Travail de fin d'études et stage[BR]- Travail de fin d'études : Reverse engineered modelling for structure stiffness analysis: application to automotive chassis[BR]- Stage d'insertion professionnelle

Auteur : Bellefroid, Jean-Charles
Promoteur(s) : Duysinx, Pierre
Faculté : Faculté des Sciences appliquées
Diplôme : Master en ingénieur civil mécanicien, à finalité spécialisée en technologies durables en automobile
Année académique : 2021-2022
URI/URL : http://hdl.handle.net/2268.2/14562

Master thesis

Reverse engineered modelling for structure stiffness analysis : application to automotive chassis

M.Sc. in Mechanical Engineering

Jean-Charles Bellefroid

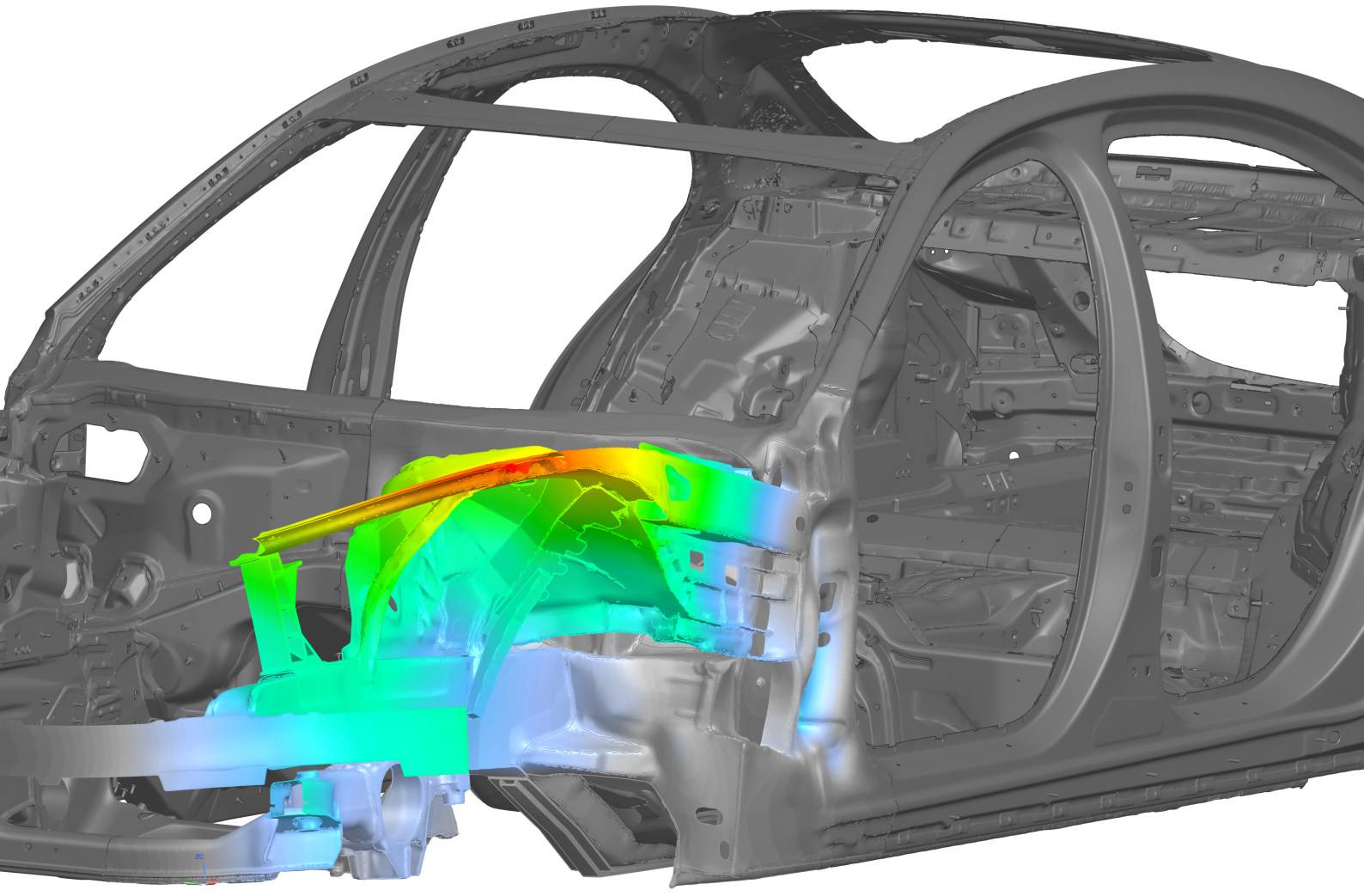

LIÈGE université
Sciences Appliquées

CARAT
Duchatelet®

Master thesis

Reverse engineered modelling for structure stiffness analysis : application to automotive chassis

Graduation Studies conducted for obtaining the Master's degree in Mechanical Engineering by

Jean-Charles Bellefroid

Student Name	Student Number
Bellefroid Jean-Charles	s173407

Academic year 2021-2022

Academic promoter:	Pr. Pierre Duysinx
Industrial promoter:	Vincent Lambert
Institution:	University of Liège
Place:	Faculty of Applied Sciences, Aerospace and Mechanical department
Project Duration:	February, 2022 - June, 2022

Abstract

Producing high quality secured vehicles starting from mass-produced ones involves a strong re-engineering of the initial product, for which only a 3D scan and a few additional data are available. Especially, this work intended to suggest structural stiffener elements to the front compartment of a car body through the analysis of a front left quarter part of the whole automotive body.

The geometrical modelling aimed at generating a suitable numerical model. Based on a particular reverse engineering process, it consisted in various operations on facets of the 3D scan. From this step results a geometric model approaching the physical chassis and composed of several connected parts consisting of sheet metals or massive parts, and made from various materials and/or thicknesses.
It involved strong assumptions and simplifications since the 3D scan does only provides partial information about external surfaces.

The Finite Element Analysis, led through the two most important load cases that are bending and torsion ones, validated the mechanical consistency of the model with respect to the physical chassis. It concluded that the model is accurate and consistent enough for global structure stiffness analysis, especially when working with relative notions. What concerns absolute results, experimental testing is needed to provide a scaling between real and numerical results.

Further improvements that are the addition of the subframe in the model and the investigation of load transfer through the suspension mechanism have been added.

Concrete applications about structural stiffness analysis of the built model have been suggested through three stiffening possibilities. It resulted that the piece resulting from the enterprise's know-how was quite effective even as a stand alone, while the combination of the strut tower's strapping with the flexural reinforcement part was the most effective with a limited additional deformation of the armoured vehicle compared to the classic unarmoured one.

Key words: reverse engineering, geometric reverse engineering, 3D scan, scan cleaning, structure stiffness, car body stiffness, automotive

Acknowledgments

This thesis represents the outcome of five years of hard but pleasant work to become a competent Mechanical Engineer.

First, I want to thank my academic promoter, Professor Pierre Duysinx, for his key support during this thesis realisation, but also during the whole master. Then, I would like to thank Professor Eric Béchet for his punctual help.
I would also like to thank the professors of the Faculty of Applied Sciences for giving me the necessary baggage to face the professional world.

Secondly, I am grateful to Vincent Lambert for his trust and *Carat-Duchatelet* employees for their help and their welcome.

In addition, I would like to sincerely thank Sébastien Guibert from the *Siemens Support Center* for his precious help concerning the software's possibilities and without whom I would undoubtedly not have succeeded in carrying out this project.

Finally, I want to thank my relatives for the support, help and encouragement they have shown during these five long years.

Choose a job you love, and you'll never have to work a day in your life.

Contents

List of Figures

List of Tables

Nomenclature

Abbreviations

Abbreviation	Definition
VIP	Very Important Person
B2B	Business-to-Business
RE	Reverse Engineering
CAD	Computer-Aided design
CAE	Computer-Aided Engineering
CAM	Computer-Aided Manufacturing
B-Rep	Boundary Representation
CoG	Center of Gravity
BIW	Body-In-White
RBM	Rigid Body Mode
FEA	Finite Element Analysis
S&R	Squeak and Rattle
NVH	Noise, Vibration and Harshness
SUV	Sports Utility Vehicle
FEM	Finite Element Method
dof	Degree of Freedom
TPE	Total Potential Energy
BC	Boundary Condition
STB	Strut Tower Brace
AI	Artificial Intelligence
TO	Topology Optimization

Introduction

The product re-engineering is becoming more and more important. Modifying an existing product allows to fix problems and issues, or add new features in lowered lead-times.
The automotive sector is no exception to the rule, whether for customized vehicles such as limousines or prepared cars for racing.

When integrity is concerned, the structural behavior should be carefully analyzed and discussed. Especially, armoured vehicles are usually lengthened and suffer from a substantial additional weight that impacts its behavior.

The purpose of this work is to analyze the structure stiffness of an armoured automotive chassis, and suggest solutions to keep its structural integrity. On the one hand, this project must propose a model for leading analysis. On the other hand, this model should provide relevant results.
To synthesize, the objectives can be formulated in the following questions :

- What is the traditional procedure to re-engineer existing products?
- How to model an automotive chassis for global structure stiffness analysis?
- What are the relevant tests to analyze automotive chassis' stiffness?
- How results coming from analysis can be used to discuss structural integrity and provide industrial applications?

To answer these questions, the methodology is divided into two main parts. The first one develops the process of generating a numerical model suitable for global structure stiffness analysis. The second parts analyzes the model, discuss its limitations and proposes solutions to answer the original problem.

This work is structured in six parts. The global context is first described, as well as the initial problem. This poses the basics for a deep understanding of the subject. Then, the literature review gives the necessary knowledge about geometric reverse engineering, structural analysis of automotive body, finite element method, and software used. The third part describes the procedure to recover a suitable numerical model starting from a 3D scan, after what comes the analysis and validation of the generated model. Improvements are proposed and criticized. The fifth parts concerns potential solutions to answer the problem initially stated. Finally, some perspectives are introduced for further reflection and improvements.

1 | Context and project description

This project, carried out in enterprise, takes place in an industrial context. Its understanding is primordial for a deep apprehension of this thesis, and especially to appreciate choices, assumptions and simplifications made.

This Chapter begins by setting the general context. It describes the enterprise and its general business model. Then, the problem is stated, objectives are listed and limitations are pointed out.

1.1 General context

1.1.1 Need for secured vehicles

A VIP armored vehicle is a traditional car with reinforced structure in order to keep occupants safe from various assaults such as bullets, blasts, fire, etc [36]. Generally, such a car is essentially composed of bulletproof plates and glasses.
There is one major difference between military and VIP armoured vehicles: the VIP one is externally extremely similar to the original model. The ultimate goal of secured vehicles' manufacturers is to produce secured cars that couldn't be differentiated from normal ones. The Figure 1.1 shows a secured limousine.

Figure 1.1: *Carat-Duchatelet* Carat 1000 secured vehicle [9]

Nowadays, armoured vehicles are widespread all around the world, especially in unstable regions such as Africa or Middle-East.
Secured vehicles are essential for many people such as businessmen, heads of State or royal families [34]. For these people, the objective is to stay safe in most situations imaginable while keeping the highest level of comfort.

1.1.2 Enterprise

Carat-Duchatelet is a Belgian company founded in 1968 and located in the city of Liège [9]. It is known as the world leader in manufacturing specialty vehicles in the automotive industry. Far away from mass and series production, each vehicle is unique and based on the needs of the particular customer. The company provides the highest quality vehicles, the ultimate

objective being combining exclusivity with security.

Carat-Duchatelet develops vehicles on demand of customers, but focuses on one major base model : the Mercedes S Class. Starting from this car, different versions are manufactured, depending on the lengthening, the degree of protection and other options that the customer wants.

The new model (W223) of the Mercedes S Class was presented in September 2020 [37], which is the seventh generation of the S Class and replaces the previous version that was produced since 2013.

Carat-Duchatelet develops thus models of secured vehicles based on this new generation, through re-engineering of the initial product.

Data sharing between Mercedes and *Carat-Duchatelet*

Generally, data sharing between businesses can be very lucrative to both data suppliers and users since it allows to develop for the two sides new business models and new products or services [3].

Unfortunately, Mercedes does not provide any data about its vehicles to *Carat-Duchatelet*. It is quite convenient for large companies, especially for car manufacturers, to not share any data about their products to other companies if there is no specific partnership between them. This is mainly due to industrial reproduction and espionage, as well as safety and security requirements.

1.2 Motivations

Producing high quality secured vehicles starting from mass-produced ones involves a strong re-engineering of the initial product. Lengthening of the car modifies the chassis, and armoring the vehicle induces the addition of numerous ballistic windows and steel plates. This induces a significant extra weight that the car is not designed for.

These two features lead to potential stiffness issue.

The first objective is thus to discuss the structure stiffness of the chassis for both classic and armored situations, and suggest ways to improve its rigidity when armoured.

The enterprise has also a second motivation: investigate a new manufacturing process for its modified vehicles. Traditionally, armored and lengthened cars are based on the initial integral body. However, the design's complexity, especially in terms of materials and geometries, is strongly increasing so that the actual general process to lengthen the body becomes quite complicated.

This new process would consist in building a whole new survival cell directly made from ballistic plates. Both front and rear compartments of the original chassis would be bonded to this new cell to form the secured car body.

In order to make feel secure with the bonding between compartments and survival cells, a mechanical support would stiffen and strengthen these junctions. To sum up, the second objective of this work is thus to investigate a mechanical support between front/rear and central compartments.

1.3 Available resources

As developed in Section 1.1.2, there is no numerical model made available by Mercedes so that an alternative way has to be found.

Although the 3D scan does not correspond to original technical data coming from the car manufacturer, it is an interesting way to dispose of information about the product when there is no specific data sharing.
The 3D scan provides (partial) geometric information. Associated with other data types such as product's materials constitution or thicknesses of scanned surfaces, there is a way through reverse engineering (RE) process to lead some specific analysis.

In this way, *A2Mac1*, an automotive benchmarking provider [2], dispenses a 3D scan of the automotive body as a whole and information about thicknesses and/or material constitution for different locations.
The Figure 1.2 shows the full 3D scan of the chassis.

Figure 1.2: 3D scan of the full Mercedes S Class chassis by *A2Mac1*

1.4 Objectives and limitations

There are several objectives in relation to the project itself. They reside in the following items:

- Development of a geometric reverse engineering modelling procedure specific to modern softwares for global stiffness analysis of an automotive chassis;

- Development of a methodology for structure stiffness analysis of an automotive body;
- Application to the stiffening of an automotive body's front compartment.

On the other hand, objectives also concern personal aspects, listed below:

- Familiarisation with a modern CAE software;
- Knowledge development about reverse engineering, automobile body structure design, and automotive sector in general;
- Improvement of the work method specific to engineers.

However, the project suffers from limitations that are listed below:

- The time limit. It is generally a key factor in professional environment and always leads to concessions.
  In this project, this constraint concerns a first strong choice: the limitation to a quarter front model instead of the whole body. This point is further discussed in Section 1.4.1;
- Presented results are not optimal in every respect. Each part can be further developed and improved such as the mesh generation, the sequence involved in model processing, etc.
  At every moment, one has to keep in mind limitations, assumptions and simplifications made;
- The proposed application with chassis bracing does not consist in dimensioning phase. It only suggests ways to answer the initial problem but it does not claim to present a working prototype.

1.4.1 Time limit constraint

The time available for answering the problem is limited to some months. The choice to focus the project on the front compartment was made and is justified by the following arguments:

First, the armoured central compartment is supposed to be extremely stiff so that there is no interest in studying this specific portion. The study can focus on front and/or rear compartments specifically.

Secondly, the armoured central compartment directly receives efforts coming from the rear axles. It results that the rear compartment does not suffer from significant efforts. There is little interest in investigating the rigidity of the rear part.

Furthermore, the front compartment can be considered as being symmetric with respect to the central vertical plane so that considering only the half of the front compartment is sufficient.

Finally, a real physical experimentation on the car body exhibited that the front compartment is more critical because it is more subject than the rear one to deformation with respect to the central compartment. It also showed that deformations are very similar for both left and right parts in front compartment, so that considering a half part of the front compartment is enough to study its complete behavior.

To conclude, this thesis focuses on the front left quarter part of the automotive chassis.

2 | Literature review

As a preliminary step in this work, it is interesting to synthesize all the stuff that might be necessary to know in order to fully and completely understand the content of this work. In other words, it resumes the literature about the different subjects discussed along this thesis. In addition, it also describes and justifies the software that have been used.

This Chapter begins with the description of the geometric RE. The general steps of the RE process leading to a Computer-Aided Design (CAD) model starting from the real physical model are addressed. Secondly, the theory about structural analysis of automotive chassis is discussed. All the load cases are defined, and especially the most important ones. Then comes a short explanation of the Finite Element Method (FEM). Finally, this Chapter ends with the software description, as well as the justification of its use for this subject.

2.1 Geometric reverse engineering

2.1.1 Definition, applications and interest

RE has multiple definitions which all highlight inverse methods [22]. More specifically in mechanical engineering, geometric RE can be defined as the redesign of an existing product based on several informations such as its geometrical shape, involved manufacturing processes and assemblies, functionality or documentation.

Explained in another way, the redesign consists in the reconstruction of a CAD model starting from the product, this redesign being as close as possible from its original shape [5]. It aims at inferring a model and its parameters from experimental data.
It is also known as the RE of shape [33], where real parts are transformed into engineering models and concepts.

Applications

There are several applications of geometric RE in practice [23]. This process is used to copy existing parts when there is no drawing or documentation available. For instance, RE is able to provide relevant 3D models for quite old products that no longer have drawings. A second typical application of RE concerns the re-engineering of existing products. It can concern new features added to the product, or real-scale clay models modelled by stylists and that need to be converted into a 3D CAD model. For instance, the automotive industry works with this methodology for the aesthetic of the automobile. A third usage deals with custom fits to human surfaces, as for prostheses, helmets and other mating parts.

Interest

Usually, it is intended that the parametric representation resulting from the RE process would be compatible with at least one widespread CAE software.

Since the CAD model consists in a more compact and concise representation of the geometry, the design is more qualitative and efficient, manufacturing is improved as well as

analysis.

The practical usefulness of the generated model is variable and is dependent on several factors. The faculty of recovering the 'perfect' design is the most important one. Indeed, a 'close' representation is generally not sufficient for engineering applications. Specific properties such as parallelism or exact dimensions are nearly always primordial.

The geometric RE process is divided into four basic steps, as shown in Figure 2.1. The first consists in the data capture. The existing product is scanned to convert its geometry into a numerical form. Then, the preprocessing prepares the raw data for next steps by cleaning the model from some specific defects. The third step concerns the segmentation and surface reconstruction. It is the most critical one because it requires a great deal of reflection. Finally, the CAD model is generated by connecting surfaces and applying some properties through feature recognition such as parallelism, dimensions, etc.

Although appearing sequential, these steps are generally overlapping and some iterations are necessary.

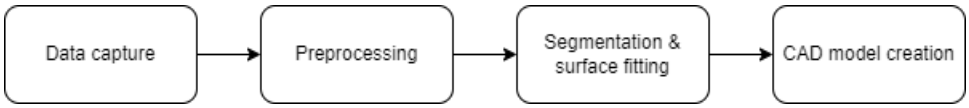

Figure 2.1: Geometric reverse engineering steps

At the top of its art, the RE is an intelligent process able to directly create the CAD model from the scanning step, without any human intervention. However, it is a particularly complex problem that still requires laborious work. The following Sections describe these general steps.

2.1.2 Data acquisition

The data capture corresponds to physical measurements through the scanning operation to collect data on its shape. It is thus strongly limited by physical considerations.
A partial resolution of this issue involves the merging of multiple scans. However, there is still some unreachable zones that are impossible to scan. It results an incomplete 3D scan.

On the other hand, approximate or incomplete models may be sufficient for certain particular applications.

There are several methods to scan a part, each of them having strengths and weaknesses. All interact with the surface or material through different phenomena such as optical, tactile, acoustic or magnetic methods.

In practice, data acquisition is subject to various issues :

Calibration and accuracy It is dependent to the technology and the model of the scanner.

Accessibility Configuration and topology of the part impact the accessibility.

Occlusion It corresponds to the blocking due to shadowing or obstruction.

Fixturing and multiple views Fixturing of the part can be fixed using multiple views. However, multiple views introduce errors because of the combination process.

Noise and incomplete data It is a hard issue because of the multiple factors leading to noise and incomplete data. Filtering methods are generally useful.

Statistical distribution of products The scanning of the part corresponds to one single part for which the fabrication involves tolerances and defects. It results that the scanned part represents only one single sample in a distributed population.

Surface finish Smoothness and material coatings affect the result of scanning. In addition, Noise can also be induced due to properties of the surface, depending on the interaction between surface and scanning technology.

Accuracy at borders Borders are characterized by the absence of data along it so that the scanner is not able to smooth the border by comparing it to its vicinity. It results strong inaccuracies at surface's borders.

These issues involve a post-processing that may be particularly laborious and time-consuming.

From a point cloud to a surface mesh The scanning step provides a variable density point cloud. It is necessary to convert it into a piecewise smooth and continuous model. The point cloud is transformed into a mesh of elementary surfaces, such as triangles.
The standard file format for such a triangular mesh is the STL, which is broadly and widely supported by numerous engineering softwares.

Other data types

Scanning of the part is not the only raw data that can be useful for RE processes. Additional information about the product such as constitutive materials, interaction with its environment or with other parts, etc are generally extremely useful and even primordial to generate an accurate model.
Additional data can also be used for cross-checking information, in such a way that the model comes out more representative.

The main advantage of disposing of the real physical part or other data types than the 3D scan is the ability of reconstruct a more meaningful model regarding to functions of the part.

2.1.3 Preprocessing

As explained in previous Section , the 3D scan suffers from defects and inaccuracies. It is necessary to clean certain types of defects before pursuing the geometric RE process.

The goal of the preprocessing is to prepare the 3D scan for the next steps. Generally, it is most manual and consists in some operations on the mesh such as removing details, smoothing surfaces, etc. It is dependent on the software used and its capacities.

2.1.4 Segmentation and simple surface fitting

In most of mechanical engineering's applications, the mesh emerging from the 3D scan is not the best suited because it does not provide a perfect representation of surfaces. Indeed, manufacturing methods depend on surface type, *i.e. if a surface is a plane, a circle, a random surface, etc.*

It is a quite easy process for an engineer to recognize the type of surface. Nevertheless, it is a deeply complicated task for a computer. For instance, it strongly depends on tolerances with respect to surfaces, but these surfaces suffer from several defects and inaccuracies.

Therefore this differentiation of surface type, also called segmentation, is a step in its own right. The goal of the segmentation and surface fitting is to extract from the triangular mesh forming a general surface of the part a higher level representation of the shape.

Segmentation

The segmentation aims at dividing the point set into subsets, each subset corresponding to a natural surface such as a plane, a cylinder, a sphere, etc. Then, the classification identifies the type of surface for each subset. Finally, a best fit surface is built for each subset. The least-square method is commonly used for this last step.

There are two ways for segmentation: the edge-based and face-based methods. Generally, face-based methods provide better results; it is nowadays based on the curvature of the surface that highlights surface types, as shown in FIGURE 2.2.

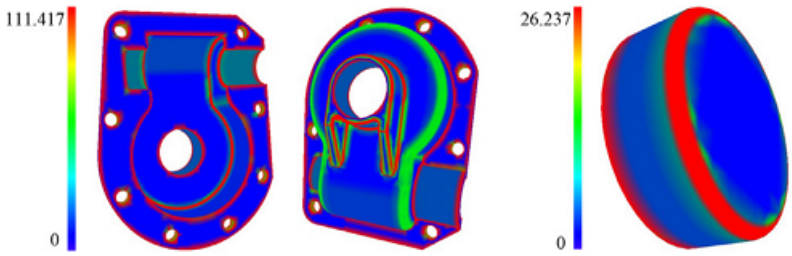

Figure 2.2: Curvedness map example [22]

In practice, these three steps of segmentation and surface fitting are not sequential, but are conducted in parallel.

Free-form geometry

In contrast to simple surfaces such as planes, spheres, etc, the free-form surfaces are particular and lead to difficulties that do not appear for the first ones. Indeed, free-form surfaces have much more internal parameters because of their geometric complexity. They are thus strongly dependent on the definition of the surface itself.
However, it is non-trivial to identify and choose where faces start and end. The resulting segmentation process is crucial. There is four approaches that are commonly used:

Global approximating surfaces A best-fit surface is shaped on a large roughly approximating four-sided surface. If tolerances with respect to the original surface are too large, the surface is subdivided. An iteration process is created until tolerances are encountered.
The FIGURE 2.3 illustrates the working principle of the global approximating surfaces method. The concept is simple and requires no user interaction. However, the initial surface delim-

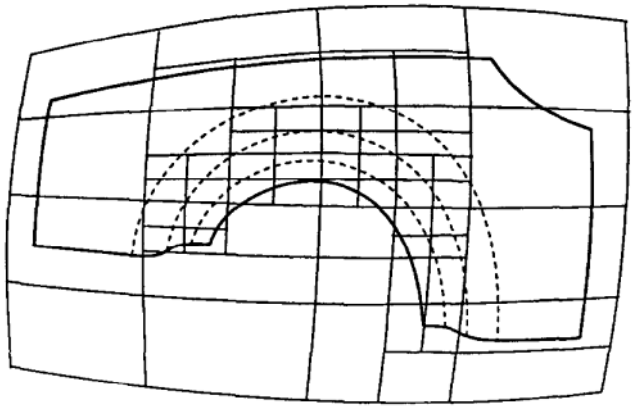

Figure 2.3: Global approximating surface [33]

itation should be determined carefully for accurate refining. There is also no attempt for understanding the shape.

Curve network based surfaces The surface is divided from characteristic curves to define four-sided surfaces, as shown in FIGURE 2.4 Although the patches reflect the structure of the

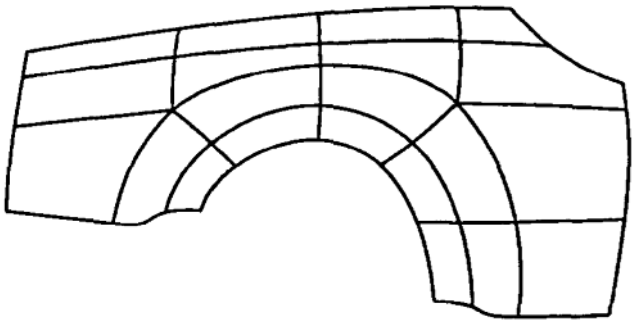

Figure 2.4: Curve network based surface [33]

surface, defining the characteristic curves is tricky and may be unreliable. Indeed, only local parts of the data (that suffer from noise issues) are used to determine these curves.

Arbitrary topology surfaces This approach consists in a combination of the two previous ones. A global approximating surface is created with an arbitrary topology. Then, the generation of the patch structure comes from the simplification of the global approximating surface.

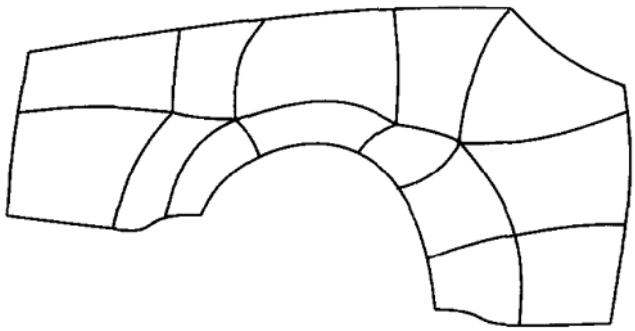

Figure 2.5: Arbitrary topology surface [33]

The FIGURE 2.5 illustrates this method. The collection of smooth connections between patches fits rather well to the topological structure of the surface, even if this structure does not represent the functional structure of the shape.

Functionally decomposed surface The goal for this method is to attempt to identify how the surface was shaped and thus try to perform the same operations, as shown in FIGURE 2.6. This seems to be the best method providing an appropriate engineering decomposition of the

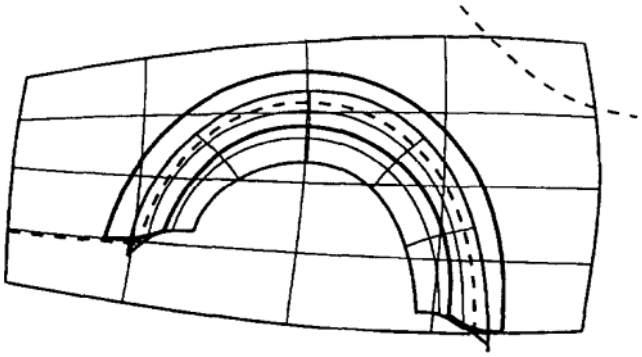

Figure 2.6: Functionally decomposed surface [33]

shape, although requiring a large amount of interaction or a detailed knowledge of the part.

To conclude about free-form surfaces, the most used method consists in surface patches with four boundary curves, such as Bezier patches. Nevertheless, the ideal method would combine all the approaches detailed above.

2.1.5 CAD model creation

The last step of the geometric RE process aims at creating a geometric product using a Boundary Representation (B-Rep). In that way, the fitted surfaces must be connected together using

explicitly stored adjacency relationships and mathematical formulation for edges and curves. This last step also concerns geometric properties in the model such as dimensions, parallelism, perpendicularity, etc.

Intersections between surfaces

In some cases, as using edge-based methods or free-form curves network, the explicitation of boundary curves is created during segmentation. However, it does not happen for models made of disjoint surfaces, where no consistency have been created between them during segmentation and surface fitting step. There are diverse cases when connecting disjoint surfaces:

Two-surfaces intersection By extending two surfaces, the intersection between them is easily created and proper edge curves are generated.
However, it is not always the best way to intersect two surfaces. Sometimes, it is better to consider a blend or to adjust parameters of the surfaces in order to smooth the intersection;

Multi-surfaces intersection If surfaces meet in a sharp intersection, this intersection corresponds to a unique point. In contrast, it is more difficult when smooth edges or more than three edges meet. This happens for example due to inaccuracies. One possible solution is to adjust surface parameters to improve intersection between surfaces;

Blending surfaces Sometimes blends are explicitly present in the model. Sometimes they are not but help to artificially bridge gaps due to imperfections.

Geometric properties

Up to now, the CAD model is built but it is still generally not suitable because important geometric properties such as symmetry, parallelism, orthogonality, concentricity, etc are still missing. These are essential informations, especially for manufacturing, as already explained before. The definition of these properties should be done with extreme care.

The issue of identify ”where” and ”what” to apply as geometric constraints needs a high level of information. This requires a strong user interaction, or possibly artificial intelligence.

The manufacturing knowledge and functional analysis may be particularly useful [1], as it already is for the segmentation and surface fitting.

2.2 Automotive body structure : design and analysis

2.2.1 Functions of the car body, design constraints and restrictions

The car body has several main functions [13]:

Transport It has to carry passengers and goods, that act as a load, over a certain distance with speed and safety requirements. For passengers, it corresponds to safety and comfort such as fatigue reduction, insulation and protection against external perturbations (wind, rain, sound, dusts, etc), or space. For freight, it is more about maximizing efficiency by increasing space and facilitate loading/unloading;

Structural It acts as the backbone of the vehicle. It has thus a structural function because diverse components are attached to it: engine, drivetrain, seat, etc;

Mechanical Chassis structures are stressed by both external and internal loads [24]. External loads come from aerodynamic resistance all around the body, and from tire-ground contact through the suspension mechanism. Internal loads are due to the mass of the vehicle and its payload. Important internal loads are also caused by the reaction forces of the powertrain that is attached to the chassis;

Aerodynamic and aesthetic On the one hand, the car body should minimize the aerodynamic resistance through the aerodynamic coefficient C_x and the frontal area of the car S. This is mainly related to the shape of the body. On the other hand, the aesthetic aspect is primordial since cars are produced to be sold, and *"Ugly sells less well"*.

Design constraints and restrictions

When designing an automotive body structure, it is necessary to consider several design constraints and restrictions:

- Taking care of structural and mechanical aspects, the stiffness must be high enough while minimizing the weight. This particular point is further discussed in Section 2.2.4.

  Stress levels are also important for fatigue and durability considerations.

  Finally, the design for crashworthiness becomes more and more important for modern vehicles: the mechanical function also requires the safety and protection of passengers in the event of an accident. It mainly concerns a non-deformable survival cell located between two deformable energy absorption zones;
- The car body must be easy to manufacture, assembly, dismantle, recycle, maintenance, and repair, while minimizing manufacturing costs. Viability of car manufacturer is at sake;
- The vehicle stability and handling is of prime importance. The position of the Center of Gravity (CoG) and the stiffness in bending and torsion mainly characterize the vehicle dynamic;
- The performance matters through aerodynamic and mass, as do the safety through deformable and non-deformable zones;
- Habitability considerations lead to restrictions because of interior volume and easiness of loading/unloading requirements;
- Operating costs are also restrictive. They includes maintenance and energy consumption.

2.2.2 Integral chassis

Previously, there was a difference between automotive chassis and body. The chassis is defined as the structural frame usually combining beams and bar connected either by welding or by connection elements such as bolts, rivets, etc. On the other hand, the body is the shell of the car. It is characterized by the number of doors, the seat arrangement, the roof structure, etc.

Nowadays, modern passenger vehicles generally have an integrated construction of chassis and body, as illustrated in FIGURE 2.7. It results an integrated chassis made of stamped steel of various shapes designed to resist to tensile and compressive or bending and torsional loads depending on the location of components in the structure [15]. Sheet metals are usually joint using spot welding [21].

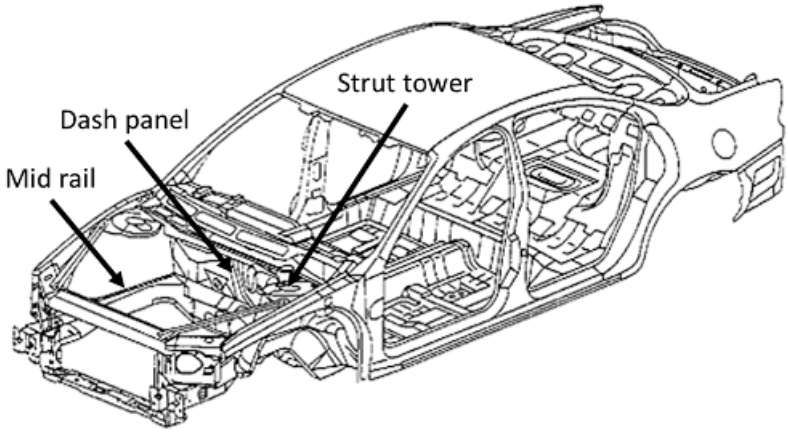

Figure 2.7: Typical passenger car integral chassis [19]

In an integral chassis, structural components have double function: structural and body parts. Such an arrangement is more rigid than separated configuration. The structural stiffness takes benefit of all components [30], especially the ones which are far from the neutral axis such as roof panels. It has one of the highest stiffness-to-weight ratio compared to solutions based on separate chassis and body.

Note that the separation between chassis and body is still valid for commercial and heavy vehicles, because of the great ability to accommodate to variety of shapes and body types.

2.2.3 Load cases

A set of loads and Boundary Conditions (BC's) applied to a system forms a load case, that is used to study the response of the aforementioned system to these loads and BC's.
The structural behavior of a car body can be analyzed through different load cases [12]. In normal running conditions, loads arise from uneven ground and from maneuvers performed by the driver [14].

There are five major load cases : bending, torsion, combined bending/torsion, lateral loads, and longitudinal loads. The most severe ones are bending, torsion, and combined bending/torsion. Additionally, it is common to find that the torsion case is the most difficult one to design for so that the torsion stiffness is used as the main indicator about car body performance.

Although lateral and longitudinal load cases being less significant on the structure as a whole, they are important for the suspension design.

There are also other particular load cases such as efforts in hinges when opening doors or else efforts due to seats and seat belts during brutal deceleration caused by crash or emergency braking.

Bending

The chassis is loaded in the vertical plane xz due to the weight of the components along the chassis, as showed in FIGURE 2.8, and causes bending about the y-axis.

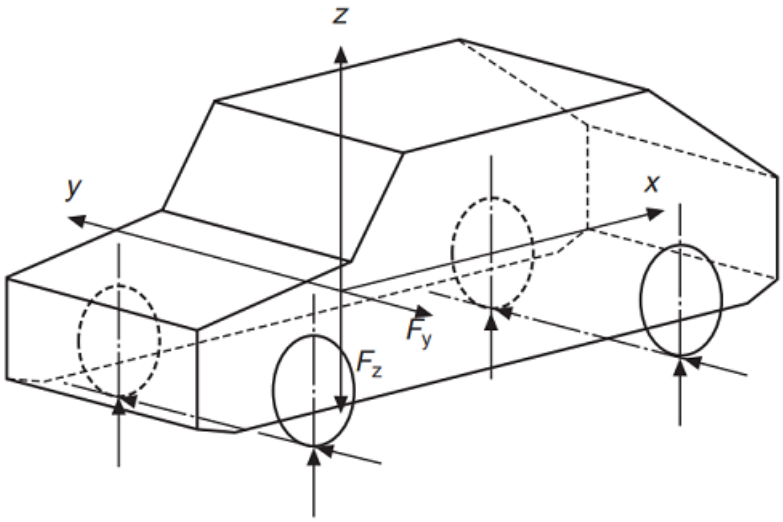

Figure 2.8: Vehicle bending case [14]

The bending conditions are determined by the weight distribution of major components in the vehicle, as well as the payload. Unsprung masses such as wheels or suspensions do not participate to this weight distribution because it does not impose loads on the structure.

Dynamic considerations It should be better to consider dynamic loads since the vehicle faces uneven road surface, such as when it overtakes a road bump. In the case of a sufficient vehicle speed, the wheels leave the ground. When impacting the ground again and even if being partially damped by the suspension, the load under the wheels increases severely and is more important than in static loading.

Car manufacturers have found that dynamic loads can be taken into account by applying a magnification factor to the static loading. For road vehicles, this magnification factor is about $2.5 - 3$ whereas it is up to 4 for all-terrain operations.

Torsion

The vehicle is subject to a torque by applying 2 opposite vertical forces at both ends of the axles, at the knuckle, as illustrated in FIGURE 2.9. It results in a twisting action about the longitudinal x-axis.

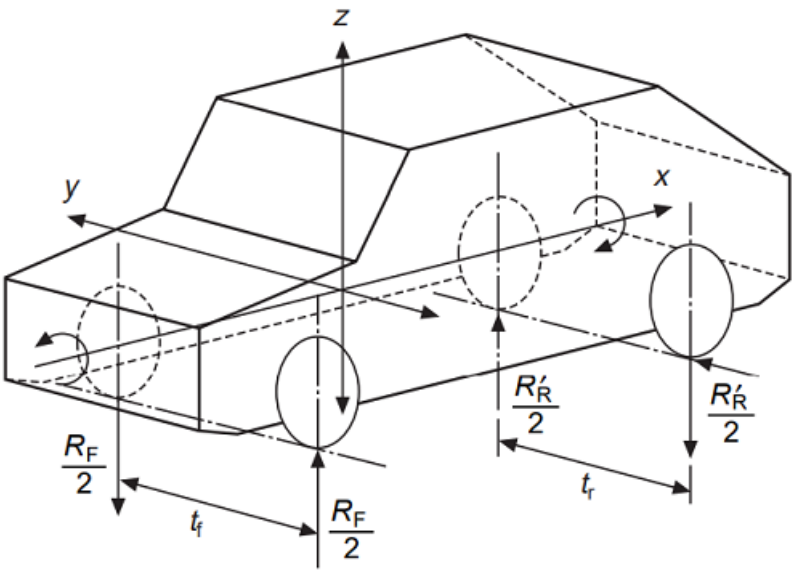

Figure 2.9: Vehicle torsion case [14]

A pure torsion load being applied under one axle, the other is subject to a reaction moment. The base torque is calculated with the vertical forces under the lightest axle. Its value is :

$$M_x = R_F \frac{t_F}{2} = R_R \frac{t_R}{2} \tag{2.1}$$

Generally, t_F and t_R are different, and the lightest axle is often the rear axle, such that $R_R < R_F$.

Dynamic considerations As explained in Section 2.2.3 for bending, dynamic loading should better be considered instead of static loading. This can also be estimated using a magnification factor on the static loading. For road vehicles, it amounts to 1.3, while it is 1.8 for all-terrain vehicles.

Combined bending and torsion

Pure torsion load case is more theoretic than realistic. In practice, the gravity always acts during the torsion, and it is reasonable to consider the simultaneous application of bending and torsion loads.
The most critical situation corresponds to the case of one wheel of the lightest axle lifts off the ground. It happens when the other wheel of the lightest axle is raised on a bump of sufficient height. The vertical force under this wheel vanishes and the vertical force of the axle is completely withstood by a single wheel. This load case is represented in Figure 2.10.

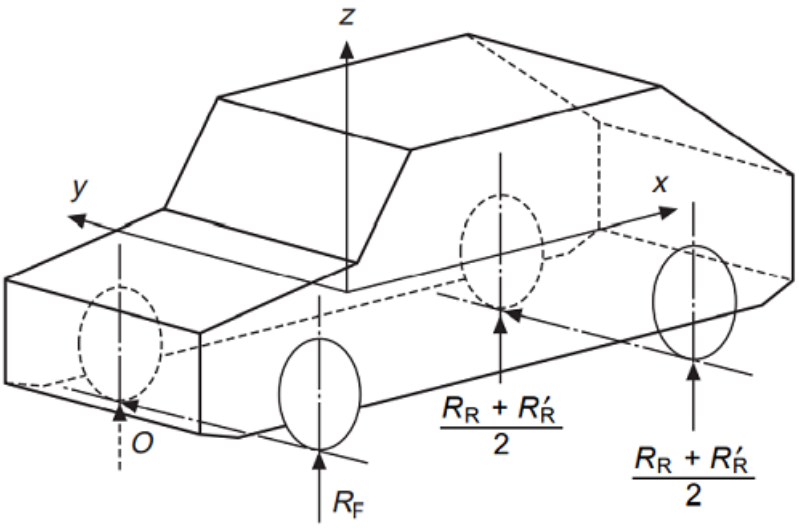

Figure 2.10: Vehicle combined bending and torsion [14]

Lateral

When the vehicle is turning, tires develop lateral forces to counterbalance the centrifugal acceleration MV^2/R. The FIGURE 2.11 illustrates the critical situation, when the car is about to roll over because the whole vertical load is transferred on the external wheel. Loads are along the y-axis so that the structure is subject to bending in the xy plane.

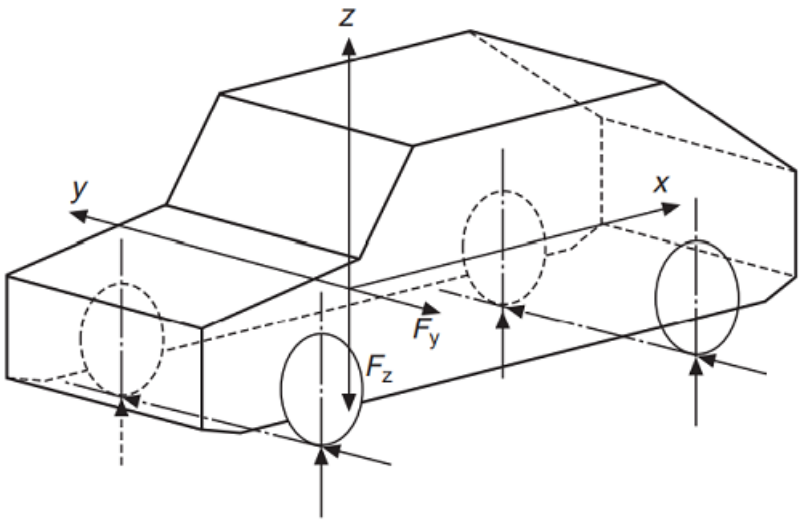

Figure 2.11: Vehicle lateral loading [14]

In practice, the usual position of the CoG as well as the limitation of the adherence coefficient are such that this situation never occurs. Indeed, the roll-over situation corresponds to a lateral acceleration of about $1.42g$ while the road adherence involves a limit lateral acceleration of about $0.75g$. In other words, the vehicle will loose its tire-surface adherence before undergoing roll-over.

In addition, the lateral load case is not a critical design criteria because of the large bend-

ing moment inertia of the car body in the xy plane. However, it is a severe load case for attachment points of suspension to the body since it must withstand high loads during shocks. Safety considerations usually lead to consider a magnification factor of 2 between static and dynamic loadings.

Longitudinal

The weight transfer between front and rear axles involved by large accelerations or braking maneuvers develop inertia loads of components onto the chassis. These loads are along the x-axis. Such a load case is represented in FIGURE 2.12.

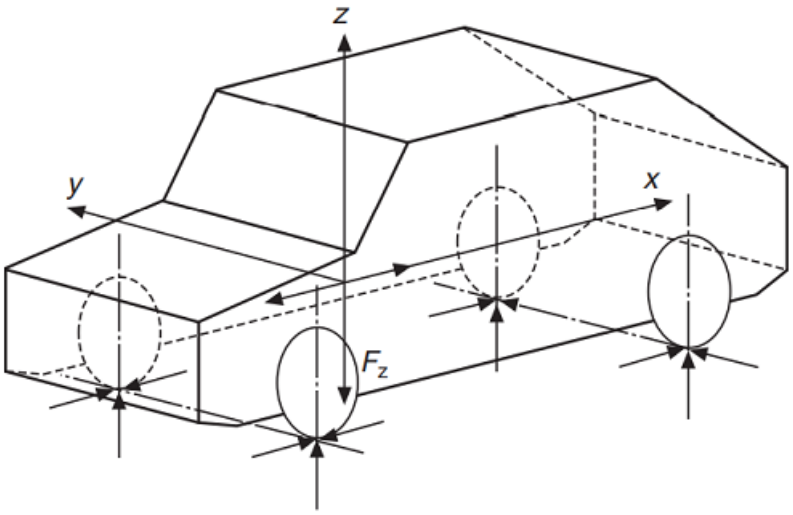

Figure 2.12: Vehicle longitudinal loading [14]

The braking and acceleration forces are limited by the tire-ground adherence. It results thus that this load case is less significant than others.

2.2.4 Car body stiffness

Strength and stiffness

Strength and stiffness are the two main indicators of vehicle structure performance [19]. Designing a vehicle structure aims at achieving high enough strength and stiffness levels while considering design constraints such as mass, cost, manufacturing processes, etc.

Strength is about the maximum force the structure can withstand. This implies that no part of the body loses its function when normally loaded.

Stiffness relates the deflection of the structure when loaded at a certain level, in the elastic domain.

The FIGURE 2.13 schematizes the difference between strength and stiffness.

Structure stiffness can alternatively be defined as the ability of a structure to resist deformation when external forces are applied onto it. It refers to the rigidity concept.

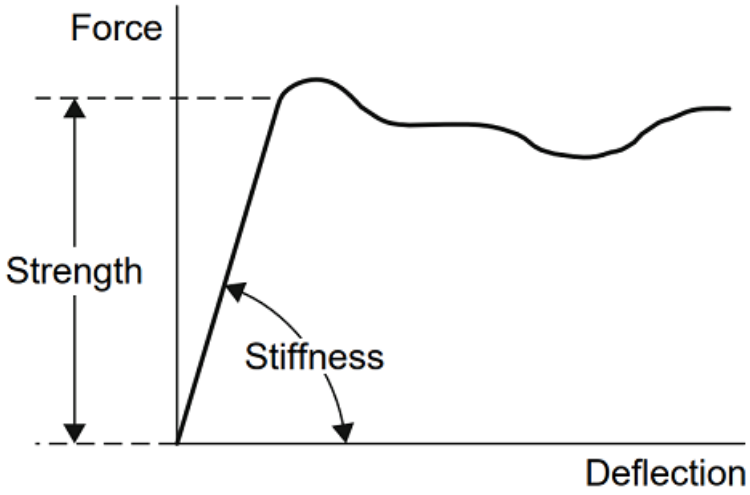

Figure 2.13: The concepts of strength and stiffness [19]

The stiffness can be further divided into overall and local stiffness. Here is only discussed the overall stiffness.

As mentioned above in Section 2.2.3, there are two main forms of body's deformation. They are linked to the two main load cases : bending and torsional solicitations.
Bending stiffness is defined as the ratio between an external applied force and its corresponding bending deformation. Its unit is the $[N/mm]$.
Torsion stiffness if defined as the ratio between an external applied torque and its corresponding torsional deformation. Its unit is the $[Nm/^{\circ}]$ or equivalently $[Nm/rad]$.

Stiffness requirement

Sometimes, the stiffness requirement is more important than the strength one. Indeed, even if a structure resists to its loads, *i.e. even if it has a sufficient strength*, its mission may not be completely fulfill if it is too compliant. Stiffness is an important indicator for vehicle's driving quality and performance [25]. There are various ways to specify the required stiffness, such as tolerant gaps for assemblies, vibration and noise transmission, road holding, etc.

Insufficient body stiffness issues Body stiffness determines the vehicle's driving quality and dynamic performance. A too compliant body causes Squeak and Rattle (S&R), Noise, Vibration and Harshness (NVH), handling, collision safety, and reliability. Furthermore, a lack of stiffness can also induce a feel of "unsafe" vehicle in the eyes of customers.

Car body and full vehicle stiffness The car body, also called Body-In-White (BIW), being the core of the full vehicle, its stiffness mainly characterizes the stiffness of the car. The eigenfrequencies of the full vehicle and the BIW are different, but the overall mode shapes are very similar although the numerous accessories.

Studying the car body stiffness provides an easier way for analyzing the full vehicle stiffness.

Modal parameters and stiffness The body's bending and torsional stiffness is closely related to its modal frequencies and shapes in bending and torsion respectively. Thus, studying the modal parameters of the structure is very useful to characterize its stiffness since it does not need to consider any particular external loads. Indeed, modal parameters are fixed for linear systems such that they are independent of external loads applied.

Bending stiffness

The bending stiffness must be large enough. For instance, the doors should be opened and closed without interference with the car body. Furthermore, stiffness of the floor is necessary for passenger acceptance. Finally, it also contributes to reduction of the vibration generation and transmission in the various panels.

Concerning integral chassis, the bending rigidity derives mostly from the inertia of the transmission tunnel and from the longitudinal beams. If necessary, additional rails are added in the inner part of the body. Solid square or round cross-section steel beams would be ideal but the goal in automotive design is to maximize the stiffness-to-weight ratio instead of the stiffness itself [16]. Therefore solid cross-section is nearly never used.

Order of magnitude Economy sedans with windshield show a bending stiffness from 8000 to 10000 $[N/mm]$, mid-sized sedans with windshield ranges from 10000 to 16000 $[N/mm]$, and Sports Utility Vehicles (SUVs) with windshield have bending stiffness of about $8000 - 14000$ $[N/mm]$.

The full vehicle would have a bending frequency in the range of $22 - 25$ $[Hz]$ in order to be far enough from major exciting forces and to be in a range at which humans are less sensitive to vibration. This gives that generally, the first bending mode of economy sedans' car body gives frequency in the range of $40-50$ $[Hz]$, while it is in the ranges of $45-55$ $[Hz]$ for mid-sized sedans and SUVs. Note that windshield has a small influence on the bending modal frequencies.

Vehicles that have a higher mass loading or cars with a longer overall length require a higher static bending stiffness in order to achieve the same frequency target.

Torsion stiffness

The torsional stiffness is essential for structural behavior. A too low stiffness induces difficulties for the doors opening and closure, and dynamic performance issues.

The roof is a major contributor to the global torsion stiffness, as well as the windshield whose contribution can be as high as 40 $[\%]$. The integral chassis torsion rigidity mainly comes from the dashboard panel, from the side skirts and from the rear bulkhead.

Order of magnitude Economy sedans with windshield show a bending stiffness from 700 to 900 $[kNm/rad]$, mid-sized sedans with windshield ranges from 900 to 1300 $[kNm/rad]$, and SUVs with windshield have bending stiffness of about $1000 - 1300$ $[kNm/rad]$.

As for bending stiffness, the full vehicle would have a desirable torsion frequency in the range of $22-25$ $[Hz]$. Generally, the first torsional mode of economy sedans' car body gives

frequency of about $40\ [Hz]$, while it is in the ranges of $40 - 50\ [Hz]$ and $35 - 40\ [Hz]$ for mid-sized sedans and SUVs respectively. Finally, the first torsional modal frequency of a chassis with windshield is about $3 - 10\ [Hz]$ higher than without windshield.

Comment about joint and adhesive bonding stiffness

The stiffness of a structure composed of multiple elements does not only depend on the constitutive parts' stiffness. The joint stiffness is a also crucial parameter strongly impacting the whole structure stiffness.
In addition, adhesive bonding has also an influence on the overall body stiffness. The proof is that its use stiffens the body, increasing thus the body's modal frequencies.

2.3 The finite element method

The Finite Element Method (FEM) is widely used for engineering analysis since it is applicable to any field problem (stress analysis, heat transfer, etc) and there is no geometrical restriction [28]. The general concept is to subdivide the structure into small and simple subparts, called finite elements.

For solids and structure mechanics, the displacement method is the standard formulation of the mathematical problem. It aims at developing the structure's global stiffness equations with specified BC's [10]. These equations are described under the form of a linear algebraic system reflecting the interaction between nodal displacements of finite elements, applied forces and moments, and BC's. The solution of this algebraic system provides the structure's displacements at nodes of finite elements.

The process of FEA, schematized in Figure 2.14, states that every finite element problem starts from a physical problem that has been translated into a mathematical form. Its finite element solution involving a numerical procedure, it is necessary to assess its accuracy.

Otherwise, it should be kept in mind that the FEM solves only the mathematical model, with its assumptions. The latter will be reflected in the solution. Therefore the choice of the mathematical model is primordial to represent accurately the physical problem [7].

Although it is impossible to compute *exactly* the real behavior, the FEA is anyway able to provide relevant results. The key way in engineering analysis is thus to select a mathematical model for the physical problem that is reliable and effective in predicting the desired quantities.
The heart of the finite element procedure is the definition of the finite elements.

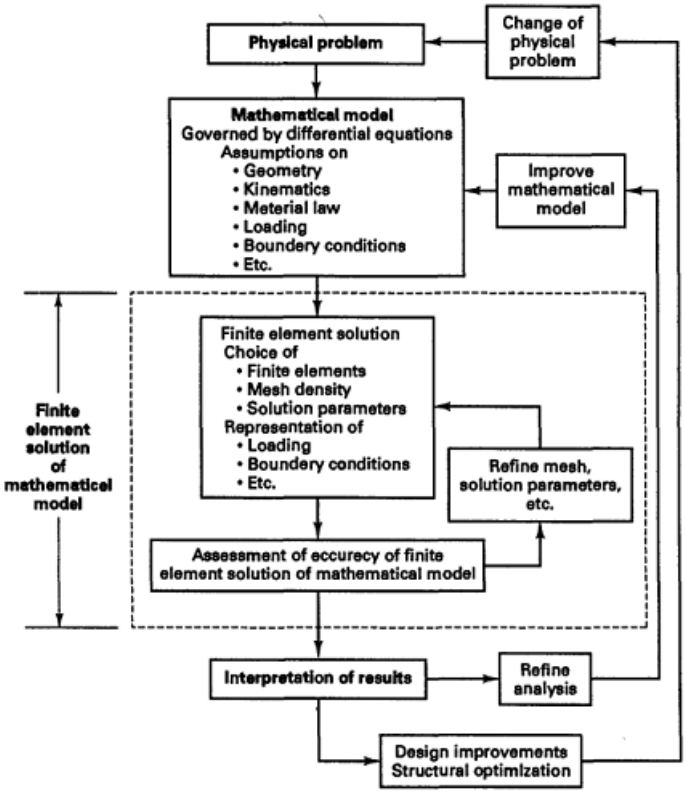

Figure 2.14: The process of FEA [7]

Static analysis

The general equation to be solved is:

$$\mathbf{Kq} = \mathbf{g} \tag{2.2}$$

where $\mathbf{K}$ is the stiffness matrix, $\mathbf{q}$ is the vector of displacement, and $\mathbf{g}$ is the load vector of the finite element system.

Dynamic analysis

The equations of equilibrium governing the linear dynamic response of a system of finite elements are:

$$\mathbf{M\ddot{q}} + \mathbf{C\dot{q}} + \mathbf{Kq} = \mathbf{g} \tag{2.3}$$

with $\mathbf{M}$, $\mathbf{C}$ and $\mathbf{K}$, respectively the mass, damping and stiffness matrices, the vector of externally applied loads $\mathbf{g}$, and $\mathbf{q}$, $\dot{\mathbf{q}}$ and $\ddot{\mathbf{q}}$ the displacement, velocity and acceleration vectors of the finite element assemblage.

More particularly, the eigenfrequencies and corresponding mode shapes of the system are solution of the following eigenvalue problem [29]:

$$\mathbf{Kq} = \omega^2\mathbf{Mq} \tag{2.4}$$

where ω is the eigenfrequency.

2.3.1 Application to vehicle design

Nowadays, integral chassis, which is the current design of car body structures, strongly requires FEA. It has become a fundamental in the design process because of the increasing complexity of chassis.
The FEM allows to study both sub-parts of a chassis to get more manageable problems and the whole chassis to analyze its complete structural behavior.

2.4 Software description

This work having a direct industrial application, the arbitrary choice of using an existing and relatively widespread software was laid. After some short researches, the Siemens NX1980 software and its solver Samcef have been chosen for multiple reasons:

- These softwares seem at first to have convenient capacities and functionalities for this work;
- These are well-known softwares and I have experience with them;
- The *Siemens Support Center* is particularly useful and is of a great help when difficulties are encountered.

That Siemens NX1980 version was released June 2021. It is one of the newest versions and it brings many additional functions in RE domain. Therefore this version is preferred over older versions.

One tool in the CAD section has been widely used : the *Polygon Modelling* task. This tool, also called convergent modelling, works on faceted models. In other words, it is able to directly work on STL files, which is the file format of the 3D scan. The faceted model resulting from the STL file importation into the software is called *Convergent body*.
This framework allows to fix defects of the 3D scan in order to generate a model suitable for meshing and simulations. Its interest is to get rid of laborious RE steps such as manual shape creation. Indeed, results obtained using only polygon modelling are good enough for this work.

From this tool, it results a major time saving. Indeed, the model generation process becomes a 'simple' model cleaning process.
Note that if the process is much more simple and direct than traditional RE processes, the model generation remains a time-consuming and strongly manual work. In addition, there are still some defects and features that are particularly hard to fix.

3 | Geometrical Modelling

This work aims at analyzing and improving the structural behavior and especially the stiffness of the Mercedes S Class chassis. As explained in Section 1.1.2, the CAD model is not available so that it is necessary to find an alternative way to generate a numerical model.

In such manner, a 3D scan and some additional information are available so that a RE modelling, also called *scan-to-CAD*, is possible and seems to be the most appropriate way to recover a numerical model suitable for structural analysis.

This Chapter describes the procedure followed to generate the numerical model starting from the 3D scan of the chassis. It begins with a discussion about the general approach followed for this scan-to-CAD processing, as well as the motives justifying the need for this procedure. Then, the model cleaning process is described. It is articulated as follows: the methodology used for each defect type is exposed. Finally, the model and its characteristics are listed and discussed in order to preview the model before going into the in-depth analysis of the latter.

3.1 Why and how to conduct the scan-to-CAD process

In the most common way, the scan-to-CAD process is a laborious work. Redesigning a front quarter model of automotive chassis may require a very long time. However, only matters the global stiffness for this work. Local comportment is not of interest and there is no intent at all to use the model for remanufacturing. Therefore a 'close' representation may be suitable.

Starting from this postulate, the use of the Siemens NX1980 software is justified since it is able to generate a finite element mesh from a cleaned 3D scan; the objective becomes to provide a cleaned model of the 3D scan. In other words, instead of following the whole traditional geometric RE process described in Section 2.1, the procedure stops at the preprocessing step. Nonetheless, this preprocessing waypoint needs a more substantial and careful work.

3.1.1 Necessity of cleaning the 3D scan

As discussed in Section 2.1.2, a 3D scan suffers from numerous defects that mainly come from accessibility and occlusion. They must be fixed.
For instance, hidden elements and surfaces can not be identified such as reinforcement parts located between two panels or details' invisibility at the junction of different welded or bonded elements. Furthermore, the 3D scan corresponds to a real manufactured part. Irrelevant elements such as bolts and rivets should be removed. Accessibility issues also need to be fixed. Finally, general defects due to the scanning process such as the orange peel effect must be fixed.

Once these issues are resolved, the resulting faceted mesh emerges suitable for meshing and FEA. Do not perform this cleaning process would lead to incapacity of the software to mesh the model. In addition, even if the software would have been able to perform the

meshing operation, results coming from simulations would have no consistence with the real behavior of the car body.

3.1.2 Software working principle about 3D scan modification

As explained in Section 2.4, Siemens NX1980 directly works on facets of the model through different operations such as removal or addition of facets, modification of relative position of facets in relation to others, or else facet subdivision or combination.

These elementary operations are intelligently used to provide specific functions aimed at achieving specific goals.

3.2 Model cleaning process

This Section is articulated around the different defects types present in the 3D scan. The way to fix each defect and recover a useable and accurate enough model is presented and illustrated.

Note that these procedures, although described as sequential, are absolutely not and the process is in practice more about parallel progress.

3.2.1 Splitting and remeshing

There are two different reasons to use this *Splitting* procedure. The first lies in the fact that this project is limited to the study of only the front left quarter part of the whole chassis while the original 3D scan corresponds to the complete chassis. It is therefore required to reduce the initial 3D scan to the portion of interest.

The second motivation is to save computational time and ease the processing. Indeed, the quarter model remains heavy. Subdivide it into multiple sub-parts to work on renders the model easier to clean and saves time. Once sub-parts are cleaned, these are merged to recover the full quarter model.

The division of the convergent body is conducted using the function *Snip Facet Body* with option *At plane*. The option *Plane dialog* allows to define easily the plane corresponding to the location of splitting.
The plane definition is arbitrary; the only interest being the reduction of computational time during processing.

Remeshing

The initial meshed body is made of facets whose size strongly varies depending on the location. Unfortunately, functions of the *Polygon modelling* task are dependent on facets. It would be more appropriate to work with a more uniform and smaller facet mesh.

The solution is the create a new finer mesh using the function *Remesh Facet Body*. The option *Facet Size* is taken as variable with an arbitrary maximum size of $3\ [mm]$, which is sufficient to work properly on the model while keeping processing time reasonable.

Note that the mesh size is chosen as variable to keep accuracy where a smaller facet size than $3\ [mm]$ is more appropriate.
One can see in FIGURE 3.1 that the mesh is finer and much more uniform when refined compared to the initial case.

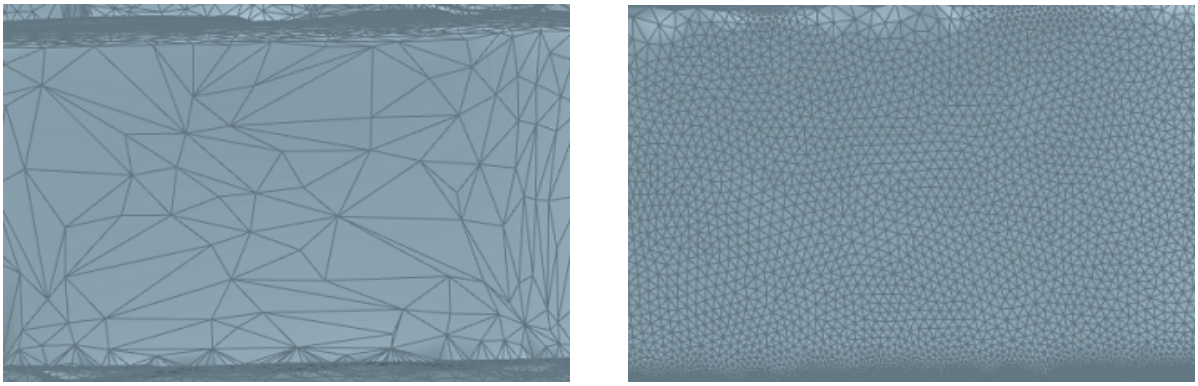

(a) Initial mesh **(b)** Refined mesh

Figure 3.1: Model cleaning - Remeshing operation

Re-assembly

Once the sub-parts are globally cleaned, these are merged together to recover the full model. The sub-parts are imported into the same CAD model. Since they have the same referential, the location of the latter match. Then, these are merged two at once using the function *Combine Facet Bodies*.

However, if the border of sub-parts have been modified, even slightly, the junction has some defects. The solution is to smooth this junction, whose procedure is further discussed in SECTION 3.2.6. The FIGURE 3.2 shows two sub-parts before and after merging.

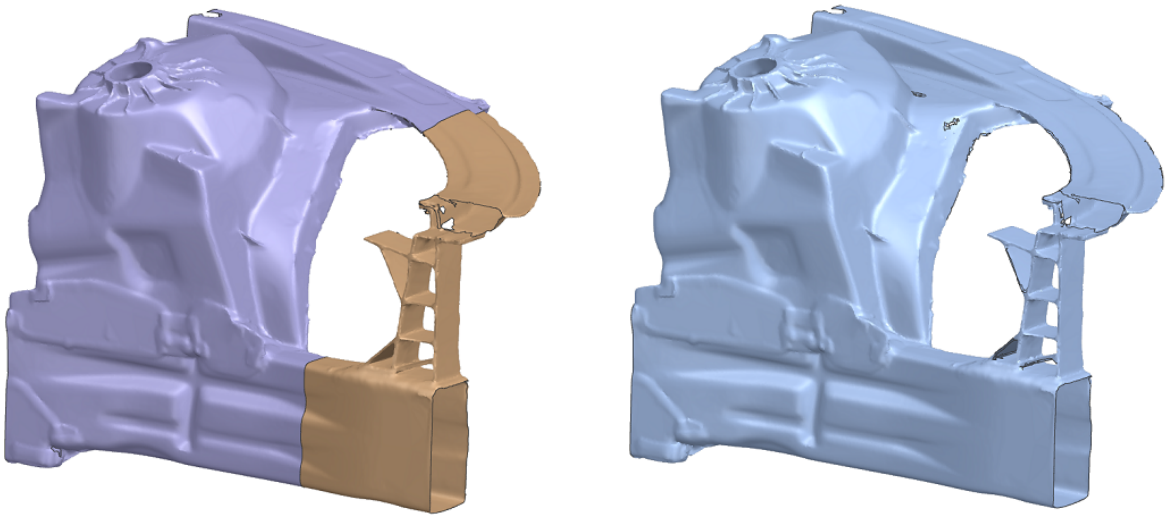

(a) Sub-parts before merging **(b)** Sub-parts after merging

Figure 3.2: Model cleaning - Re-assembly of splitted parts

3.2.2 Holes

Holes corresponds to locations where there is no scan data. It occurs because of the lack of accessibility or because of the scanning process itself. The function *Fill Hole* with option *Fill Hole* is used to fix this issue.
The FIGURE 3.3 illustrates a hole in the scan and the corresponding surface after filling operation.

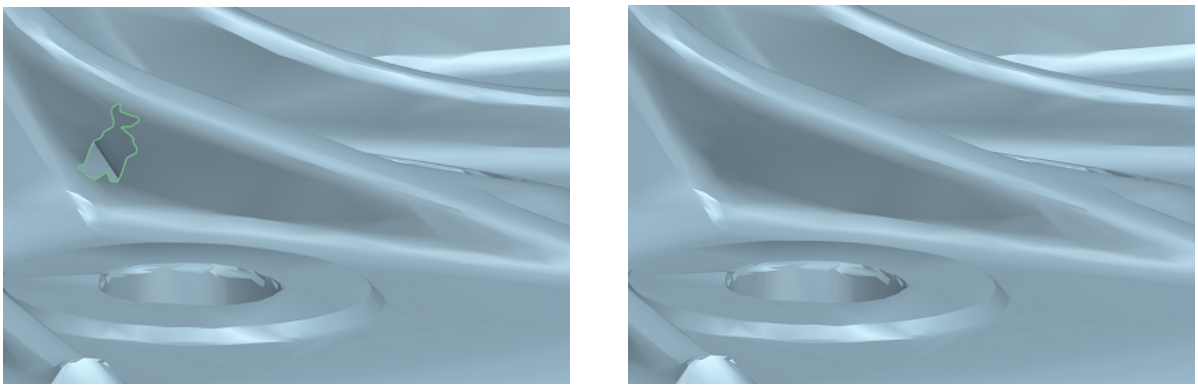

(a) Surrounded in green : initial hole **(b)** Filled hole

Figure 3.3: Model cleaning - Holes : classic approach

Defective borders

A 3D scan often suffers from strong inaccuracies at the latter's borders, as already explained in SECTION 2.1.2. Therefore sometimes hole's border has defective facets that need to be suppressed, as shown in FIGURE 3.4a, in order to correctly fill the hole next.

To suppress these defective facets, the function *Snip Facet Body* with option *By region* is used in the surrounding of the hole. It results in a larger hole, but with a cleaner border that can be filled as in classic *Fill Hole* operation.
The FIGURE 3.4 shows the cleaning steps on a defective hole, before pursuing traditional *Fill Hole* operation.

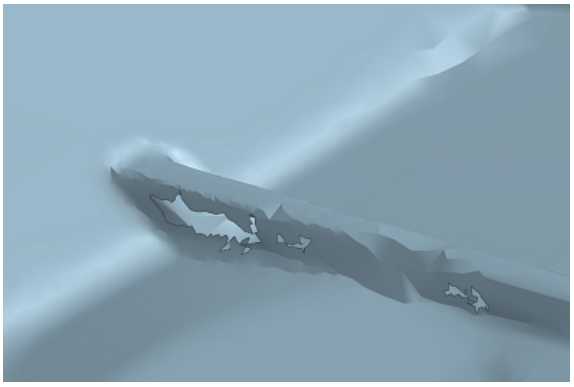

(a) Surrounded in green: Very defective hole

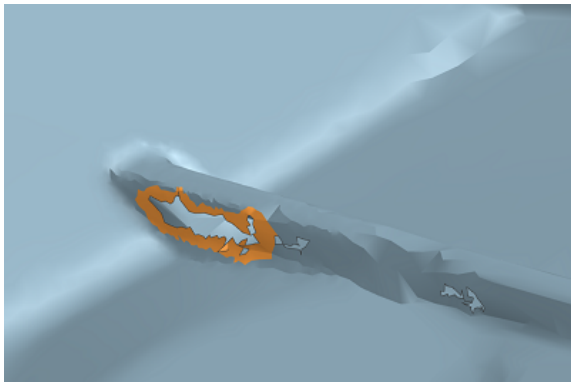

(b) In orange: defective facets to be removed

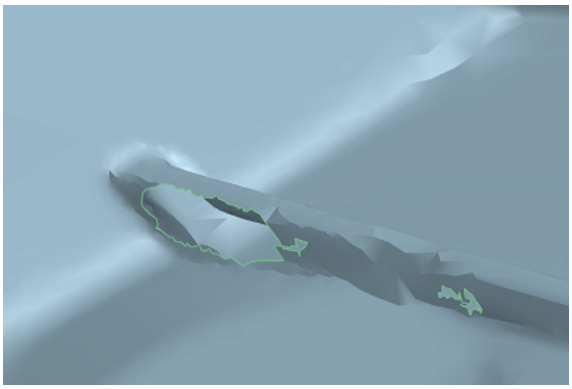

(c) Surrounded in green: Hole after snip operation

Figure 3.4: Model cleaning - Holes : defective surrounding

Large and complex holes

Sometimes holes are located in a corner or on a non-flat surface and the *Fill Hole* function represents reality rather badly, as shown in FIGURE 3.5b.
Luckily, there is a solution to get better results than using directly the *Fill Hole* function. The principle lies in creating a connection between the two sides of the hole at the corner, as represented in yellow in FIGURE 3.5c. This is done using the function *Fill Hole* with option *Bridge Gap*, that connects two of the open sides of a facet body hole with a bridge of triangles. Then, it remains to fill the two remaining holes using the traditional *fill hole* procedure. The result is finally shown in FIGURE 3.5d.

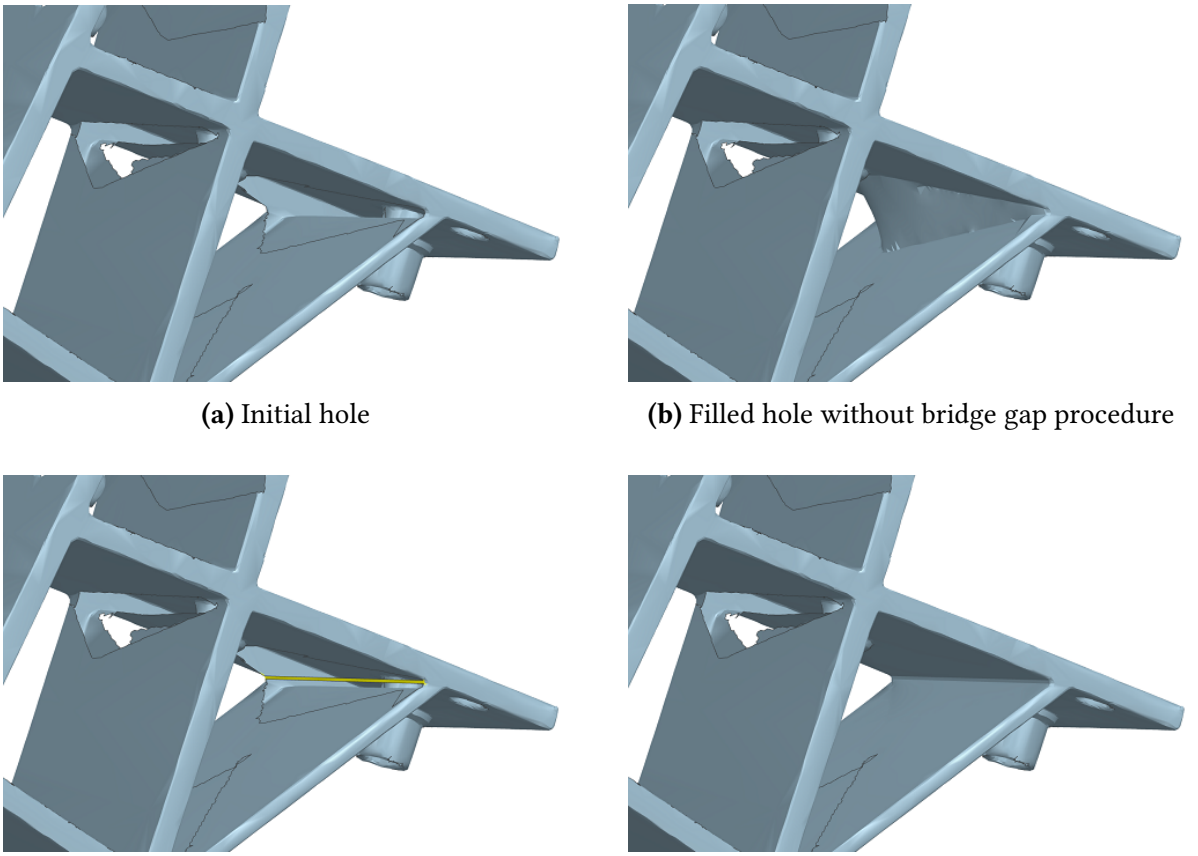

(a) Initial hole

(b) Filled hole without bridge gap procedure

(c) In yellow : bridge gap

(d) Filled hole using bridge gap procedure

Figure 3.5: Model cleaning - Holes : bridge gap procedure

3.2.3 Irrelevant details

Another important aspect in the model cleaning step is the suppression of irrelevant details. Indeed, there is numerous features that are not relevant for the structural analysis in which only the global behavior of the chassis is interesting. In the non-exhaustive list, one can notice screw holes, marks such as stamped brand logo, stud bolds, etc.
These details need to be deleted since it does not noticeably participate to the structural behavior of the chassis while greatly increasing the complexity of the problem, and thus leading to heavy computational cost and rendering results' analysis harder. In addition, Most of these details are extremely defective, as shown in FIGURE 3.6a. It would have been extremely difficult and time-consuming to clean these zones.

The solution is to suppress the facets associated to these irrelevant details using the function *Snip Facet Body* with option *By Region*. It results a simple hole one can fill using the classic *Fill Hole* process.
The FIGURE 3.6 shows the removing of an irrelevant detail.

(a) Initial surface

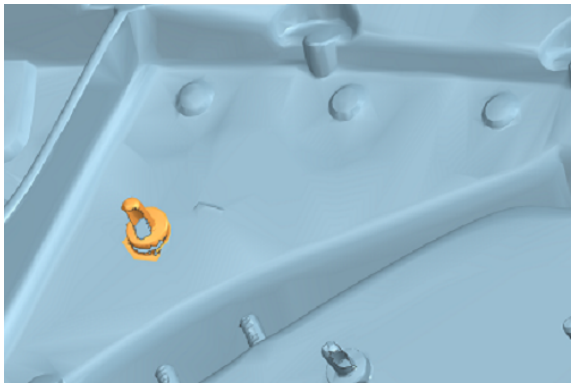

(b) In orange : Irrelevant detail to remove

(c) In green : Hole to fill

Figure 3.6: Model cleaning - Irrelevant details

3.2.4 Identification of main parts

One of the major difficulties about the model creation is to identify the main constitutive parts of the chassis. Indeed, the latter is made of several parts assembled together using different techniques, made from different constitutive materials, with different thicknesses and involving various manufacturing processes. However, an accurate simulation of the structural behavior requires these informations.

Since there is a few technical data available to identify all the individual constitutive parts, this step involves strong assumptions based on knowledge and feeling. Furthermore, it is quite hard or even impossible to identify all these parts.
The subdivision of the model is thus carried out at the extend possible with regard to available data and time limit. As a result, the model is relatively arbitrarily divided into different parts, depending on the identified manufacturing processes (massive parts or sheet metal) or depending on the identified assemblies. The general parts are furthermore subdivided later to differentiate materials and thicknesses.

Although being a strongly approximating process, it consists in the best *-or the least worst-* modelling process considering available data and time limit. The key feature is then to validate this generated model.

To get each part individually, the procedure starts from the full model. The identified sub-part is isolated from the rest of the model using the function *Snip Facet Body* with options *By Boundary* or *By Region*, depending on the easier way to delete facets that do not belong to the sub-part.

3.2.5 Hidden surfaces

Once the sub-part is isolated, it is sometimes necessary to reconstruct some surfaces that were hidden by the rest of the 3D scan because of occlusion or accessibility. Even if some surfaces are quite easy to reconstruct, others are very tricky.

Classic hidden surfaces

The FIGURE 3.7a shows a part where the need for reconstruction is easy and consists in a simple link between the two opposite surfaces.
The objective is to generate a hole that can be filled using the *Fill Hole* function. This is done using smartly the option *Bridge Gap* of the *Fill Hole* function. The different steps are shown in FIGURE 3.7.

As a conclusion, there are several zones where this procedure is sufficient and allows to reconstruct hidden surfaces.

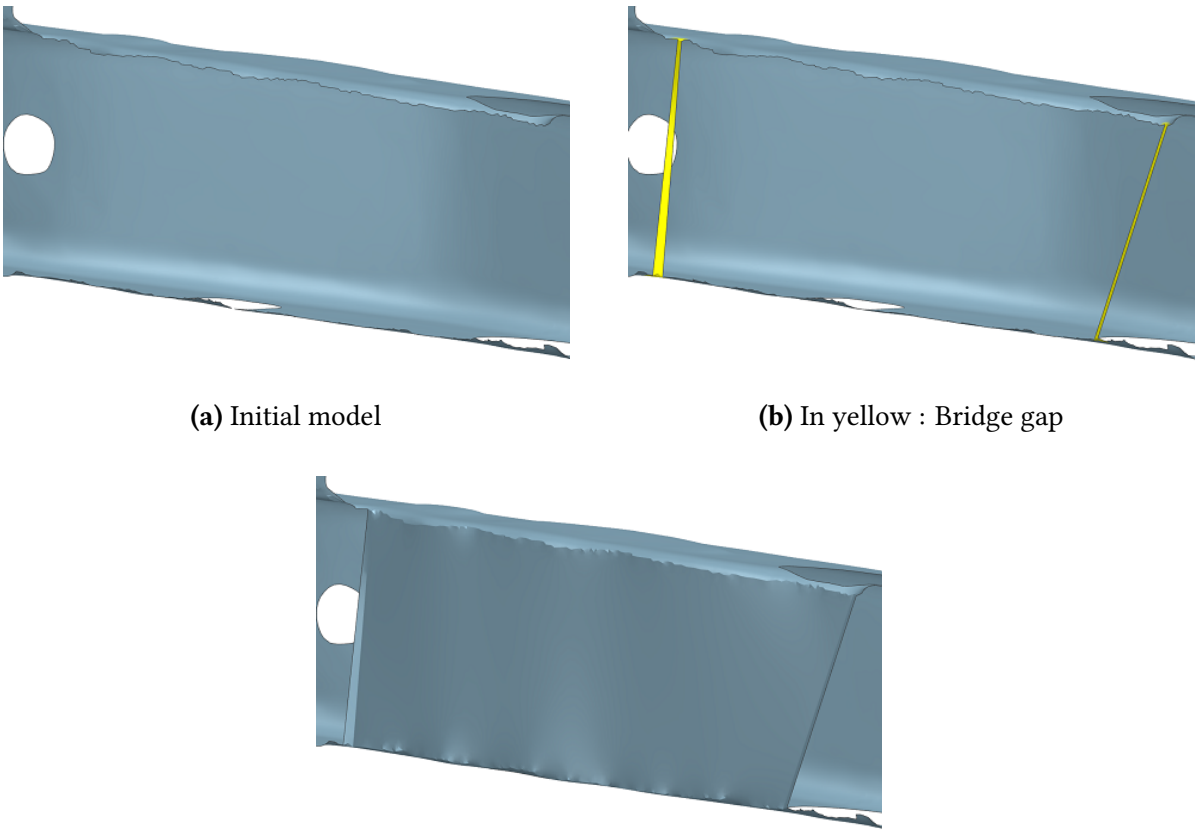

(a) Initial model

(b) In yellow : Bridge gap

(c) Reconstructed surface

Figure 3.7: Model cleaning - Simple hidden surface

Complex hidden surfaces

Sometimes, hidden surfaces are remarkably complicated and need a complex procedure to try to reconstruct suitable surfaces. To describe the process, let's consider two different examples that meet for final steps. The first uses initial surfaces of the convergent body to add for instance thicknesses. The second considers surfaces built using traditional CAD approach.

For seek of simplicity, let's consider the simple example of adding a cylindrical extrusion to the top surface of a cube, as shown in FIGURE 3.9e.

The first step is to construct the top surface of the cylindrical extrusion. There are two different ways to do so: use the initial convergent body, and consider traditional CAD. The use of one method instead of the other depends of the particular application.

Use of initial convergent body The function *Local offset* is used with option *Edit a copy* to generate a new additional body that will be merged with the initial one later. The *Offset distance* is set so that the offset surface is correctly located. Finally, the *Transition* method is set to None. This gives sharp edges, which allow an easier suppression of non-interesting facets.
Then, time is to isolate the surface of interest resulting from the *Local offset* from the rest of the new convergent body. This is done by snipping the sharp edge all around the local offset using the function *Snip* with option *By region*. It remains finally the top surface of the cylinder extrusion.
The FIGURE 3.8 shows the result with the whole offset surface in yellow.

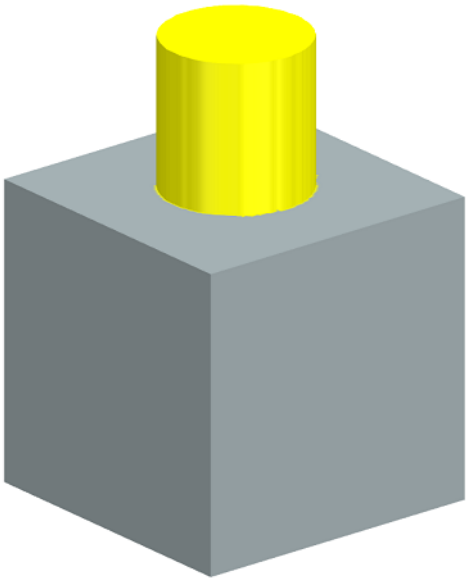

Figure 3.8: Model cleaning - Complex surface: local offset in yellow

Use of traditional CAD approach The top surface of the cylinder extrusion is constructed using traditional CAD method. Then, it is simply converted into a convergent body to be

compatible with the cubic convergent body.

Once the top surface is constructed, a circular hole is created on the top face of the cube in order to connect that hole's border to the circular surface previously created.
However, linking the generated surface to the initial body simply and directly using the *Fill Hole* function with option *Bridge Gap* gives bad result with inverse links, as shown in Figure 3.9b. This happens because the normals of the top surface's facets are misdirected with respect to the one of the cube.

The solution to correctly align the normals is to thicken the surface, and delete the facets that do not belong to the surface. This is done using the function *Thicken*. Note that the thickness does not matter since the facets are directly snipped to recover only the initial surface. This has for effect to correct the orientation of normals.

The last steps are identical to the one described in Section 3.2.5 for classic hidden surfaces.

3.2.6 Smoothing

Even if the parts are free of particular defects, the surface remains quite rough. This effect has already been discussed in Section 2.1.2.
A smoothing step is thus necessary and is performed using the function *Smooth Facet Body*. The *Smoothing factor* was generally set at 20 to give best results but sometimes, a lower or higher factor has been used, depending on results expected and impact on the model. The option *Iterations* is set at 1 to keep a strong control on the process. If necessary, the process is manually repeated.

3.2.7 Mesh imperfections

The faceted mesh results from the initial 3D scan, as well as from various operations and modifications led onto the latter. Resulting facets can suffer from individual defects, including degenerate facets, *i.e. facets with one long edge*, inconsistent normals with respect to the neighboring, self intersections between facets, etc [31]. The function *Cleanup Facet Body* automatically fixes these issues.

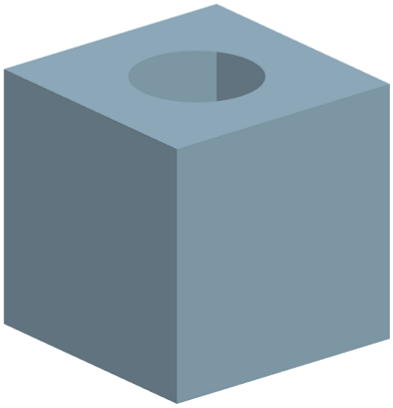

(a) Snip: base cylinder hole creation

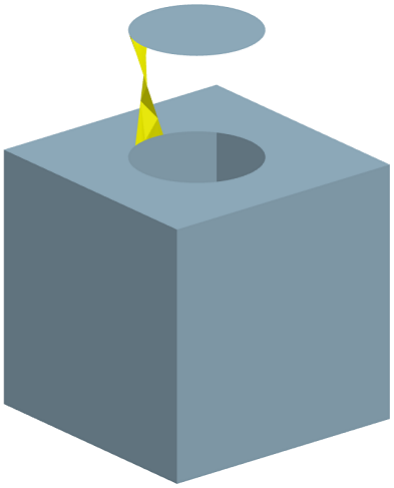

(b) In yellow : bridge gap - misaligned normals

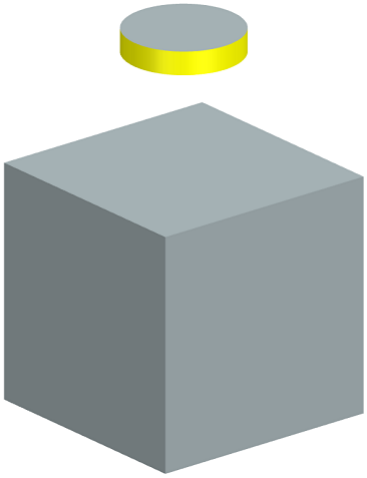

(c) Thicken of surface - in yellow: snipped regions

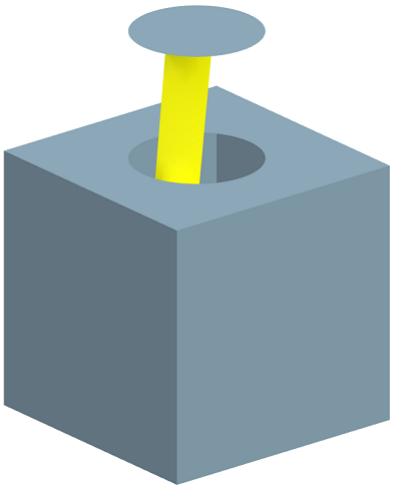

(d) In yellow : bridge gap - aligned normals

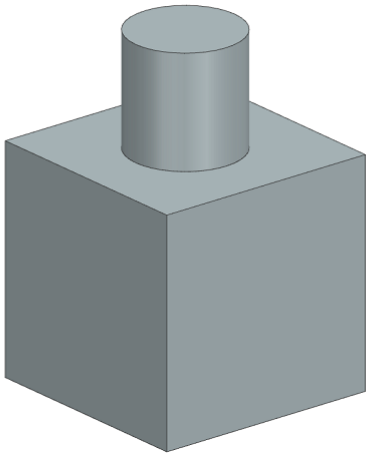

(e) Final result

Figure 3.9: Model cleaning - Complex surface reconstruction

3.2.8 Particular case of simple forms

The previous Sections describe the procedure to follow to extract a CAD model from a 3D scan. However, it is a laborious process and seems to be best suited for complex components.

In case of simple geometries, directly rebuild the geometry using a traditional CAD approach is often easier and faster than using geometric RE procedures.
For instance, the car body has simple extrusion parts, as the one shown in Figure 3.10. For this application, the simplest and most accurate way to recreate the geometry consists in the redesign of the cross-section starting from 3D scan or other data in a classical CAD drawing and extrude it to get the part. The result is shown in Section 3.3.3.

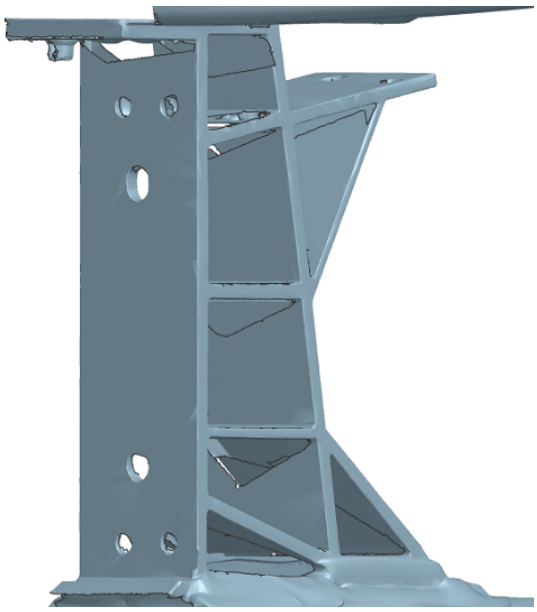

Figure 3.10: Model cleaning - Simple extrusion part

3.3 Model description

Previously, the 3D scan has been used to construct a suitable numerical model made of several parts. In this Section , the model is presented so as to enable a fine understanding of the further analysis. First, each constitutive part is addressed, especially about material constitution and thickness. These two data are provided by the 3D scan supplier, *i.e. A2Mac1*. Then, connections between these constitutive parts are discussed and a brief Section covers the materials definition in the numerical model.

> Note that the notation of parts is completely arbitrary and will be used for the rest of this writing.

The initial model with its eight main constitutive parts is illustrated in Figure 3.11. More views are shown in Appendix A.1.
There are also three additional parts that do not belong to the initial model but will be added to the latter later.

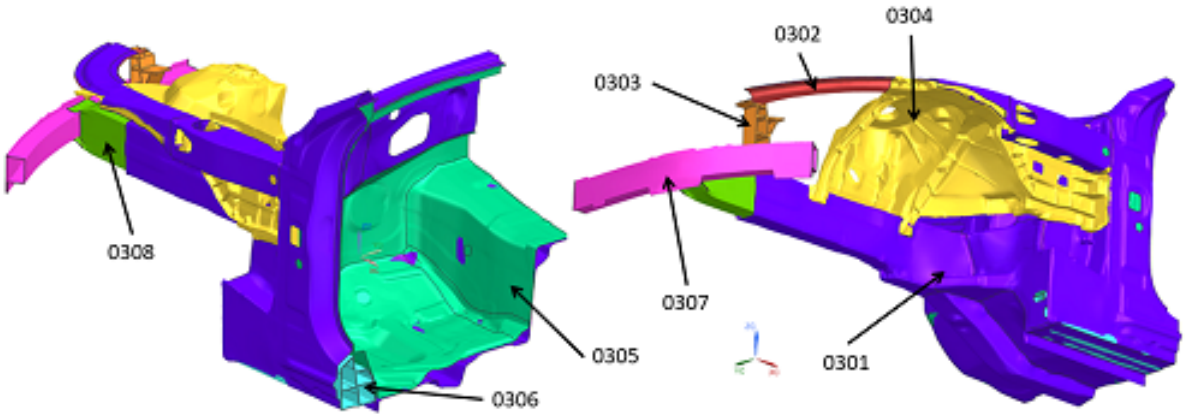

Figure 3.11: Model description

3.3.1 0301 - outer sheet body

This part corresponds to the external sheet metal of the chassis. It is in reality composed of sub-parts welded, bonded or riveted together. However, for seek of simplicity and because there are nearly no technical data describing all these sub-elements, this body is considered as one single general body. It is then subdivided into different sub-bodies in order to differentiate as much as possible materials and thicknesses.
The Figure 3.12 shows the outer sheet body while the Figure 3.13 presents the referencing of the sub-parts made of different materials and/or thicknesses. These informations are resumed in Table 3.1. Note that the value indicated for the material corresponds to the tensile strength.

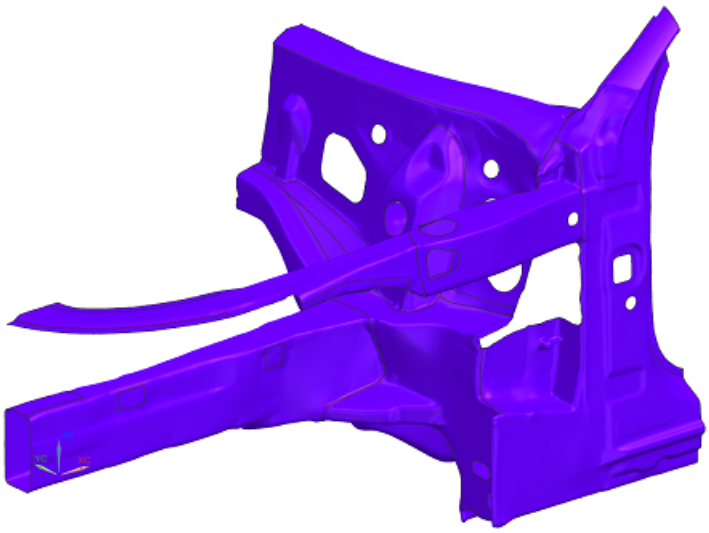

Figure 3.12: Model description - 0301

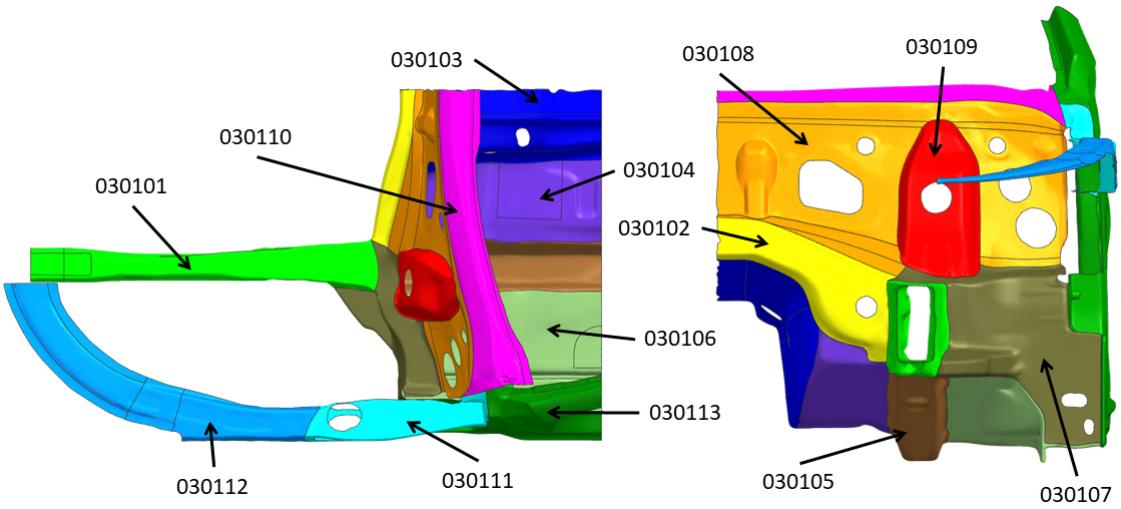

Figure 3.13: Model description - 0301 : sub-parts differentiation

Element code	Material	Thickness [mm]
030101	Aluminium	3.7
030102	Steel (635 MPa)	1.3
030103	Steel (563 MPa)	1.16
030104	Steel (522 MPa)	0.74
030105	Steel (1696 MPa)	1.58
030106	Steel (522 MPa)	0.74
030107	Steel (1751 MPa)	1.76
030108	Steel (519 MPa)	0.95
030109	Steel (1743 MPa)	1.34
030110	Aluminium	1.83
030111	Aluminium	1.77
030112	Aluminium	1.86
030113	Aluminium	1.2

Table 3.1: Model description - constitutive materials and thicknesses of part 0301

3.3.2 0302 - small sheet metal

This part corresponds to a small sheet metal essentially connected to the front of the part 0301. It is made of aluminium and is $1.82\ [mm]$ thick. It is illustrated in FIGURE 3.14.

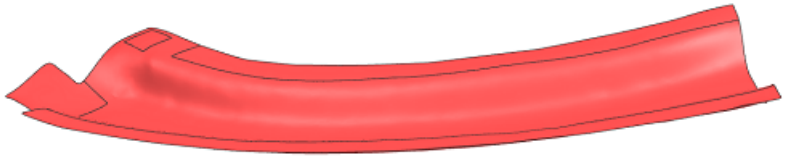

Figure 3.14: Model description - 0302

3.3.3 0303 - Extrusion element

The extrusion element is a massive aluminium-made link between the part 0302 and the mid rail, located in the part 0301. It is shown in Figure 3.15.

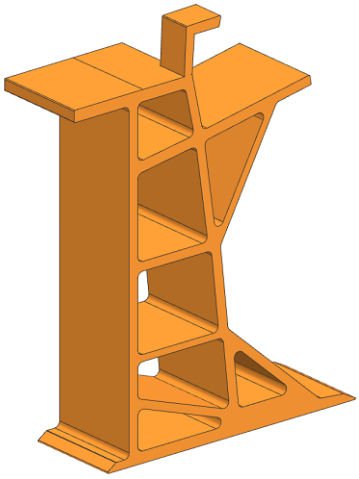

Figure 3.15: Model description - 0303

3.3.4 0304 - Front strut tower

This massive component made of aluminium is located above the wheel and mainly receives suspension efforts coming from the spring-damper element. It is illustrated in Figure 3.16.

Although corresponding in practice to multiple massive elements, this part is considered as one single component.

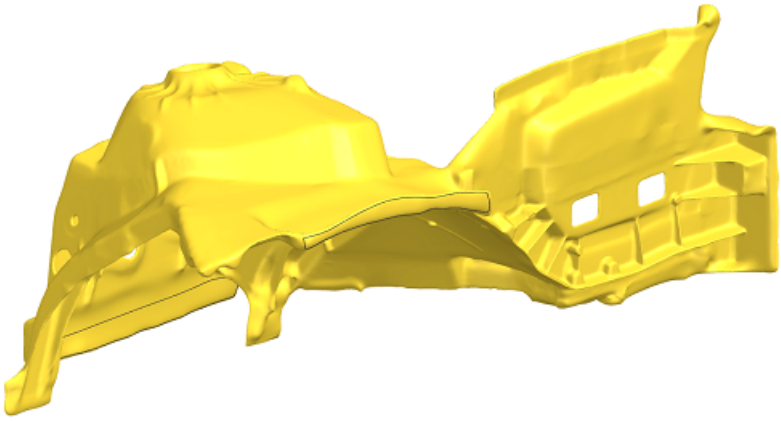

Figure 3.16: Model description - 0304

3.3.5 0305 - Inner sheet metal

This part corresponds to the internal sheet metal of the chassis. As for the part 0301, it is in practice composed of numerous sub-parts welded, bonded or riveted together. This body is

thus also considered as one single general body subdivided into different elements in order to differentiate as much as possible materials and thicknesses.
The FIGURE 3.17 shows the component while the FIGURE 3.18 presents the referencing of the sub-parts made of different materials and/or thicknesses. These informations are resumed in TABLE 3.2.

Figure 3.17: Model description - 0305

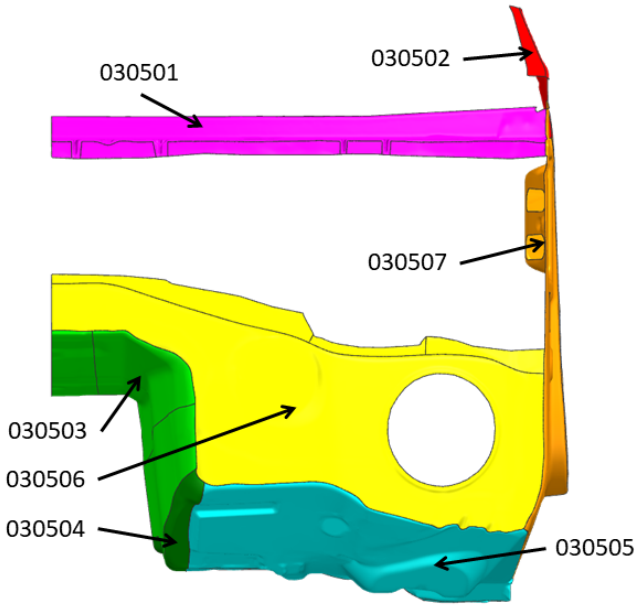

Figure 3.18: Model description - 0305 : sub-parts differentiation

Element code	Material	Thickness [mm]
030501	Aluminium	3
030502	Aluminium	2.38
030503	Steel (1870 MPa)	1.44
030504	Steel (1361 MPa)	1.52
030505	Steel (1787 MPa)	0.92
030506	Steel (519 MPa)	0.95
030507	Steel (539 MPa)	2.08

Table 3.2: Model description - constitutive materials and thicknesses of part 0305

3.3.6 0306 - Side rail

This beam is located between inner and outer sheet metals parts. This massive aluminium part is illustrated in FIGURE 3.19.

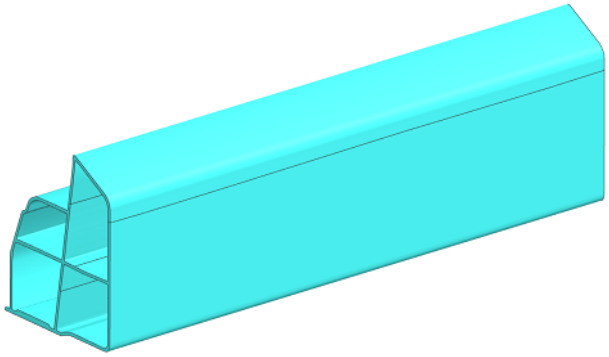

Figure 3.19: Model description - 0306

3.3.7 0307 - Bumper

The bumper, which is a $2.92\ [mm]$ thick aluminium sheet metal, is located all ahead of the model, as illustrated in FIGURE 3.20.

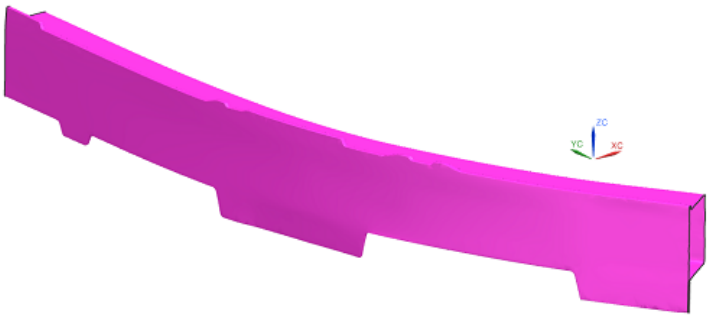

Figure 3.20: Model description - 0307

3.3.8 0308 - Bumper mounting

The bumper mounting serves to fix the bumper to the mid rail. It is made of an aluminium sheet metal and is $2.02\ [mm]$ thick. The FIGURE 3.21 illustrates this part.

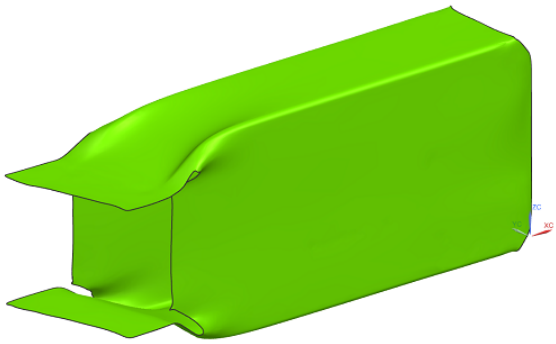

Figure 3.21: Model description - 0308

3.3.9 0309 - Subframe *(Additional part)*

The subframe is a structural component that withstands suspension loads. It is also usual to fix the engine and gear box mountings on the subframe. It is attached to the chassis via the part 0301 and is made of an $4\ [mm]$ aluminium sheet metal.
The FIGURE 3.22 shows the subframe alone while the FIGURE 3.23 shows its integration into the initial model.

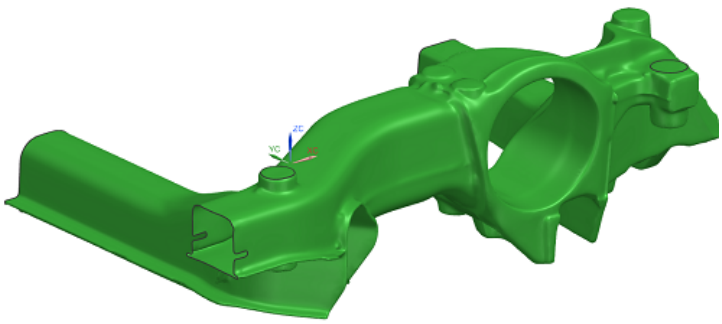

Figure 3.22: Model description - 0309

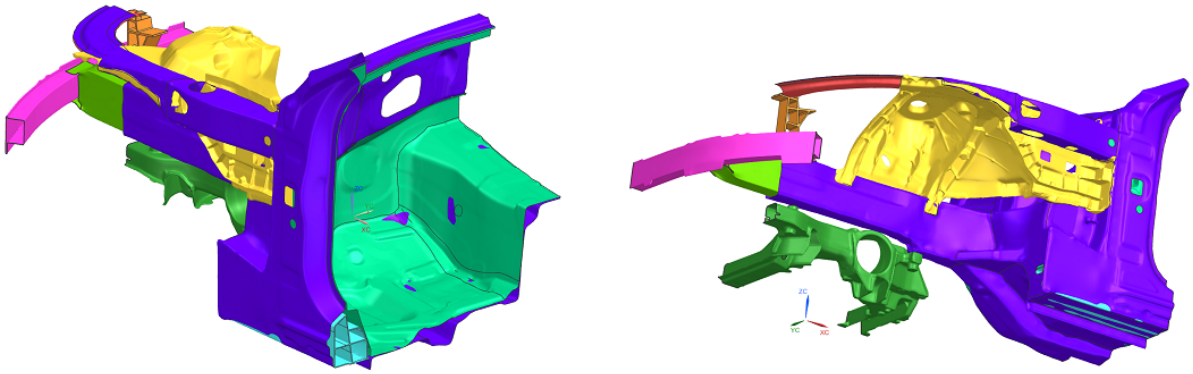

(a) View 1 **(b)** View 2

Figure 3.23: Model description - integration of part 0309 into the model

3.3.10 0310 - *Carat-Duchatelet* reinforcement element *(Additional part)*

This reinforcement part, designed by the enterprise *Carat-Duchatelet* and inspired by the reinforcement part developed by Mercedes itself for their previous armoured models of the S Class chassis, is a massive strapping part made of steel. The thickness is of 3 $[mm]$.

Note that this part is considered to be completely and rigidly bonded to the strut tower. The FIGURE 3.24 shows the part while the FIGURE 3.25 illustrates its incorporation into the full model.

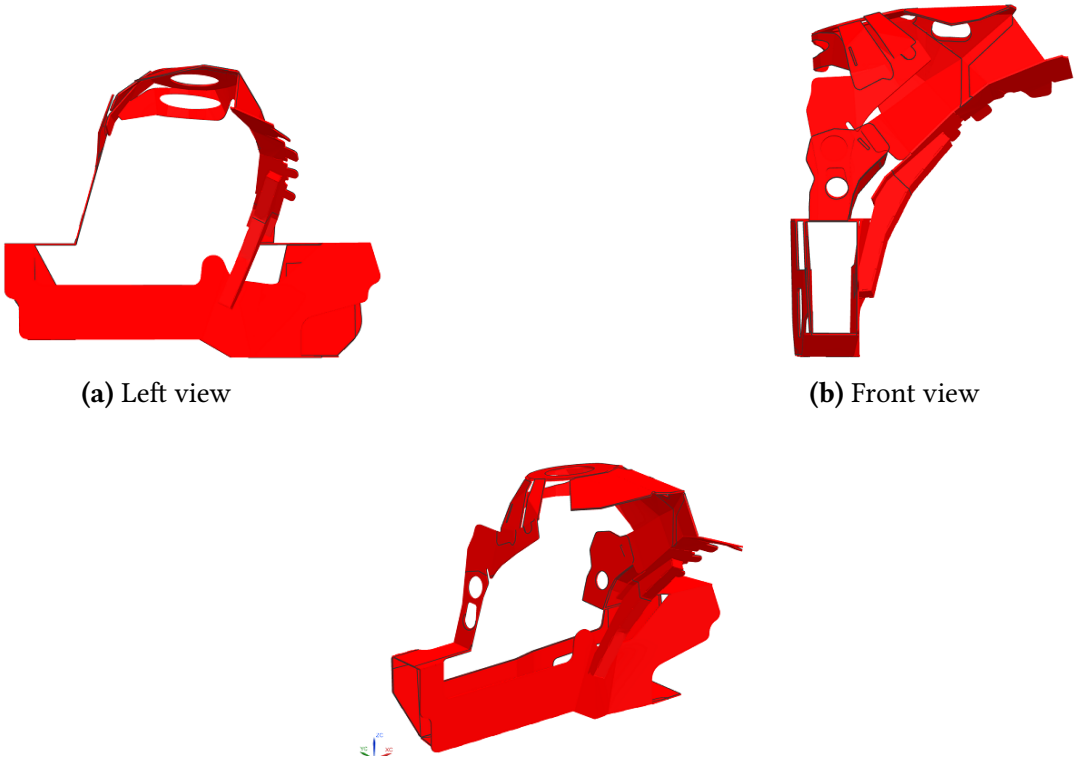

(a) Left view **(b)** Front view

(c) 3D view

Figure 3.24: Model description - 0310

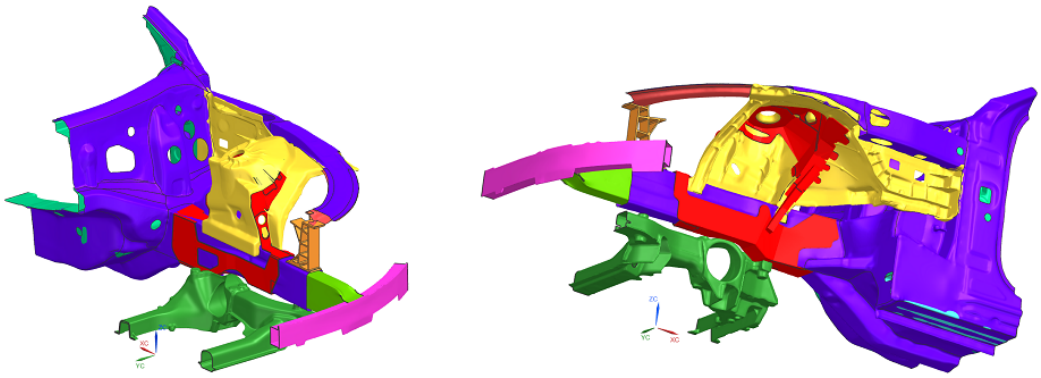

(a) View 1 **(b)** View 2

Figure 3.25: Model description - integration of part 0310 into the model

3.3.11 0311 - Flexural reinforcement element *(Additional part)*

This part is the reinforcement design imagined as a mechanical support for the junction between the motor compartment and the armored survival cell, as introduced in Section 1.2.

As the 0310 component, it is a massive part of 3 $[mm]$ thick steel completely and rigidly bonded to the model that aims at taking up essentially bending efforts.
The Figure 3.27 shows the part while the Figure 3.26 illustrates its incorporation into the full model.

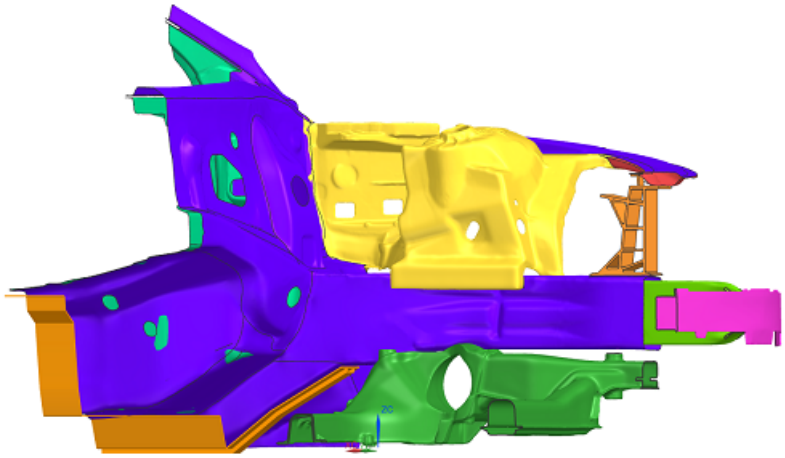

Figure 3.26: Model description - integration of part 0311 into the model

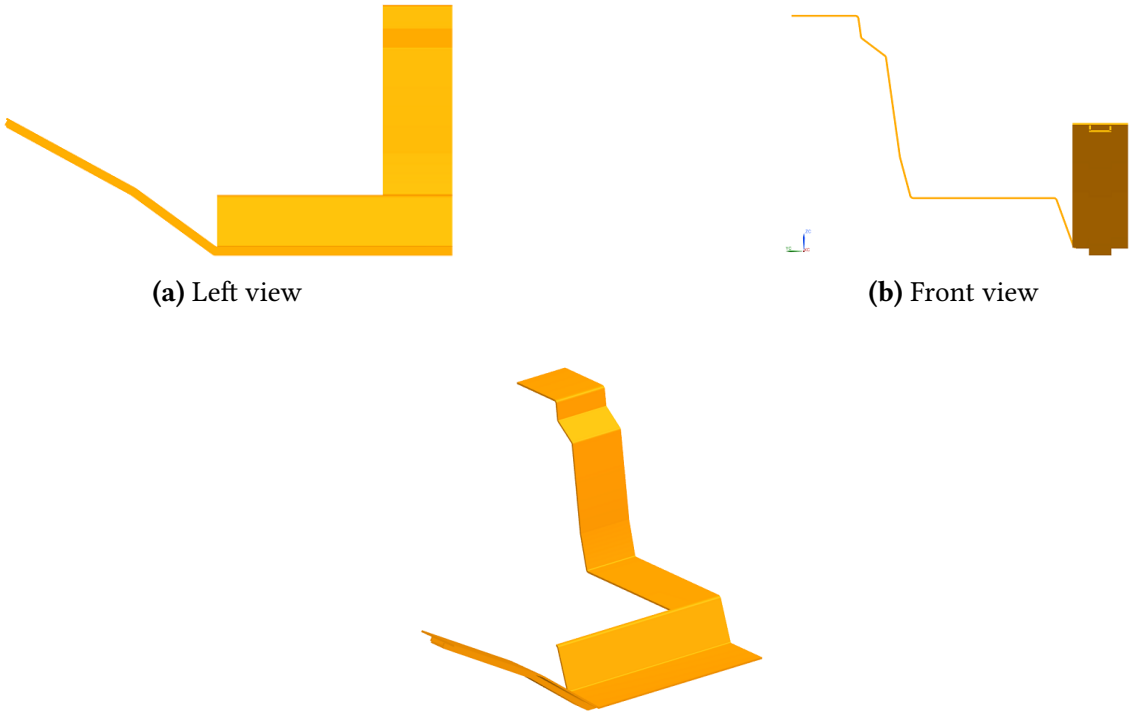

(a) Left view

(b) Front view

(c) 3D view

Figure 3.27: Model description - 0311

On the other hand, the FIGURE 3.28 displays the integration of both 0310 and 0311 reinforcement elements into the complete model.

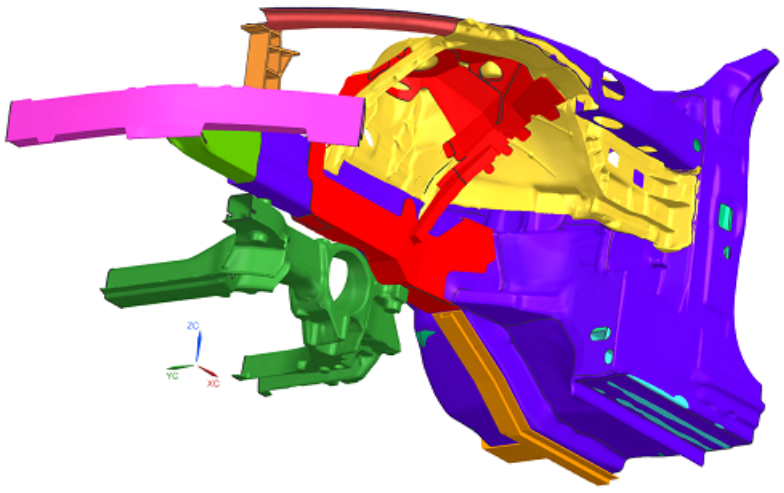

Figure 3.28: Model description - integration of parts 0310 and 0311 into the model

3.3.12 Connections between parts

It has already been developed in Section 2.2.4 that links between components in an automotive body have a significant influence on its structural behavior. This Section discuss the physical connections between the parts and its translation into the numerical model.

Physical connections

The first step is to identify connections' locations. However, there is no available information about connections. Once again, this topic will concern strong assumptions and simplifications.

There are four types of connections considered in the model. The first is the welding of two sheet metal connected at their extremities by a small surface dedicated to welding. This is for example the case to join the parts 0301 and 0305 at the door location, as shown in Figure 3.29a.

The second connection case is the welding of one part's edge to another part's surface. This is the case to join the parts 0301 and 0304, as shown in Figure 3.29b.

Thirdly, a quite widespread connection is the bonding of parts. The surfaces of two components are connected by a gluing operation. This is for example the case to join the parts 0301 and 0303, as shown in Figure 3.29c.

Finally, the last connection concerns the connections of sub-parts composing 0301 and 0305 parts. As a reminder, the latter are considered as unique parts but have been subdivided in order to differentiate materials and thicknesses.

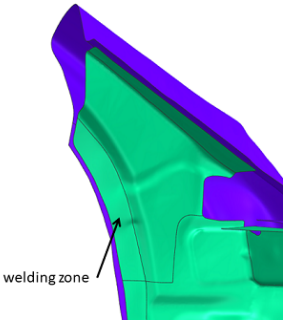

(a) Welding of two faces

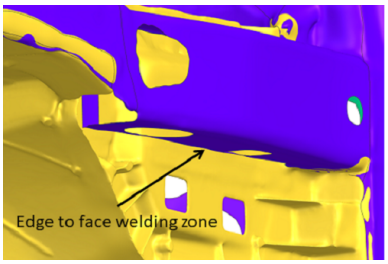

(b) Welding of edge onto a face

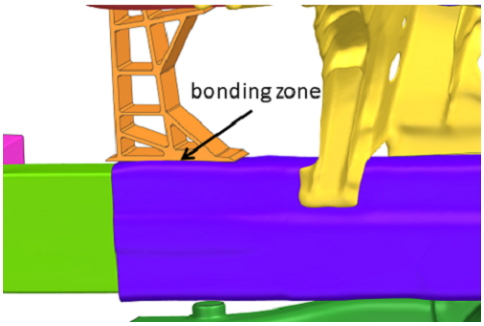

(c) Bonding of faces

Figure 3.29: Model description - Connection types

Numerical translation

Once all connections are physically identified, it is necessary to translate it into the numerical model. This is done during the meshing of the model using the *1D connection* function with different options depending on the nature of the connection.

For both welding and bonding of faces, the *1D connection* function is used with option *face to face* while it is with the option *edge to face* for the welding of edge onto a face. Concerning the linking of sub-parts, the option *Edge to edge* is used.

The model is a strong approximation of the real physical chassis: parts do not perfectly correspond to reality, structural parts are missing, connections are quite artificial and do not correspond to the physical car body, etc.
In reaction, it wouldn't make sense or interest to consider some flexibility in connections, even if it is in reality the case for welds and gluing. Therefore the connections are defined as completely rigid by defining the *Properties* of the *Connecting element* as *Rigid link*.

Partial validation There is one simple way to (partly) validate connections (location and type): analyzing the modes shapes of the model through a modal analysis. Indeed, curious mode shapes allow to easily identify some issues about missing or misplaced connections between parts.

3.3.13 Materials

As implied previously, the model is constituted of three different materials: aluminium, steel with a tensile strength of about $500 - 600$ $[MPa]$, and steel with a high tensile strength of about 1500 $[MPa]$.
However, there is no more information about constitutive materials. Furthermore, the interest of the project being to study the stiffness, the main interest about materials is the Young's modulus, and the latter remains in the same order of magnitude for general material type.

In reaction, this may be satisfactory to simply consider materials available in the database of Siemens NX1980 , being traditionally used in the automotive sector and corresponding as much as possible to identified materials, especially about tensile strength.
To synthesize the materials used in the numerical model are respectively:

Aluminium 6061 With a Young's modulus of 68.98 $[GPa]$, the *Aluminium 6061* is commonly used in aerospace and automotive sectors since it has good mechanical properties and has a good weldability [27]. It is for instance widely used in the *Audi A8* chassis [32];

AISI 304 stainless steel annealed This steel, that has excellent forming properties [6], has a Young's modulus of 190 $[GPa]$ and an ultimate tensile strength of 572 $[MPa]$. It is notably used for aerospace and automotive components such as chassis for buses and trucks, internal and external trim, etc [17];

Maraging steel It is a high strength steel characterized by a Young's modulus of 186 $[GPa]$ and an ultimate tensile strength of 1515 $[MPa]$. It is generally used in aeronautic and automotive applications when operating temperatures are far from the heat treatment of the material [8].

4 | Finite Element Analysis

The previous Chapter has described the procedure to extract an appropriate numerical model from a 3D scan for which a mesh can be generated. However, two different validations must be assessed, as mentioned in Section 2.3: accuracy and consistency.

Accuracy concerns the finite element solution itself. Mesh size must be such that the solution is independent of the later. In other words, further refining of the mesh would not provide much different results.

On the other hand, consistency of computed results with respect to the physical problem must be assessed taking care of the intended purpose of the model, *i.e. a global structure stiffness analysis only*. Even if simulations provide accurate results, results have no interest if they do not correspond to the physical model. Put another way, the mathematical model trying to represent the real physical problem must be validated.

Once accuracy and consistency have been validated, the numerical model can be used for practical applications. This is the subject of the Chapter 5.

This chapter is decomposed into five main parts. First, the mesh accuracy is assessed. Then load cases are presented, in particular BC's and applied loads. The third Section presents the finite element simulations, with static and modal analysis. Finally, the two last parts propose two different model improvements: the addition of the subframe into the model and the consideration of load paths into the suspension mechanism.

4.1 Mesh accuracy assessment

4.1.1 Element type

The CAD model previously generated is a particular and not conventional one. Indeed, it is not made of simple surfaces; it consists in faceted surfaces and bodies. Therefore the mesh generation can not be done using traditional techniques to get 'clean' meshes. Siemens NX1980 is only able to generate automatic triangular-shaped and tetrahedral elements on facet bodies.

Nevertheless, triangular elements are known to be very stiff. They generally give bad results except if there is a very high number of elements. In other words, such elements provide accurate results but involve a higher computational load because of the need for a finer mesh that increases the size of the problem.

2D mesh Finite elements used for representing sheet metals are of type *Mindlin shell T3*. These are based on the Mindlin first order shear deformation plate theory [4].

3D mesh Finite elements representing massive components are conventional 3D tetrahedral elements of type *Solid T4*.

4.1.2 Mesh generation

As already introduced previously, faceted geometry is too complex for traditional meshing algorithms that mathematically flatten surfaces. The function *2D mesh from facets* generates thus a mesh of linear triangles directly from the facet geometry.

For the rest of this work, when the mesh size is mentioned, it corresponds in practice to the *target element size*. All other parameters are set to default values. In particular, the *maximum growth rate*, that specifies the maximum rate at which the element size can change, is set at 1.3 $[-]$, and the *minimum element size* specifying the length of the shortest element edge compared to the target element size is set at 10.10 $[\%]$.

Note that this aspect in further discussed in perspectives, in Chapter 6.

Uniform mesh in the whole model

The choice of considering a uniform mesh size for the whole model is made. The optimal mesh size for which results converge to the solution indicates the minimum element size for critical locations in the model. However, it does not provide any information about the maximum element size for less critical locations.

Considering a uniform mesh whose element size corresponds to the minimum required size at critical locations provides accurate results but involves a larger problem. In other words, the simplicity of constructing a uniform mesh leads to a higher computational time. This can be justified by the following points:

- The model is substantial. Constructing an optimized mesh would take a long time, which is not possible with regard to the time limit;
- The interest of optimizing the mesh appears when there is numerous simulations to lead so that the time necessary to optimize the mesh is smaller than the additional computational time induced by a smaller uniform mesh. Intended simulations here are not enough to justify the mesh optimization.

4.1.3 Mesh convergence analysis

Generating a mesh is not sufficient. It is primordial to assess its accuracy. Indeed, it is requested to dispose of a model for which results converge to a solution and are independent of mesh size [18]. When converged, further refinement of the mesh is unnecessary.

To analyze the impact of mesh size on results, the bending load case with an applied force on the wheel axle of 1000 $[N]$ is analyzed. Note that this load case is described in Section 4.2 and will be further used for each mesh convergence analysis.
The Figure 4.1 shows the evolution of the Total Potential Energy (TPE) in function of the number of dofs[1]. In parallel, this Figure also shows the corresponding computational time in function of the number of dofs. Note that the computer's characteristics are: 11th Gen Intel(R) Core(TM) i7-1165G7 2.80 GHz processor with a RAM of 16 Go.

[1] And equivalently the mesh size

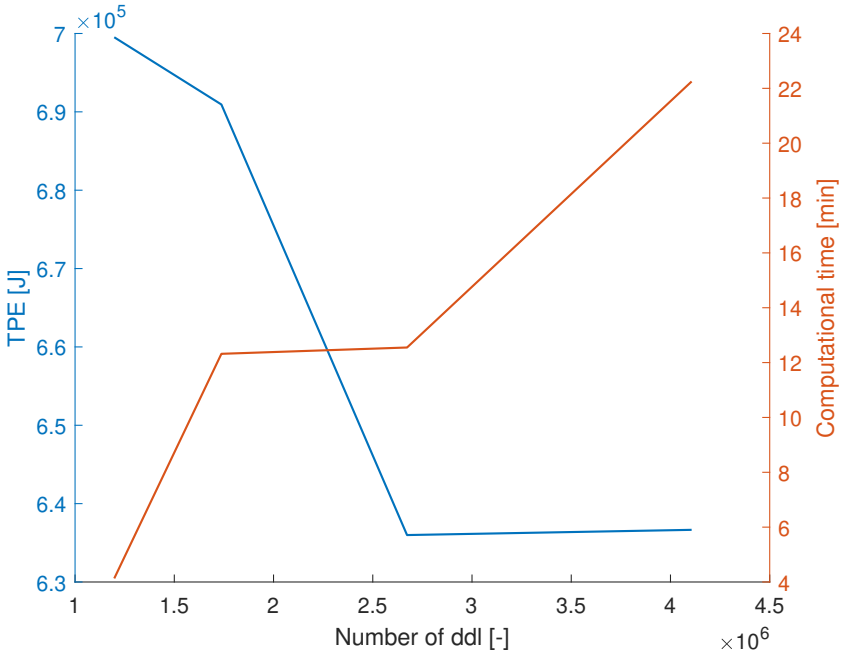

Figure 4.1: Initial model - Mesh convergence: TPE and computational time in function of the number of dofs.

TPE converges starting from an element size of $5\ [mm]$, for which the relative difference with the smallest mesh size computed, *i.e.* $4\ [mm]$, is of $0.10\ [\%]$. Working with a smaller mesh size than $5\ [mm]$ would have no interest in terms of accuracy while requiring a larger computational time.
To sum up, the optimal element size is of $5\ [mm]$. All the results are also summed up in Appendix B.1.

4.2 Load cases

As developed in Section 2.2.3, there are two main load cases for structural analysis of an automotive chassis: the bending and torsion deformation modes. This Section discuss the BC's as well as the external applied load to mimic these two load cases for linear static analysis. On the other hand, the modal analysis is also addressed at the end of this Section .

4.2.1 Realistic load under the wheel

Based on postulates of Section 2.2.3, a realistic load under the wheel taking dynamic effect can be defined as :

$$F = k \cdot W \tag{4.1}$$
$$= k \cdot mg \tag{4.2}$$

where $F\ [N]$ is the external load to apply under the wheel to take into account dynamic effects, $k\ [-]$ is the magnification factor equal to 3.0 for bending simulation and 1.3 for torsion,

W $[N]$ is the weight of the quarter chassis and m $[kg]$ its corresponding mass.

Once the vehicle is armoured, its weight considerably increases. Its structural behavior is altered with higher deformations. The ultimate goal of this project being to stiffen the chassis of the armoured vehicle to get a deformation similar to the initial unarmoured chassis. Thus, it is necessary to simulate both initial and armoured vehicles.

Initial vehicle

The weight of the complete classic vehicle is of 2360 $[kg]$ [20] and one considers four people of 80 $[kg]$ each into the car. Supposing an ideal weight distribution onto the four wheels, it can be concluded a static weight per wheel of:

$$m = \frac{1}{4}\left(2360 + 4 \cdot 80\right) = 670\ [kg] \tag{4.3}$$

Finally, the loads under the wheel for the two load cases are:

$$F_{clas,bend} = 3.0 \cdot 670 \cdot 9.81 \approx 19\,720\ [N] \tag{4.4}$$

$$F_{clas,tors} = 1.3 \cdot 670 \cdot 9.81 \approx 8\,550\ [N] \tag{4.5}$$

Armoured vehicle

The heaviest vehicle produced by *Carat-Duchatelet* is a S Class Maybach Mercedes X222 lengthened by 100 cm with a roof raised by 10 cm, armoured with the highest protection *B7/B6+*. Its weight is of 4890 $[kg]$ with a front/left distribution of $2270/2620$ $[kg]$. Supposing an ideal left/right distribution under the front axle and an ideal weight distribution of the four same people as for the classic vehicle, the static weight per front wheel is:

$$m = \frac{1}{2} \cdot 2270 + \frac{1}{4}\left(4 \cdot 80\right) = 1\,215\ [kg] \tag{4.6}$$

Finally, the loads under the wheel for the two load cases are:

$$F_{arm,bend} = 3.0 \cdot 1215 \cdot 9.81 \approx 35\,750\ [N] \tag{4.7}$$

$$F_{arm,tors} = 1.3 \cdot 1215 \cdot 9.81 \approx 15\,500\ [N] \tag{4.8}$$

4.2.2 Load transfer to the structure

The loads estimated above correspond to the one applied under the wheel. But these are transferred from the wheel axle to the chassis via the suspension mechanism. Actually, the suspension mounted on the Mercedes S Class X223 is a multi-link suspension. Loads are transferred to the chassis and the subframe through several paths.

As a first step, the load is supposed to be transferred directly and only through the spring-damper element from the wheel axle. The surface of application on the model corresponds to the contact surface between the strut tower and the spring-damper element.

The location of the wheel center is determined by physical measurements and it is defined as a single point where the load is applied. The representation of an infinitely rigid

spring-damper element is realized through the use of the function *1D connection* with option *point to face* between the wheel center and the surface contact between the spring-damper and the strut tower. The *Property* of the *Connecting element* is set at *Rigid link*.

Note that the load transfer through the full suspension and its impact on the structural behavior of the chassis is the subject of the Section 4.5.

4.2.3 Boundary conditions

Defining appropriate BC's for load cases is primordial to get relevant results. The model consisting in a quarter front part of a whole car body, it includes two different planes of separation: the *limit plane* separates the front compartment from the rear part of the chassis. It is located just after the dashboard panel and it is parallel to the yz plan. The second one is the *symmetry plane* separating the left side from the right side.

Limit plane BC

For both bending and torsion, the full chassis load cases involve the same condition for the rear axle : a clamping BC. To transpose the BC of the full chassis to the quarter model, the clamping BC is imposed to the limit plane. In other words, all the dofs of nodes located on this plane are fixed.
The Figure 4.2 schematizes the BC for the limit plane, which is identical for both bending and composed torsion simulations.

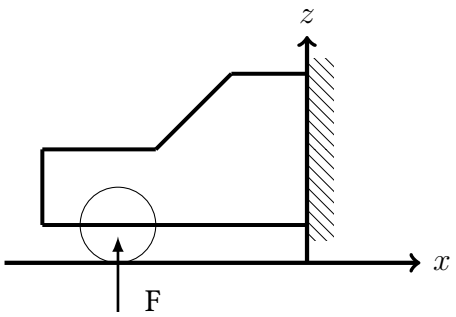

Figure 4.2: Limit plane BC

Symmetry plane BC's

There is also a BC to deal with the symmetry plane xz of the quarter model. The loading on the front axle of the full vehicle being symmetric in bending and anti-symmetric in torsion, the conditions associated to this plane of symmetry differ depending on the load case.

In bending, the BC aims at forcing the symmetry with respect to the xz plane. For that, the movement of the model at that boundary is constrained to stay in the xz plane. Especially, the dof of nodes located on the symmetry plane and related to translation in y direction is fixed while the five other dofs remain free.

Concerning the torsion, a pure torsion simulation would require a complete half model to apply anti-symmetric loads and to not be embarrassed by the symmetry plane. However, the disposable model is only a quarter front model so that a pure torsion mode of the full vehicle cannot be simulated on this latter. Only a composed torsion can be computed.
To model a composed torsion load case, all the translation dofs of nodes located at the symmetry plane must be fixed while the rotation dofs remain free.

To sum up, the FIGURE 4.3 schematizes the BC's involved by bending and composed torsion load cases for the plane of symmetry.

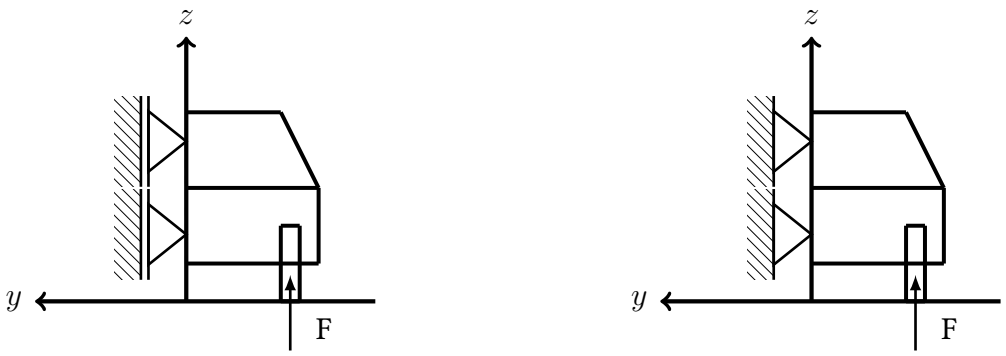

(a) Bending **(b)** Composed torsion

Figure 4.3: Symmetry plane BC's

4.2.4 Modal analysis

As explained in SECTION 2.2.4, the body stiffness is linked to the modal parameters, and especially its bending and torsion eigenfrequencies.
To compute the bending and torsion mode shapes, the same BC's as for the static analysis are applied, no external load is considered, and the first mode shape computed for each case corresponds to the expected mode shape. Explained in another way, the first mode shape computed with bending (resp. composed torsion) BC's corresponds to the bending (resp. composed torsion) mode shape.

4.3 Model analysis

Until now, the accuracy of the numerical model has been assessed. Time is now to validate its consistency with reality. On the one hand, the linear static analysis provides information about deformation mode and magnitude. On the other hand, the modal analysis allows to compare the numerical model with expected physical results about eigenfrequencies.

4.3.1 Static analysis

The FIGURES 4.4 and 4.5 respectively show the bending and composed torsion load cases. Additional views are shown in APPENDIX C.1.

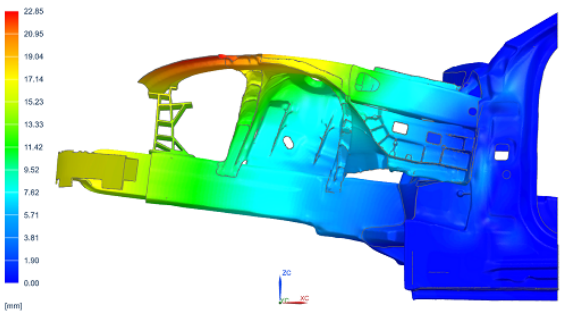

(a) Side view

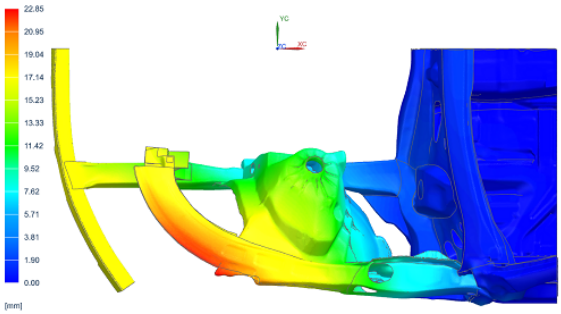

(b) Top view

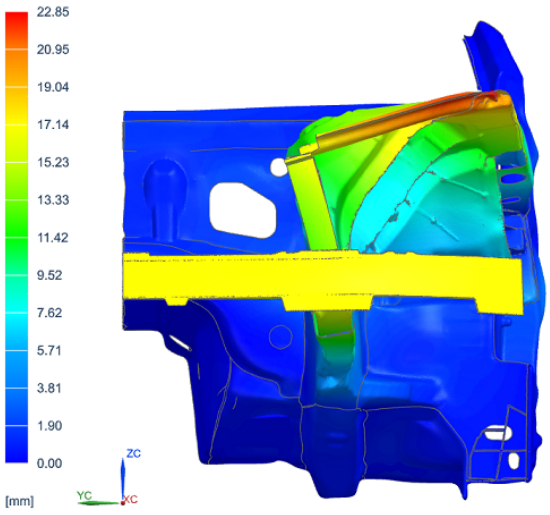

(c) Front view

Figure 4.4: Initial model - Static analysis : bending
Classic loading, 10% model deformation

The model undergoes, in bending, a global bending deformation due to soft behavior at the motor compartment-dash panel's junction. On the other hand, the rest of the structure, *i.e. the front compartment with the front strut tower and the mid rail*, seems to be quite stiff. Indeed, the mid rail has little deformation.

There is also a more local deformation mode for the strut tower that twists and slightly causes the mid rail twisting.
The magnitude of bending deformation provides a maximum deflection of $22.85\ [mm]$ for the classic load case and $41.44\ [mm]$ for the armoured vehicle.

The composed torsion load case highlights the local deformation mode of the strut tower already identified in bending. There is no bending deformation near the dash panel so that only twist of the strut tower is present.
The magnitude of composed torsion deformation provides a maximum deflection of $6.45\ [mm]$ for the classic load case and $11.70\ [mm]$ for the armoured vehicle.

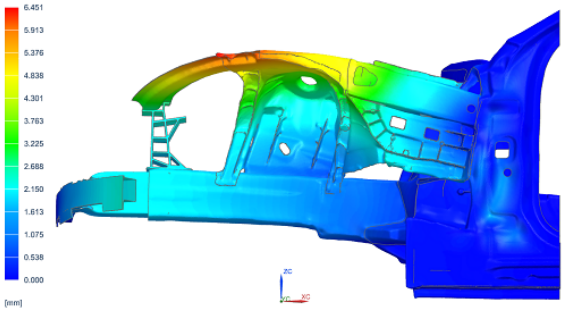

(a) Side view

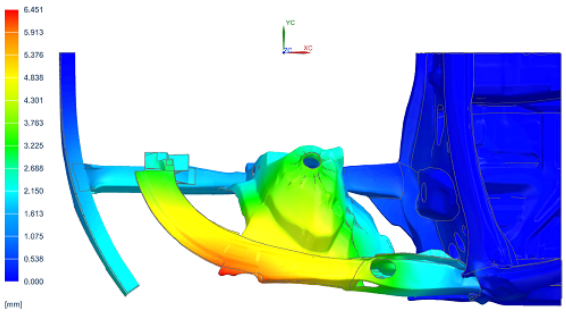

(b) Top view

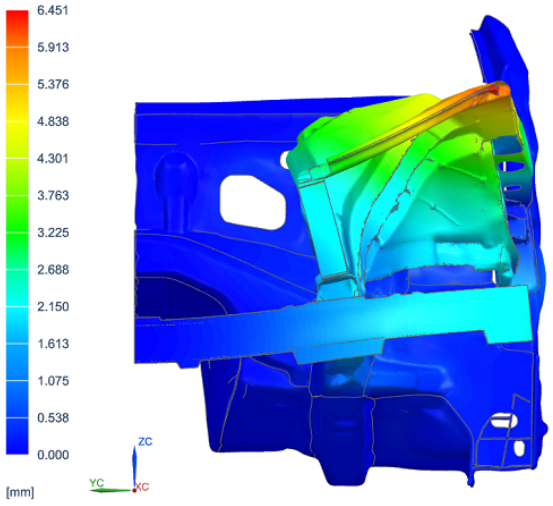

(c) Front view

Figure 4.5: Initial model - Static analysis : composed torsion
Classic loading, 10% model deformation

Critical discussion

First and foremost, the global behavior both for bending and composed torsion simulations is in line with expected results. For instance, the first observation concerning the compliance at the mid rail-dash panel's junction seems to be in line with modern design for crashworthiness. Indeed, current developments try to design plastic hinges in the structure, as shown in FIGURE 4.6.

However, it is good form to notice several details that differ from real physical deformations and result from various inaccuracies of this model. First, the massive part 0304 corresponding to the strut tower is modelled as one single part although being divided into minimum two different elements. Its stiffness is overestimated, the junction between the two real physical parts having a certain compliance. It results from this point that the deformation is displaced from that unrepresented junction to the rear side of the model near the door entry.

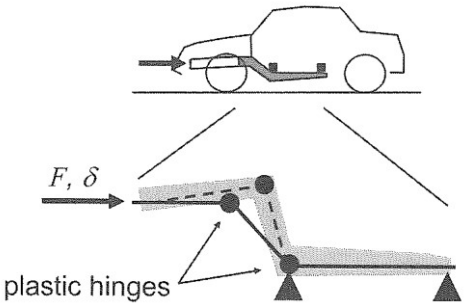

Figure 4.6: Plastic hinges in a car body [21]

Then, the rear side of the model near the door entry is softer than in reality since reinforcement parts between inner and outer surfaces are missing from the 3D scan so that they are also missing from the model.

In addition, the twisting of the part 0303 is overestimated since in the complete vehicle, the upper radiator support is connected between the two symmetrical 0303 parts, acting thus as a reinforcement against this deformation mode.

Another remark covers the junction between the mid rail and the strut tower that is oversized compared to the real chassis. It results that the mid rail's twist is also overestimated.

Concerning the magnitude of deformation, all the load cases provides quite high deformations. Since the global deformation modes seem to be globally in line with reality, this means that the whole model, and not only particular locations, is too compliant regarding to the real physical chassis.
This is not especially an issue for the goal of this work since it aims at stiffening the structure with respect to its deformation modes and not limiting the deflection to a critical specified value.

4.3.2 Modal analysis

The modal analysis computes the two first mode shapes, that correspond to bending and torsion modes. The corresponding eigenfrequencies are:

$$f_{bend} = 42.05\ [Hz] \tag{4.9}$$

$$f_{tors} = 64.24\ [Hz] \tag{4.10}$$

The Section 2.2.4 specifies that the bending eigenfrequency of an economy sedan's car body is in the range of $45 - 55\ [Hz]$. The *Mercedes S class* being a luxury sedan, its bending frequency is certainly slightly above this range. In comparison, computed bending frequency is in the same order of magnitude and lower than expected.
This matches with the static analysis which states that the model is relatively similar to physical ones with the particularity of a higher compliance.

Concerning the torsion eigenfrequency, it overestimates the frequency since the Section 2.2.4 concludes that mid-sized sedans have a torsional rigidity in the range of $40 - 50\ [Hz]$. However, only the order of magnitude can be compared since the computed torsion eigenfrequency does not correspond to a pure torsion mode but to a composed torsion mode. The

composed torsion involving a stiffer system, it is consistent to found a higher torsion frequency than expected.

4.3.3 Conclusion

To conclude, the generated model's accuracy and consistency have been assessed. Although geometry and topology are not completely respected, it has been demonstrated that the model still has an interest for a structure stiffness analysis.

By working in a relative way, the model is able to provide information about stiffness. For instance, it is possible to analyze the impact and the efficiency of a stiffeners added in the initial model. This is the red thread followed in Chapter 5.

Furthermore, it might be possible to work in an absolute way if experimental data are available. Compute a numerical simulation using the same BC's and applied loads as the ones of the experimental testing, or vice-versa, would provide a kind of "conversion factor" between numerical and physical results.

4.4 Model improvement : subframe

Although the actual model is partly consistent with the physics, it might be improved by taking into account more elements composing the full vehicle. Indeed, some additional components that are absent of the BIW are carrying loads and have a structural function. It would be more realistic to take into account more parts that carry structural function.

The most critical additional component having structural function is the subframe. The Figure 3.23 in Section 3.3.9 presents the subframe's integration into the CAD model. Additional views are shown in Appendix A.2.

4.4.1 Mesh convergence analysis

An additional component having been added, it is necessary to determine the optimal element size for the latter. As a matter of fact, the mesh being already converged for the initial model, it provides the minimum size at critical locations of the initial model. It is thus only necessary to determine the minimum size at critical locations of the subframe.
This is done by achieving a mesh convergence analysis where only subframe's element size varies. The Figure 4.7 shows the evolution of TPE and the computational time in function of the number of dofs.

TPE already converges with a rough mesh regarding the corresponding relative error compared to the finest mesh. However, the computational time remains quite constant until a mesh size of $5\ [mm]$ for which the relative difference with the smallest mesh size computed, *i.e.* $3\ [mm]$, is of $0.09\ [\%]$. With a finer mesh, the computational time considerably increases so that a mesh size of $5\ [mm]$ is ideal. The Appendix C.2 resumes all the data about this mesh accuracy analysis.

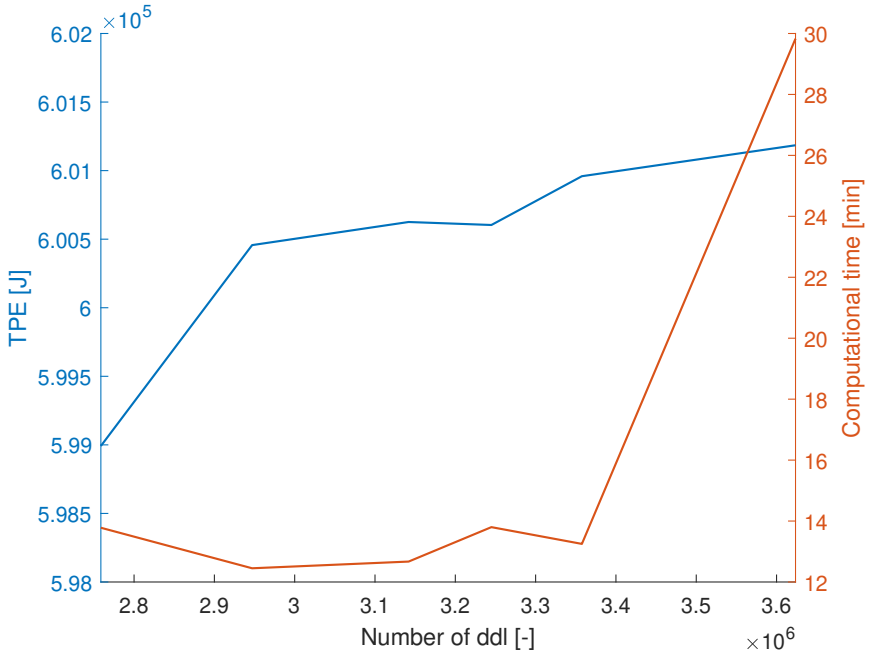

Figure 4.7: Subframe addition - Mesh convergence: TPE and computational time in function of the number of dofs.

4.4.2 Static analysis

The Figures 4.8 and 4.9 respectively show the bending and composed torsion load cases. Additional views are shown in Appendix C.2.

In terms of deformation modes, there is no significant difference with the initial model. There is still the highlighted local twist of the strut tower in the torsion load case that can be identified in the bending load case. The main difference lies in the twist of the mid rail that is decreased because the subframe is connected to this element.

However, a difference with the initial model can mainly be noticed in terms of magnitude. Indeed, the classic loading induces a maximum deflection of 21.36 $[mm]$ in bending and 5.12 $[mm]$ in torsion, while the armoured vehicle undergoes a maximum deflection of respectively 38.73 $[mm]$ and 9.29 $[mm]$ for bending and torsion simulations. This leads to a difference of 6.53 $[\%]$ in bending and 20.57 $[\%]$ in composed torsion.

4.4.3 Conclusion

To conclude about the interest of including the subframe into the initial model, let's discuss about facts and figures. As marked above, the model including the subframe is 6.53 $[\%]$ more rigid in bending and 20.57 $[\%]$ in composed torsion. This also leads to a more relevant model in terms of global behavior of the full vehicle.
Including the subframe has also a cost. Compared to the initial model, the number of dofs and the computational time are respectively 25.62 $[\%]$ and 7.42 $[\%]$ higher.

However, the interest of considering the chassis with its subframe is high enough to

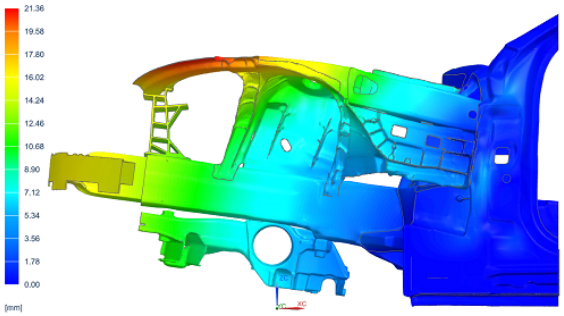

(a) Side view

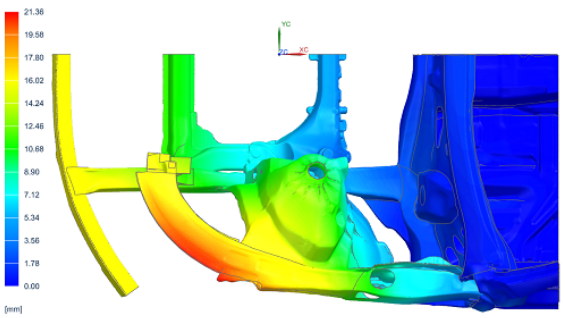

(b) Top view

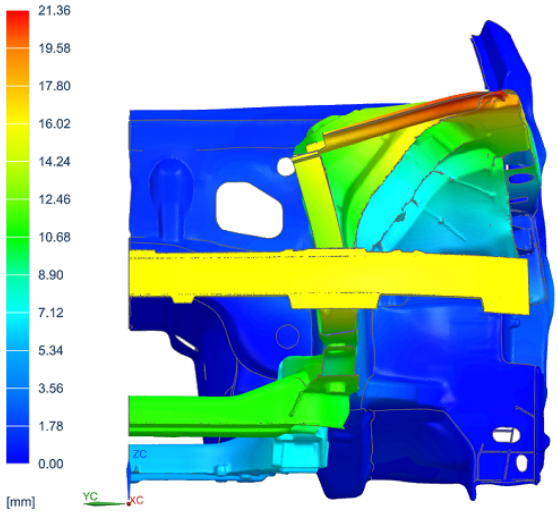

(c) Front view

Figure 4.8: Subframe addition - Static analysis : bending
Classic loading, 10% model deformation

justify the additional numerical cost.
The rest of this writing considers this model improvement.

4.5 Model improvement : suspension load paths

So far, the load cases assume a load transfer from the wheel to the model through the spring-damper element of the suspension only. At first sight, this assumption is valid since the spring-damper is the blocking element of the suspension mechanism in the vertical direction, so that applying a vertical force in the vertical direction gives rise to a transfer to structure mainly through the spring-damper.
However, the suspension mechanism is a more complex system with multiple bars that are able to pick up loads so that the vertical force applied on the wheel results in multiple reaction forces at the suspension supports.

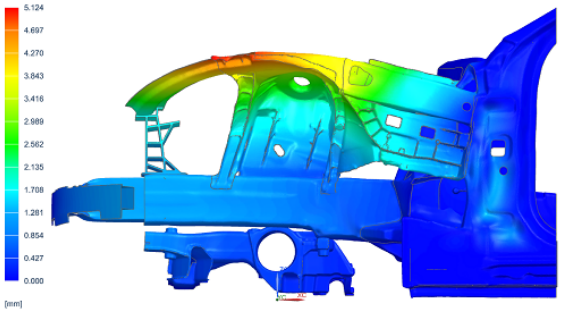

(a) Side view

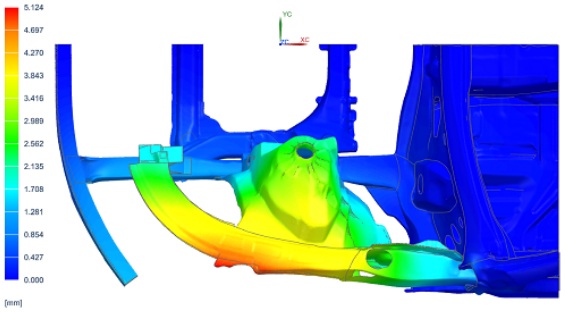

(b) Top view

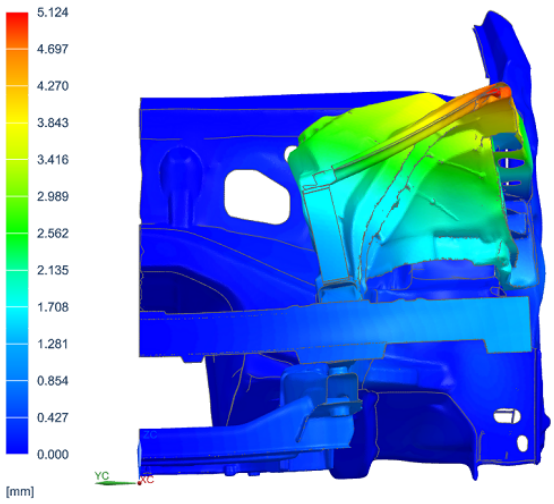

(c) Front view

Figure 4.9: Subframe addition - Static analysis : composed torsion
Classic loading, 10% model deformation

A further improvement of the present model would consist in considering the reaction forces at each suspension support instead of only at the spring-damper support on the chassis. This is the discussion of this Section .

4.5.1 Suspension modelling

To determine the reaction forces at the suspension supports, the suspension is modelled, with help of its 3D scan, with simple beam elements since the only interest is the reaction forces at the supports. The Figure 4.10 shows the 3D scan of the suspension in its close environment and the corresponding numerical model.

The Table 4.1 synthesizes the reaction forces at the suspension supports as a ratio of the reaction force component to the vertical load applied at the wheel center. The Appendix D

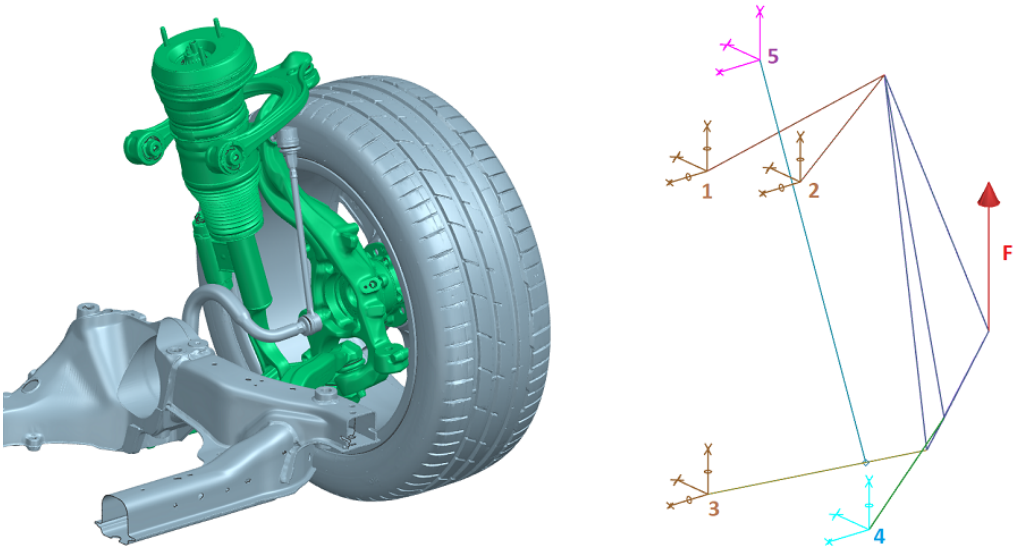

(a) 3D scan - In green: suspension mechanism **(b)** Numerical model

Figure 4.10: Suspension modelling

resumes force components on suspension supports for simulated externally applied forces.

Support	X [N]	Y [N]	Z [N]
1	-0.0305	-0.1595	0.0526
2	-0.0005	0.0009	-0.0001
3	0.0000	0.0000	0.0000
4	0.2092	-0.2919	0.0114
5	-0.1076	-0.3691	-1.5161

Table 4.1: Suspension modelling - Ratio of reaction forces components to the vertical load applied at the wheel center

As expected, the spring-damper element corresponds to the element sustaining the greatest load even if other supports are nonetheless carrying significant efforts. In addition, even if this modelling is not the most accurate one, it provides a first feeling about the impact of the suspension mechanism on the structural behavior of the car body.

4.5.2 Static analysis

The Figures 4.11 and 4.12 respectively show the bending and composed torsion load cases. Additional views are shown in Appendix C.3.

Compared to the results presented in Section 4.4.2, the deformation modes are quite similar. There is however a difference: the impact of the front attachment of suspension on the subframe. Indeed, this support induces a higher deformation of the subframe's front part. It results that the front of the subframe and the mid rail undergo a higher deformation.
In addition, the twist of the strut tower is also exacerbated.

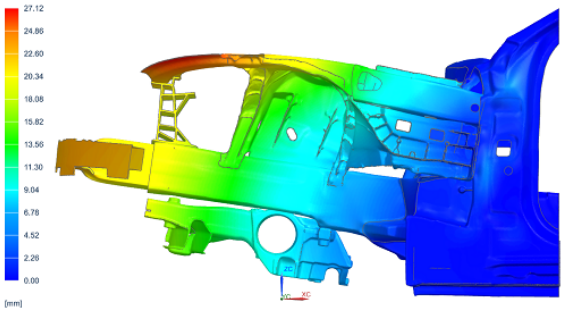

(a) Side view

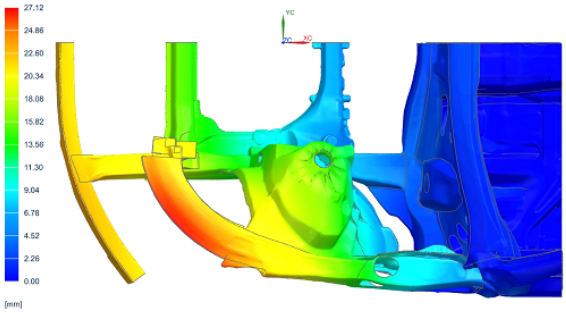

(b) Top view

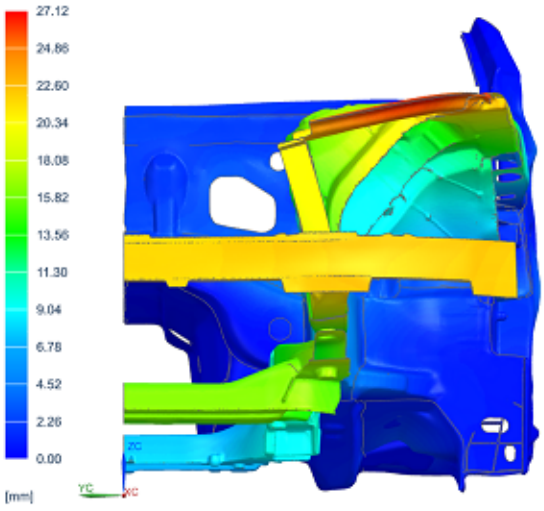

(c) Front view

Figure 4.11: Suspension load paths - Static analysis : bending
Classic loading, 10% model deformation

What concerns the magnitude, the classic loading induces a maximum deflection of $27,12\ [mm]$ in bending and $5.49\ [mm]$ in torsion, while the armoured vehicle undergoes a maximum deflection of respectively $49,18\ [mm]$ and $9.95\ [mm]$ for bending and torsion simulations. This makes a different of $+\ 26.97\ [\%]$ in bending and $+\ 7.09\ [\%]$ in torsion.

4.5.3 Conclusion

To sum up, the consideration of the real load transfer through the suspension mechanism induces a significant modification of the chassis' structural behavior. Taking this effect into account leads to a more precise and realistic model.
The rest of this project considers this model improvement.

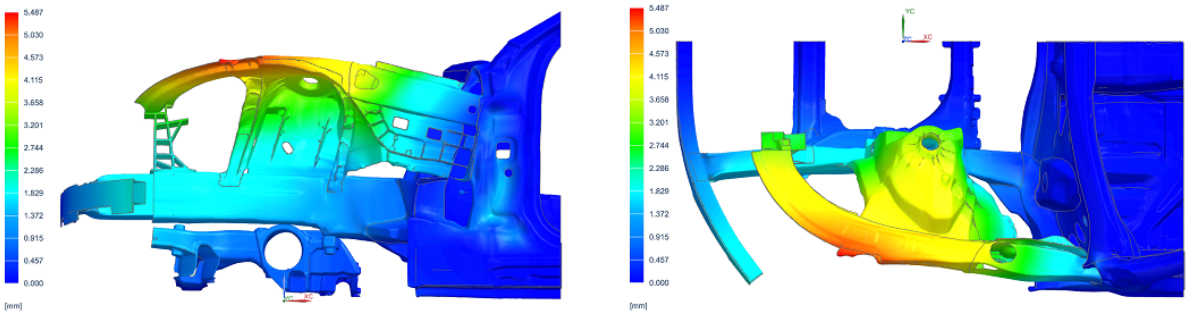

(a) Side view

(b) Top view

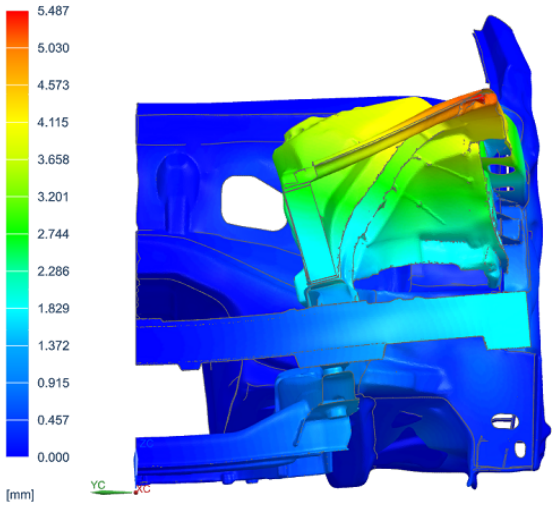

(c) Front view

Figure 4.12: Suspension load paths - Static analysis : composed torsion
Classic loading, 10% model deformation

5 | Applications

Although the numerical model of the chassis is not perfect and lies on strong assumptions and simplifications, the previous Chapter concludes that it remains suitable for certain applications involving the global behavior of the structure.
As developed in Section 1.2, the ultimate objective of this project is to suggest reinforcement components to stiffen the whole structure. this would thus limit additional deformation and withstand the excess weight caused by the armouring.

This Chapter concerns practical application of the previously modelled chassis. It is organized as follows : a first Section discuss the potential zones that could be subject to stiffening. Then, two different reinforcement components are exposed and their impact on the structure stiffness is discussed and is criticized.

5.1 Potential stiffening zones

With regard to the deformation modes exposed in Figures 4.11 and 4.12, there are two main "local" modes that can/should be minimized: the strut tower twist and the bending of the mid rail-dash panel's junction.

5.1.1 Strut tower twist

This deformation mode is the prevailing one. A too high twist of the strut tower could lead to dramatic difficulties such as motor damages, road handling issues, etc.
This deformation is already a well-known issue that becomes critical for sports cars. The typical and widely adopted solution to counter this effect is the Strut Tower Brace (STB) [11]. It consists in a bar or a system of bars tying the two strut towers together, as shown in Figure 5.1.

Figure 5.1: Mercedes S-Class (W221) STB [35]

A second possibility to stiffen the strut tower is to design a strapping that would act as a second skin around the original strut tower. This is the solution that has been used by *Carat-Duchatelet* so far. It will be further studied in Section 5.2.

5.1.2 Bending of mid rail-dash panel's junction

This deformation mode seems less important but becomes crucial with the additional weight induced by the armouring.
A possible approach is to add a flexural beam at this location in order to sustain the beginning of the mid rail and thus carry bending loads. This prospect is further developed in Section 5.3.

5.2 *Carat-Duchatelet* reinforcement

As introduced in Section 3.3.10, this reinforcement part, designed by the enterprise *Carat-Duchatelet*, is inspired by the reinforcement part designed by Mercedes for its previous armoured models of the S Class chassis. It is a massive strapping part made of steel that acts as a second structural skin for the strut tower.
The Figure 3.24 shows the part while the Figure 3.25 illustrates its incorporation into the model.

5.2.1 Mesh convergence analysis

As for the model improvement considering the subframe's addition, detailed in Section 4.4.1, the minimal element size for the reinforcing piece must be determined. The Figure 5.2 shows the evolution of TPE and the computational time in function of the number of dofs.

For a mesh size of $4\ [mm]$, TPE has converged to the solution and the relative error in terms of TPE with respect to the smallest mesh size computed, *i.e.* $3\ [mm]$, is of $0.67\ [\%]$. All the results are also summed up in Appendix B.3.

5.2.2 Linear static analysis

The Figures 5.3 and 5.4 respectively show the bending and composed torsion load cases. Additional views are shown in Appendix C.4.

As a reminder, the behavior of the model without the strut tower's strapping is shown in Figures 4.11 and 4.12. It can be seen that the mid rail-dash panel's junction behavior has a little modification in deformation mode while the strut tower is subject to a weaker twist.

In terms of numerical outcomes, the classic loading induces a maximum deflection of $22.07\ [mm]$ in bending and $4.12\ [mm]$ in torsion, while the armoured vehicle undergoes a maximum deflection of respectively $40.02\ [mm]$ and $7.48\ [mm]$ for bending and torsion simulations.

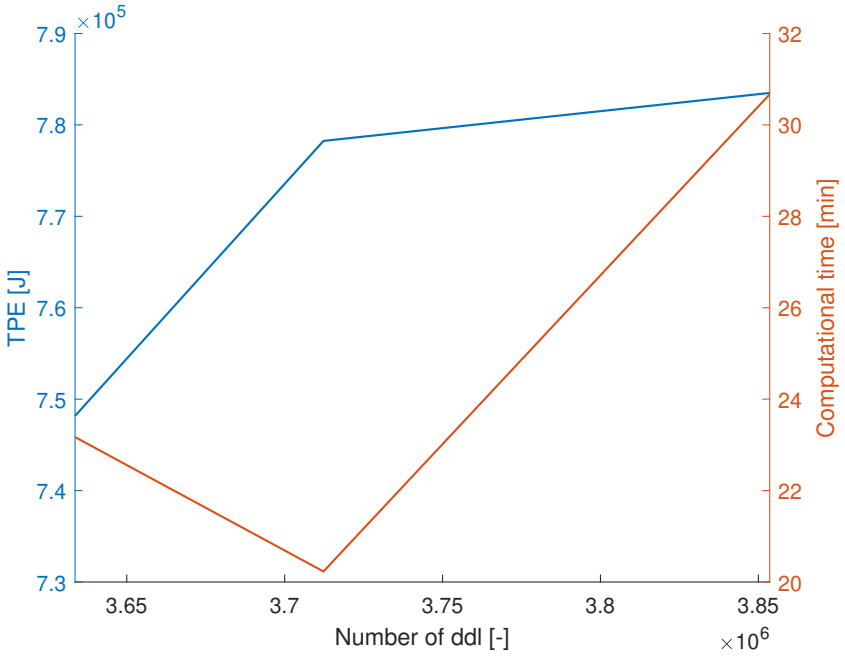

Figure 5.2: *Carat-Duchatelet* reinforcement - Mesh convergence: TPE and computational time in function of the number of dofs.

5.2.3 Conclusion

First of all, the piece has the intended effect: reduce the strut tower deformation. In practical terms, the *Carat-Duchatelet* reinforcement stiffens the front compartment considering the maximum deflection by an amount of 18.62 [%] in bending and 24.86 [%] in composed torsion.

The maximum deflection being strongly influenced by the strut tower twist when subject to bending load case, it is coherent to see an effect of the reinforcement component in bending even if it is designed for the strut tower twist.

In addition, it might be interesting to compare the maximum deflection of the armoured and reinforced motor compartment with respect to the classic un-armoured and un-reinforced one. This comparison allows to practically compare the two "real" cases encountered:

- The classic vehicle, that is characterized by its normal weight and does not need any stiffeners;
- The armoured vehicle, that is characterized by an extra weight and includes thus stiffeners.

In terms of maximum deflection, the armoured reinforced vehicle has an extra deformation of 47.57 [%] in bending and 36.27 [%] in composed torsion.

5.3 Flexural reinforcement

This reinforcement part, shown in FIGURES 3.27 and 3.26, can be seen as having two different objectives:

- Stiffen the mid rail-dash panel's junction in bending;

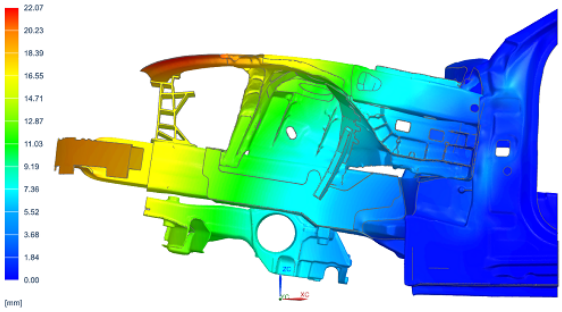

(a) Side view

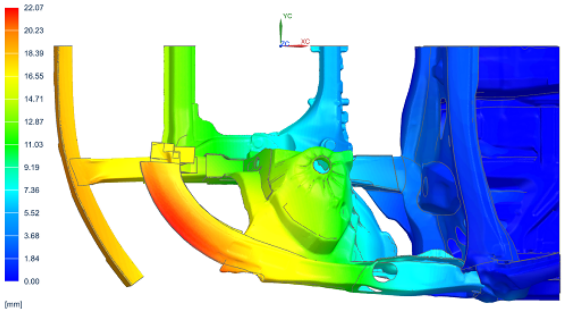

(b) Top view

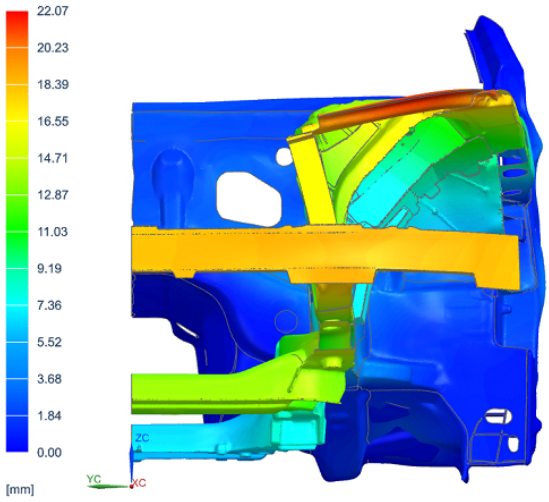

(c) Front view

Figure 5.3: *Carat-Duchatelet* reinforcement - Static analysis : bending
Classic loading, 10% model deformation

- Mechanical support for junction between front compartment and armoured survival cell. For this eventuality, the front compartment including the dash panel would be bonded to the survival cell's dash panel. The reinforcement component would secure this junction by supporting the first part of the motor compartment. This objective has been stated in Section 1.2.

5.3.1 Mesh convergence analysis

Once again, the minimal element size for the reinforcement must be determined. The Figure 5.5 shows the evolution of TPE and the computational time in function of the number of dofs.

For a mesh size of $20\ [mm]$, TPE has converged to the solution and the relative error in terms of TPE with respect to the smaller mesh size computed, *i.e.* $7\ [mm]$, is of $0.09\ [\%]$. All the results are summed up in Appendix B.4.

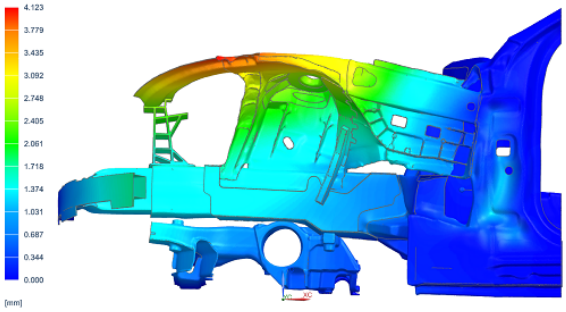

(a) Side view

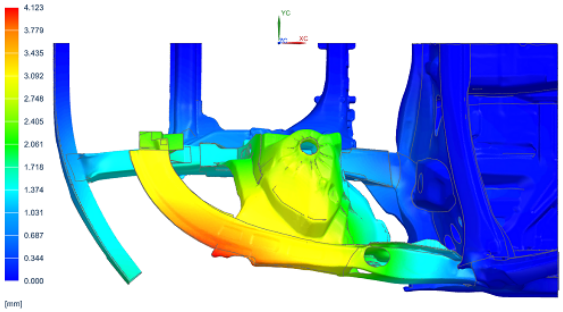

(b) Top view

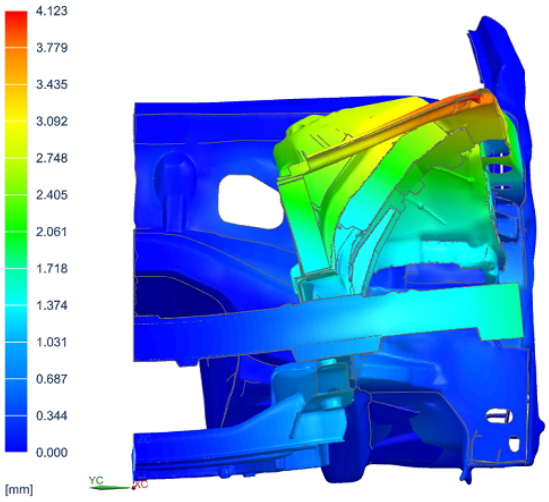

(c) Front view

Figure 5.4: *Carat-Duchatelet* reinforcement - Static analysis : composed torsion
Classic loading, 10% model deformation

5.3.2 Linear static analysis

The Figures 5.6 and 5.7 respectively show the bending and composed torsion load cases. Additional views are shown in Appendix C.5.

Compared to the behavior of the classic car body, the bending at the mid rail-dash panel's junction is decreased. However, the additional part has obviously no impact of the strut tower's twist.

In terms of numerical outcomes, the classic loading induces a maximum deflection of $22.26\ [mm]$ in bending and $5.39\ [mm]$ in torsion, while the armoured vehicle undergoes a maximum deflection of respectively $44.00\ [mm]$ and $9.78\ [mm]$ for bending and torsion simulations.

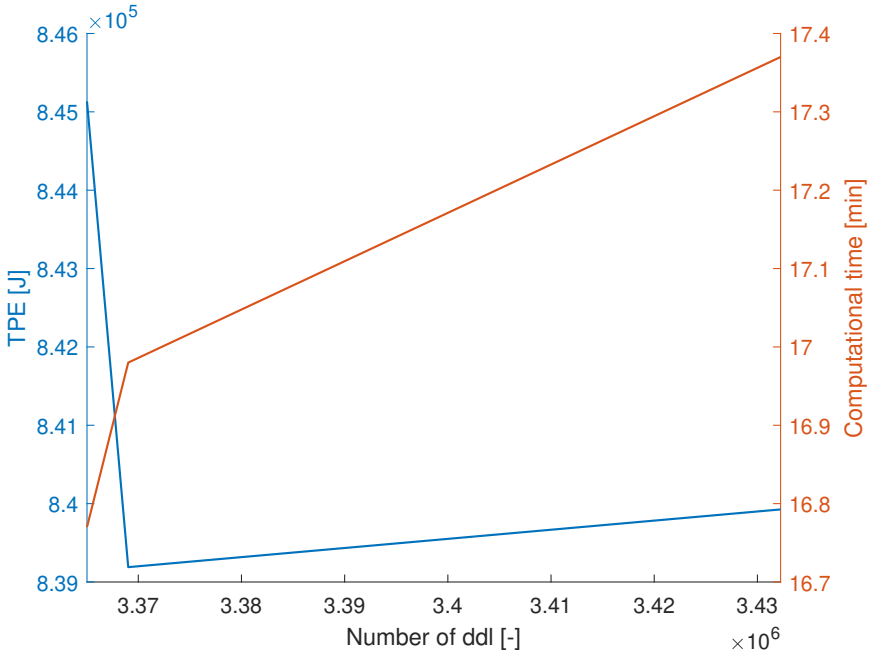

Figure 5.5: Flexural reinforcement - Mesh convergence: TPE and computational time in function of the number of dofs.

5.3.3 Conclusion

This flexural reinforcement piece allows to reduce the bending of the mid rail. This leads to an increase in stiffness in terms of maximum deflection of 10.54 [%] for the bending load case and 1.75 [%] for the composed torsion load case. These two values highlight the impact of the part: the bending is improved while it has nearly no impact on torsion.
Comparing again the initial vehicle with the armoured reinforced one, it gives that the maximum deflection of the armoured chassis is respectively 62.24 [%] and 78.18 [%] higher in bending and composed torsion.

This calls attention to the higher efficiency of the *Carat-Duchatelet* reinforcement component whatever the considered load case. On the other hand, this flexural reinforcement has a second objective: the mechanical support of the front compartment with respect to the central compartment. For this particular consideration, it seems very effective since it acts as a support for the mid rail-dash panel's junction.

5.4 Combination of *Carat-Duchatelet* and flexural reinforcements

There is an interest in studying the simultaneous combination of the two previously discussed reinforcements.

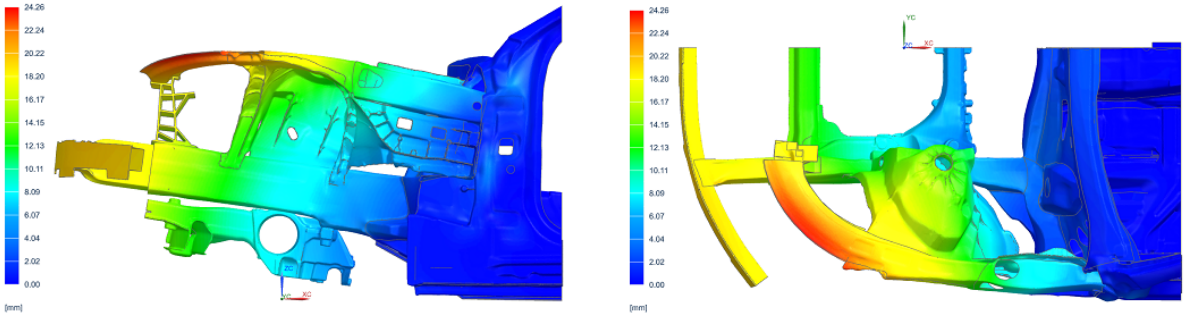

(a) Side view

(b) Top view

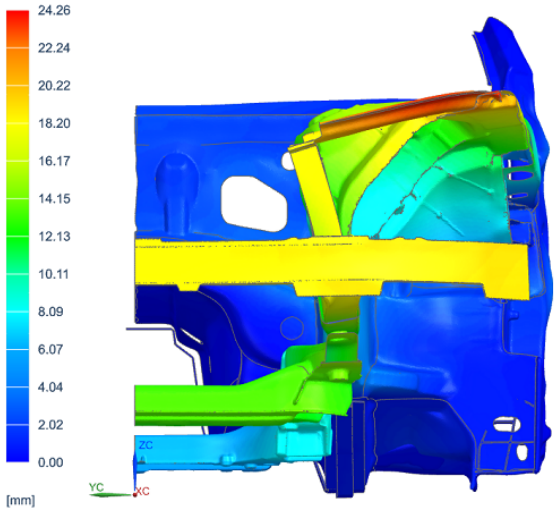

(c) Front view

Figure 5.6: Flexural reinforcement - Static analysis : bending
Classic loading, 10% model deformation

5.4.1 Linear static analysis

The Figures 5.8 and 5.9 respectively show the bending and composed torsion load cases. Additional views are shown in Appendix C.6.

Bring the two reinforcement pieces together has one interesting effect: it leads to a very similar deformation mode than the initial model. This results in the particularity that the two major local modes are stiffened by the two additional pieces.

In terms of numerical outcomes, the classic loading induces a maximum deflection of $18.70\ [mm]$ in bending and $3.95\ [mm]$ in torsion, while the armoured vehicle undergoes a maximum deflection of respectively $33.92\ [mm]$ and $7.17\ [mm]$ for bending and torsion simulations.

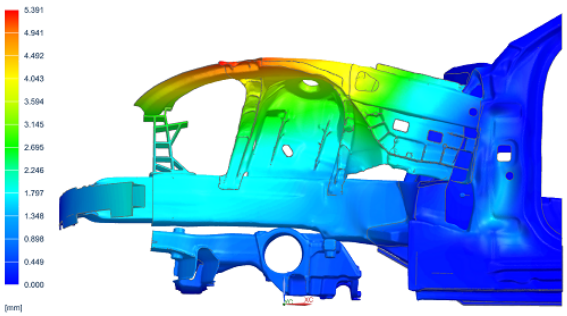

(a) Side view

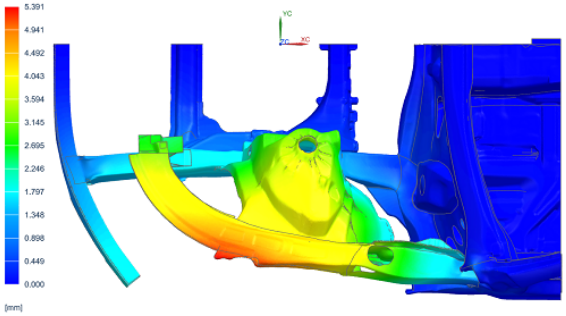

(b) Top view

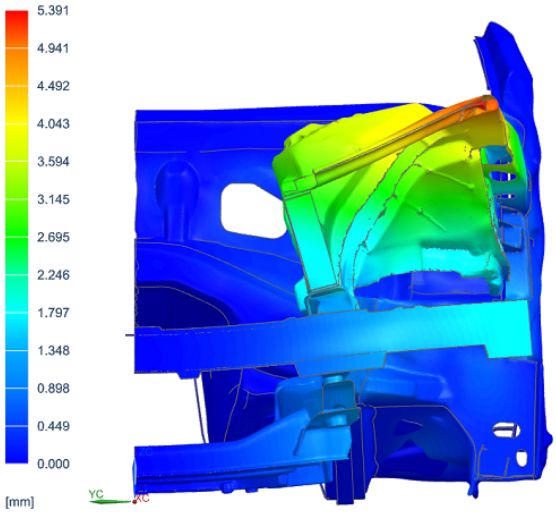

(c) Front view

Figure 5.7: Flexural reinforcement - Static analysis : composed torsion
Classic loading, 10% model deformation

5.4.2 Conclusion

This combination takes the benefits of each one. This result in a stiffening in bending of 31.04 [%] and 27.96 [%] in torsion with respect to the maximum deflection.

Furthermore, the armoured vehicle has only a maximum deflection 25.07 [%] in bending and 30.65 [%] in torsion higher compared to the initial vehicle load cases.

5.5 Conclusion

Although the impossibility for the numerical model to provide absolute results as things stand, this Chapter has shown that it remains able to have real industrial applications, especially when working with relative values.

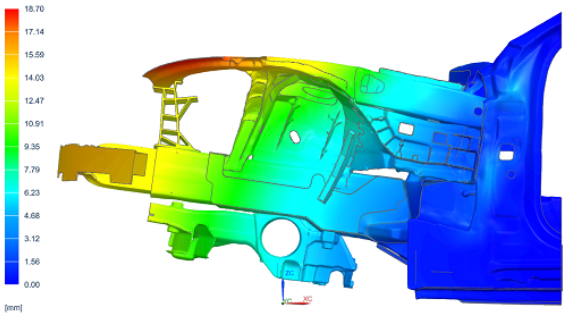

(a) Side view

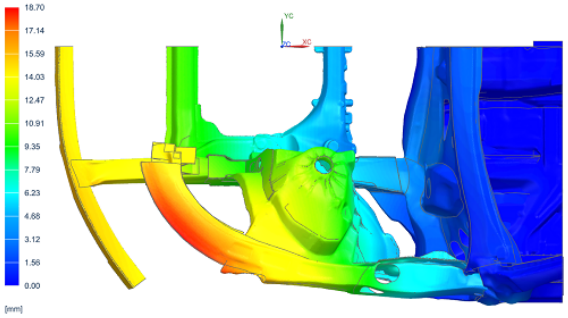

(b) Top view

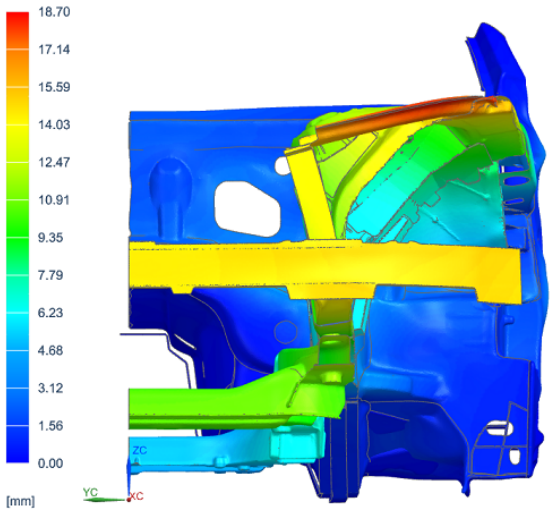

(c) Front view

Figure 5.8: Reinforcements combination - Static analysis : bending
Classic loading, 10% model deformation

The *Carat-Duchatelet* reinforcement part is very effective to reinforce the strut tower. It suggests that it would be sufficient for more usual armoured vehicles with a shorter lengthening than the one considered in this project and discussed in Section 4.2.1.

On the other hand, the flexural reinforcement component limit the bending deformation and seems to be a fairly good mechanical support for motor compartment-survival cell bonding. There is every reason to believe that the latter could be a solution to the second objective of this work stated in Section 1.2.

Finally, the last possibility combining the two reinforcements brings the advantages of the two parts together.

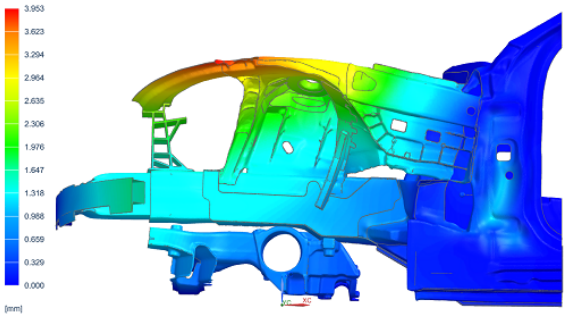

(a) Side view

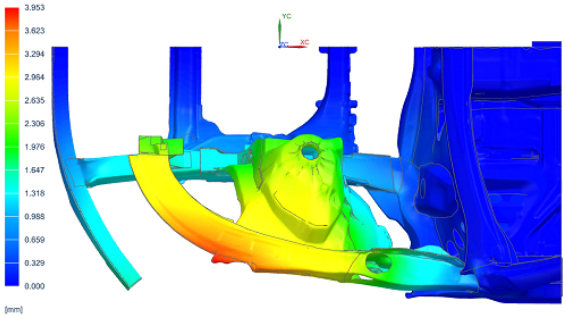

(b) Top view

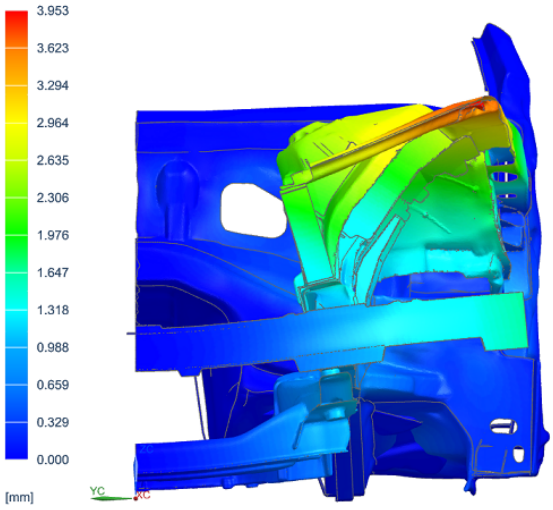

(c) Front view

Figure 5.9: Reinforcements combination - Static analysis : composed torsion
Classic loading, 10% model deformation

6 | Perspectives

The numerical modelling of a physical problem is always about compromises in accuracy and consistency with constraints. Most of the time, constraints concern time limit and available resources. The role of the engineer is to find the ideal equilibrium in this environment.

Concerning this writing in particular, the methodology led to several considerations, assumptions and simplifications. The choice of a particular software is a big part of it. In addition, the geometrical modelling of the car body can be likened to the foundations of this project. The FEA is not left behind. Finally, industrial applications are also subject to discussion. This Chapter discuss these key points.

6.1 Software

As developed in Sections 2.4 and 3.1, Siemens NX1980 is a powerful tool able to lead many operations and simulations on faceted mesh. On the other hand, it could be further improved to simplify procedures. In addition, the software selection itself may also be challenged.

6.1.1 Siemens NX1980

The *Polygon modelling* task of Siemens NX1980 edits and adjusts faceted models through various operations. It is able to answer every asked question about the model cleaning for this work, but generally in a laborious way. The ultimate goal of a RE process being to automatically transform a 3D scan into a suitable CAD model, there is an interest in automate some procedures:

Remeshing This may be the simplest feature: allow to directly select a whole body to standardize and refine the triangular mesh. At present, the refinement zone is manually selected;

Fill hole Sometimes, the *Fill hole* process fails because of defective border. The cleaning of the border during *Fill hole* operation if such an issue happens could be automated;

Irrelevant details So far, facets of the 3D scan corresponding to irrelevant details have to be manually removed in a first step, and then the generated hole is filled in a second step. These two steps could in a first approach be merged into one: the selection of irrelevant details' facets;

Smoothing As for the remeshing operation, allowing to select a whole body for smoothing operation would have an interest when the mesh suffers from general imperfections;

Misaligned normals The Section 3.2.5 describes a complex procedure to build new surfaces. The major difficulty in this process concerns the reversed *bridge gap* caused by the misaligned normals of two different surfaces. It would be particularly time saving to be able, within the *Bridge gap* function for instance, to artificially invert normals to make them coincide.

Artificial intelligence perspectives

Nowadays, Artificial Intelligence (AI) is becoming more and more important. Even for mechanical engineering applications, its potential is considerable. In particular, the geometric RE seems to be the best suited application of AI in the mechanical area. Ultimately, this will maybe lead to a fully automated process, as expected at first sight.

To conclude, the RE capabilities of Siemens NX1980 are increasing in recent years. It is already able to conduct complex operations. However, further improvements can still be glimpsed.

6.1.2 Alternatives

Siemens NX1980 is not the only software able to lead intended procedures, provide relevant results or simply answer the motivations. One can notice potential alternatives for geometrical modelling based on a 3D scan cleaning process and/or FEA. These have not been further investigated.

Here are briefly described two potential alternatives for the CAD model generation based on a scan cleaning process. Note that the use of different softwares depending on best suited tools for specific objectives could also have an interest.

MeshLab It is an open source system able to process and edit 3D triangular meshes. Although it can not create a faceted component from scratch, there is the ability to create a new component by merging two existing ones;

Autodesk MeshMixer It is a free software for processing and editing 3D triangular meshes. It is able to sculpt free-form using a selection of basic shapes, merge stl files, align and smooth surfaces, etc.

Concerning the FEA, the most important aspect concerns the mesh generation. The software must be able to generate FE meshes from faceted surfaces and bodies. This capability is generally included in most of CAE softwares such as CATIA, Hypermesh, etc.
Finally, there are also other solvers for FEA. Once the mesh has been generated on the faceted model, the choice of solver is not restricted by specific constraints involved by 3D scan considerations.

6.2 Geometrical modelling

6.2.1 Scan cleaning vs. conventional reverse engineering

The key feature in this work was to provide a suitable numerical model able to meet the needs: being consistent enough with the physical model for structural stiffness analysis.

Starting from this postulate of a structure stiffness analysis, the geometric model generation became a 3D scan cleaning, processing and editing. The Chapter 4 has shown that this procedure still provides convenient results with regard to the motivations.

For complex surfaces and bodies, the conventional geometric RE process is more laborious and involves a longer development time, but leads to a more accurate model with respect to the initial geometry. If the need for re-manufacturing or for more precise results concerning local effects arises, the conventional geometric RE modelling may become inevitable.

For simple surfaces and bodies, the conventional geometric RE becomes quite easy to such an extent that the scan cleaning method is less interesting regarding to accuracy and consistency aspects.

To sum up, each situation requires weighing the pros and cons between traditional and new RE methods, regarding to geometric complexity and intended objectives.

6.2.2 Available raw data

Through this writing, most of assumptions and simplifications came from the lack of raw data about the physical model. The 3D scan only provides external surfaces so that internal reinforcement parts are unknown. In addition, the latter corresponds to the full BIW, itself composed of numerous parts assembled together. Poor information was available on assemblies in the BIW.

Disposing of separated scans for each constitutive part, or at least a few information about assemblies would be of greatest help to recover a precise geometric model.

Furthermore, constitutive materials and thicknesses when only one face of the part is scanned would also permit to recover an accurate model concerning its mechanical behavior.

Definitely, variety, precision and completeness of raw data are key factors in generating accurate geometric models.

6.2.3 Further improvements

The most important additional part of the whole vehicle in terms of structural behavior has already been considered: the subframe. However, other components have an influence on the structural behavior of the vehicle. For instance, as said in Section 2.2.4, the windshield has a strong influence on the torsional rigidity.

In addition, the Section 4.5 introduces the influence of the suspension on the application of external load coming from the tire-ground interface. This actually only provides an overview of this phenomenon that would deserving a deeper study.

Finally, the second external load, *i.e. aerodynamic forces*, is not considered although it may be significant in dynamic situations.

6.3 Finite element analysis

6.3.1 Mesh optimization

The mesh generation and optimization is usually a time-consuming step allowing for a significant time-saving during analysis. In this work, this was not the case because of the limited number of simulations.

Variable element size As explained in Section 4.1.2, the uniform mesh size for which results converge to the solution indicates the minimum element size for critical locations in the model. However, it does not provide any information about the maximum element size for less critical locations.

A first optimization consists in adjusting the uniform mesh size component by component in the full model. This could be done by analyzing the convergence of results when varying a specific component's element size with respect to the converged fully uniformed model. This method would provide the minimum element size necessary at critical locations for each part in the full model.
It would result in a smaller problem size.

A further optimization would consist in adjusting the mesh for the each part separately.

Element parameters It is also a key feature for mesh performance and accuracy. For example, studying the impact of *maximum growth rate* and *minimum element size* may be relevant to increase mesh efficiency.

6.3.2 Load cases

It has been stated that the two most important load cases for automotive bodies are bending and torsion ones. However, it does not take into account that this project involves modified vehicles that have different behavior, road handling, characteristics, etc with respect to traditional vehicles.

Lateral and longitudinal load cases are impacted by the vehicle weight and the position of the CoG. The CoG being largely modified by armouring and extension, these load cases could lead to important efforts in the car body so that their study becomes needful.

Furthermore, only a composed torsion has been simulated since the quarter model is not suitable for pure torsion simulation using Siemens NX1980 . Two alternatives are available:

- Use a software able to define symmetry BC of the geometry on the symmetry plane, and anti-symmetric BC on the external applied load;
- Build a half model, or even a complete one, instead of a quarter chassis.

6.3.3 Modal analysis

The Section 2.2.4 states that the body's bending and torsional stiffness is closely related to its frequencies and mode shapes in bending and torsion respectively.
The modal parameters have been computed for the initial model in order to validate its mechanical behavior.

Since eigenfrequencies and mode shapes are independent of external applied loads, modal analysis is of interest for analyzing stiffness and especially comparing stiffness of different variants of the model together.

6.4 Application

This project was carried out in enterprise with a desire for concrete application of the latter. On the one hand, the proposed applications can be criticized. On the other hand, the general approach taken can also be questioned.

6.4.1 Reinforcement parts

The first remark concerns actual suggested reinforcements parts. This work only proposes ways to answer the initial problem. It does not claim to present a working prototype resulting from a dimensioning phase.

A first step would thus to lead a deeper analysis of reinforcements parts. Here is a list of what is primarily influencing reinforcement parts' efficiency:

- Material constitution (steel, aluminium, composite, etc) and thickness;
- Intrinsic geometry, especially for the flexural reinforcement's beam cross-section;
- The impact of gluing the part to the chassis or not.

Furthermore, although being suggested in Section 5.1.1 and widely used in practice, the Strut Tower Brace has not been further studied.

6.4.2 Stiffening approach

For this work, the methodology used for stiffening the front compartment was based on the deformation mode analysis.
However, recent developments in Topology Optimization (TO) show a great interest for answering present motivations. Indeed, the TO based on compliance could directly suggest most important zones for stiffness in the car body with respect to considered load cases.

Designing reinforcement elements for these locations would effectively stiffen the whole structure.

Conclusion

Producing high quality secured vehicles starting from mass-produced ones involves a strong re-engineering of the initial product, for which only a 3D scan and a few additional data are available. Especially, this work intended to suggest structural stiffener elements to the front compartment of a car body.

First, the project and its adjacent problem were described. The general context lays the foundations for a deep understanding of ins and outs. The enterprise who defined the problem and its general business model were thus introduced. Additionally, motivations with corresponding objectives and constraints were identified. In particular, the study is limited to the front left quarter part of a whole automotive body.

Then, a literature review was performed to provide the basics that might be necessary to completely appreciate this writing. The conventional geometric reverse engineering process has been presented. Furthermore, design and analysis key features about automotive body structure were also developed. Stiffness characteristics were especially discussed. Finally, a few words have been said about the Finite Element Method and the CAE software used.

The geometrical modelling aimed at generating a suitable numerical model. Based on a particular reverse engineering process, it consisted in various operations on facets of the 3D scan. From this step results a geometric model approaching the physical chassis and composed of several connected parts consisting of sheet metals or massive parts, and made from various materials and/or thicknesses.
It involved strong assumptions and simplifications since the 3D scan does only provides partial information about external surfaces.

The Finite Element Analysis, led through the two most important load cases that are bending and torsion ones, validated the mechanical consistency of the model with respect to the physical chassis. It concluded that the model is accurate and consistent enough for global structure stiffness analysis, especially when working with relative notions. What concerns absolute results, experimental testing is needed to provide a scaling between real and numerical results.

Further improvements allow to provide a more realistic model. In this way, the subframe, that is the most important additional structural component, had been added. Additionally, the load transfer from wheel center to suspension supports on the car body was studied. This gave a more truthful representation of the application of road forces onto the chassis.

Concrete applications about structural stiffness analysis of the built model have been suggested through three stiffening possibilities. It resulted that the piece resulting from the enterprise's know-how was quite effective even as a stand alone, while the combination of the strut tower's strapping with the flexural reinforcement part was the most effective with a limited additional deformation of the armoured vehicle compared to the classic unarmoured one.

The problem exposed in this work can be further extended. The geometric reverse en-

gineering is still strongly evolving, enabling more and more automated procedures. In this way, artificial intelligence seems to lead to great progress in this subject. The scan-to-CAD process is also strongly dependent on raw data. The more data available, the better the model. Otherwise, load cases that are usually of second importance may be significant for secured vehicles. Finally, Topology Optimization seems to be an effective approach to clearly identify weak zones in terms of stiffness in the model.

To conclude, the alternative reverse engineering process based on faceted mesh cleaning and editing is already able to provide accurate and consistent results, but what is the labor cost? How would it be possible for CAE softwares to generate suitable models in an automated way?

Concerning the structure stiffness analysis of a car body, static and modal analysis make it possible to identify weak zones suffering from a lack of rigidity, but is there any solution to notice these zones in a more visual or efficient way? May Topology Optimization be an answer to the previous question?

References

[1] G. Ducellier & B. Eynard A. Durupt S. Remy. "From a 3D point cloud to an engineering CAD model: a knowledge-product-based approach for reverse engineering". In: *Virtual and Physical Prototyping* 3.2 (2008), pp. 51–59.

[2] A2Mac1. *A2Mac1 website*. 2022. URL: https://portal.a2mac1.com/ (visited on 05/31/2022).

[3] C. Arnaut et al. "Study on data sharing between companies in Europe - executive summary". In: (2018). For the European Commission.

[4] C.U. Nwoji et al. "Theory of Elasticity Formulation of the Mindlin Plate Equations". In: *International Journal of Engineering and Technology* 9.6 (2017).

[5] F. Buonamici et al. "Reverse engineering of mechanical parts : A template-based approach". In: *Journal of Computational Design and Engineering* 5 (2018), pp. 145–159.

[6] Ambica. *AISI 304 Stainless Steel – One Of The Most Versatile Grades In Stainless Steel*. 2019. URL: https://www.ambicasteels.com/blog/aisi-304-stainless-steel-one-of-the-most-versatile-grades-in-stainless-steel/ (visited on 06/05/2022).

[7] K.-J. Bathe. *Finite element procedures*. Prentice Hall, Pearson Education, Inc., 2006.

[8] Book wiki. *Acier maraging*. URL: https://boowiki.info/art/inoxydable-2/acier-maraging.html (visited on 06/05/2022).

[9] Carat-Duchatelet. *Carat-Duchatelet website*. 2022. URL: https://caratduchatelet.com/ (visited on 05/16/2022).

[10] W.F. Carroll. *A primer for finite elements in elastic structures*. John Wiley Sons, Inc., 1999.

[11] Chris Teague. *What exactly is chassis bracing?* 2021. URL: https://www.carbibles.com/what-is-chassis-bracing/ (visited on 06/06/2022).

[12] P. Duysinx. "Structural design and performance of car bodies". In: *University of Liège* (2022). Vehicle architecture and components course.

[13] P. Duysinx. "The vehicle system and its major components". In: *University of Liège* (2022). Vehicle architecture and components course.

[14] J. Happian-Smith. *An introduction to modern vehicle design*. SAE, 2002.

[15] H. Heisler. *Advanced vehicle technology*. 2nd ed. Elsevier, 1989.

[16] H. Heisler. *Vehicle and engine technology*. Elsevier, 1985.

[17] ISSF. "Stainless Steel Applications – Automotive". In: ().

[18] J. Gardiner. *Finite element analysis - convergence and mesh independence*. 2017. URL: https://www.xceed-eng.com/finite-element-analysis-convergence-and-mesh-independence/#:~:text=Rouiba%5C%20Convergence%5C%3A%5C%20Mesh%5C%20convergence%5C%20determines,solution%5C%20with%5C%20decreasing%5C%20element%5C%20size. (visited on 05/25/2022).

[19] A.J. Robertson & S. Serpento J.Brown. *Automotive engineering: powertrain, chassis system and vehicle body - Terminology and overview of vehicle structure types*. D. Crolla. Elsevier, 2009.

[20] La Centrale. *Fiche technique Mercedes CLASSE S - 2022 (Routières) - VIII S 680 4MATIC MERCEDES-MAYBACH 4PL*. URL: https://www.lacentrale.fr/fiche-technique-voiture-mercedes-classe+s-viii+s+680+4matic+mercedes_maybach+4pl-2022.html (visited on 05/25/2022).

[21] D. E. Malen. *Fundamentals of automobile body structure design*. SAE, 2011.

[22] N. Anwer L. Mathieu. "From reverse engineering to shape engineering in mechanical design". In: *CIRP Annals - Manufacturing Technology* 65 (2016), pp. 165–168.

[23] C. R. Mehta. *A new reverse engineering approach to reconstruction of 3D CAD-models*. University of New York, 2005.

[24] G. Genta & L. Morello. *The automotive chassis - volume 1: components design*. Springer, 2009.

[25] J. Pang. *Noise and vibration control in automotive bodies*. Wiley, 2019.

[26] J.P. Ponthot. "An introduction to the finite element method". In: *University of Liège* (2020). Finite Element Method course.

[27] PTJ. *Is 6061 aluminum suitable for the automotive industry?* 2020. URL: https://www.cncmachiningptj.com/article-227.html (visited on 06/05/2022).

[28] M. E. Plesha & R. J. Witt R. D. Cook D. S. Malkus. *Concepts and applications of finite element analysis*. Fourth edition. John Wiley Sons, Inc., 2002.

[29] M. Géradin & D. J. Rixen. *Mechanical vibrations: theory and application to structural dynamics*. 3rd edition. John Wiley Sons, Inc., 2015.

[30] J. Erjavec & R. Scharff. *Automotive technology : a systems approach*. Delmar, 1992.

[31] Siemens. *Support Center*. 2022. URL: https://support.sw.siemens.com/fr-FR/ (visited on 05/22/2022).

[32] Stringfixer. *Alliage d'aluminium 6061*. URL: https://stringfixer.com/fr/6061%5C_aluminium_alloy (visited on 06/05/2022).

[33] R. Martin & J. Coxt T. Varady. "Reverse engineering of geometric models - an introduction". In: *Computer-Aided Design* 29.4 (1997), pp. 255–268.

[34] Tetiana. *5 Reasons Why You Should Get an Armored Car*. 2020. URL: https://www.armormax.com/blog/reasons-why-you-should-get-an-armored-car/ (visited on 05/16/2022).

[35] Ultra racing USA. *Mercedes S-class (W221) 2007–2013 - front strut (2 points)*. URL: https://ultraracing-usa.com/mercedes-s-class-w221-2007-2013-front-strut-2-points/ (visited on 06/06/2022).

[36] Wikipedia. *Armored car (VIP)*. 2021. URL: https://en.wikipedia.org/wiki/Armored_car_(VIP) (visited on 05/16/2022).

[37] Wikipedia. *Mercedes-Benz S-Class (W223)*. 2022. URL: https://en.wikipedia.org/wiki/Mercedes-Benz_S-Class_(W223) (visited on 05/16/2022).

A | Model description appendix

A.1 Initial model

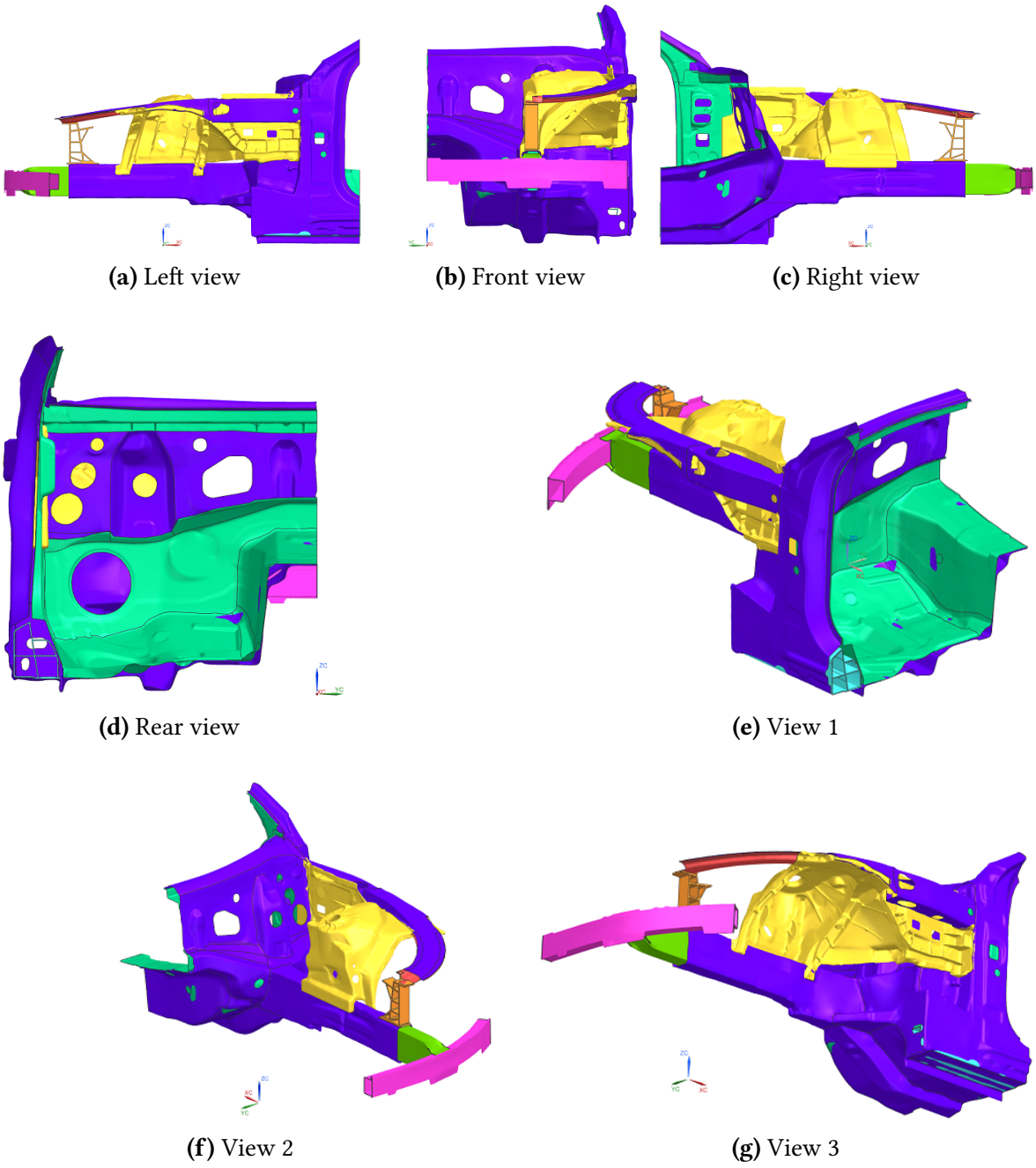

(a) Left view **(b)** Front view **(c)** Right view

(d) Rear view **(e)** View 1

(f) View 2 **(g)** View 3

Figure A.1: Model description - Additional views

A.2 Subframe

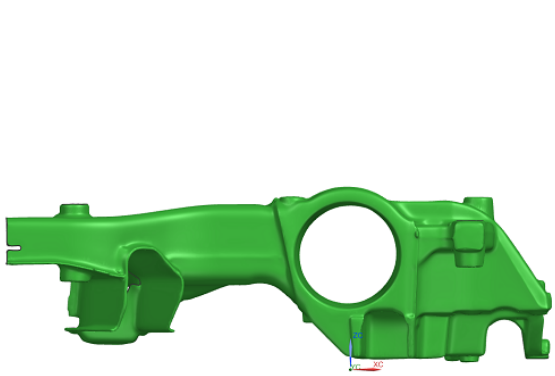

(a) Left view

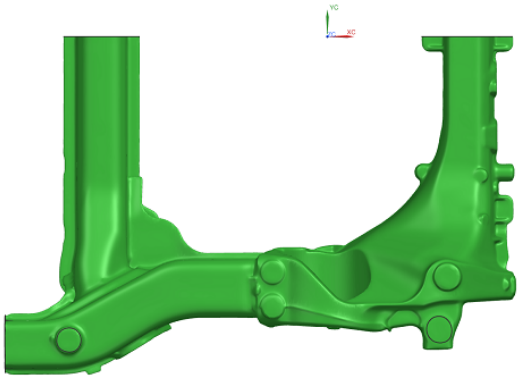

(b) Top view

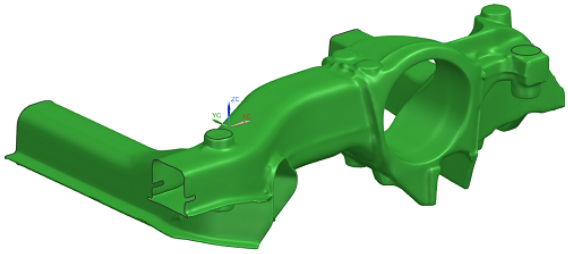

(c) 3D view

Figure A.2: Model description - 0309 (additional views)

B | Mesh convergence appendix

General remark The relative error concerns TPE and is defined with respect to the minimum element size computed:

$$relative\ error\ [\%] = \left| \frac{TPE_{current} - TPE_{min}}{TPE_{min}} \right| \cdot 100 \tag{B.1}$$

B.1 Initial model

Mesh size [mm]	Nb. dofs [-]	TPE [J]	Comp. time [min]	Rel. err. [%]
10	1 197 450	7.00e+05	4.13	9.87
7	1 737 351	6.91e+05	12.32	8.53
5	2 672 722	6.36e+05	12.55	0.10
4	4 106 574	6.37e+05	22.25	0.00

Table B.1: Initial model - mesh convergence analysis

B.2 Model improvement : subframe

Mesh size [mm]	Nb. dofs [-]	TPE [J]	Comp. time [min]	Rel. err. [%]
50	2 758 664	5.99e+05	13.78	0.55
20	2 946 998	6.00e+05	12.45	0.12
10	3 141 847	6.01e+05	13.67	0.09
7	3 244 918	6.01e+05	13.80	0.10
5	3 357 608	6.01e+05	13.25	0.04
3	3 623 604	6.01e+05	29.83	0.00

Table B.2: Model improvement : subframe - mesh convergence analysis

B.3 *Carat-Duchatelet* reinforcement

Mesh size [mm]	Nb. dofs [-]	TPE [J]	Comp. time [min]	Rel. err. [%]
5	3 633 620	7.48e+05	23.17	4.51
4	3 712 286	7.78e+05	20.23	0.67
3	3 853 601	7.83e+05	30.67	0.00

Table B.3: *Carat-Duchatelet* reinforcement - mesh convergence analysis

B.4 Flexural reinforcement

Mesh size [mm]	Nb. dofs [-]	TPE [J]	Comp. time [min]	Rel. err. [%]
30	3 365 030	8.45e+05	16.77	0.62
20	3 369 026	8.39e+05	16.98	0.09
7	3 432 245	8.40e+05	17.37	0.00

Table B.4: Flexural reinforcement - mesh convergence analysis

C | Finite element analysis appendix

C.1 Initial model

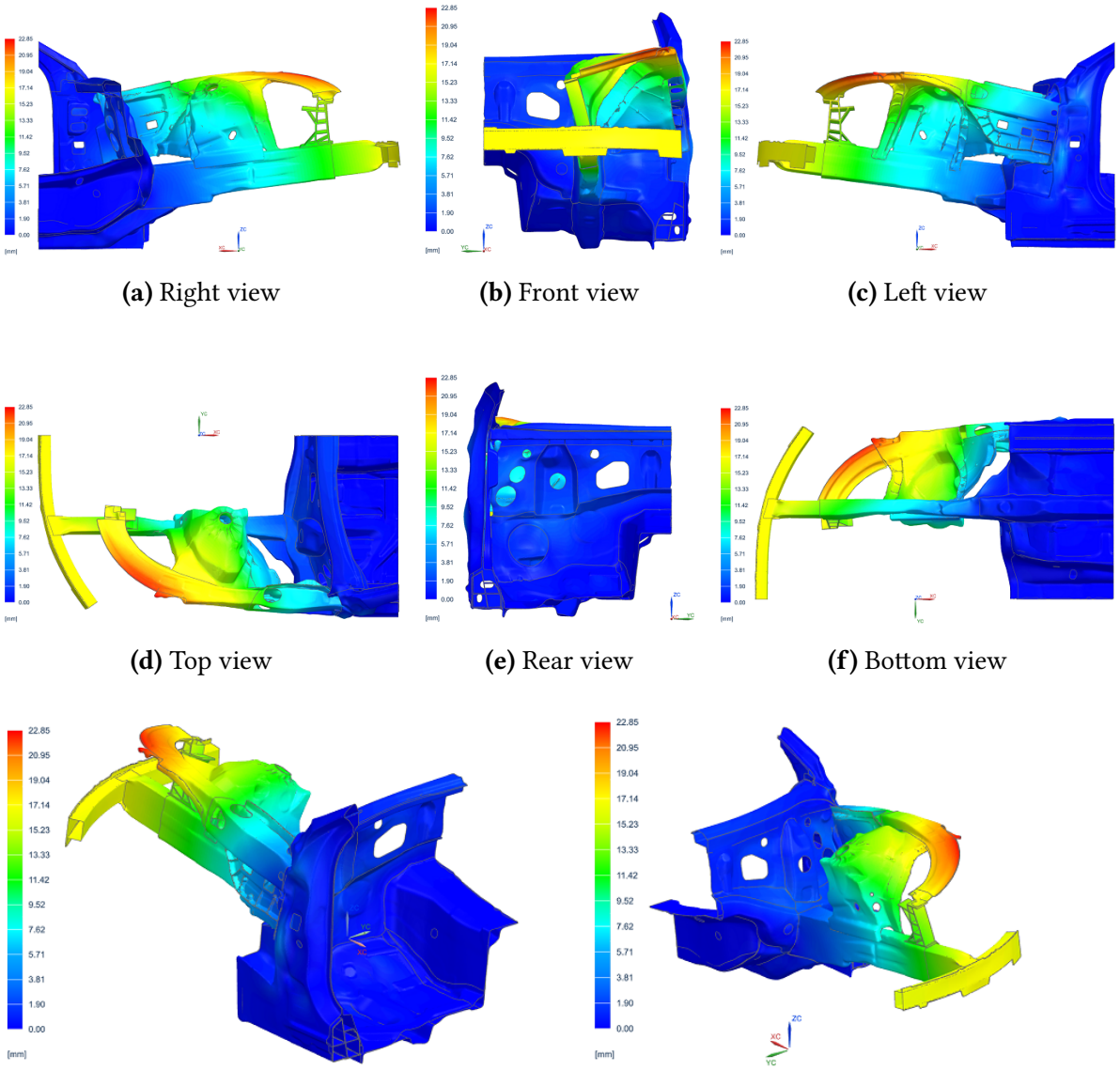

(a) Right view **(b)** Front view **(c)** Left view

(d) Top view **(e)** Rear view **(f)** Bottom view

(g) 3D view 1 **(h)** 3D view 2

Figure C.1: Initial model: Static analysis - bending (additional views)
Classic loading, 10% model deformation

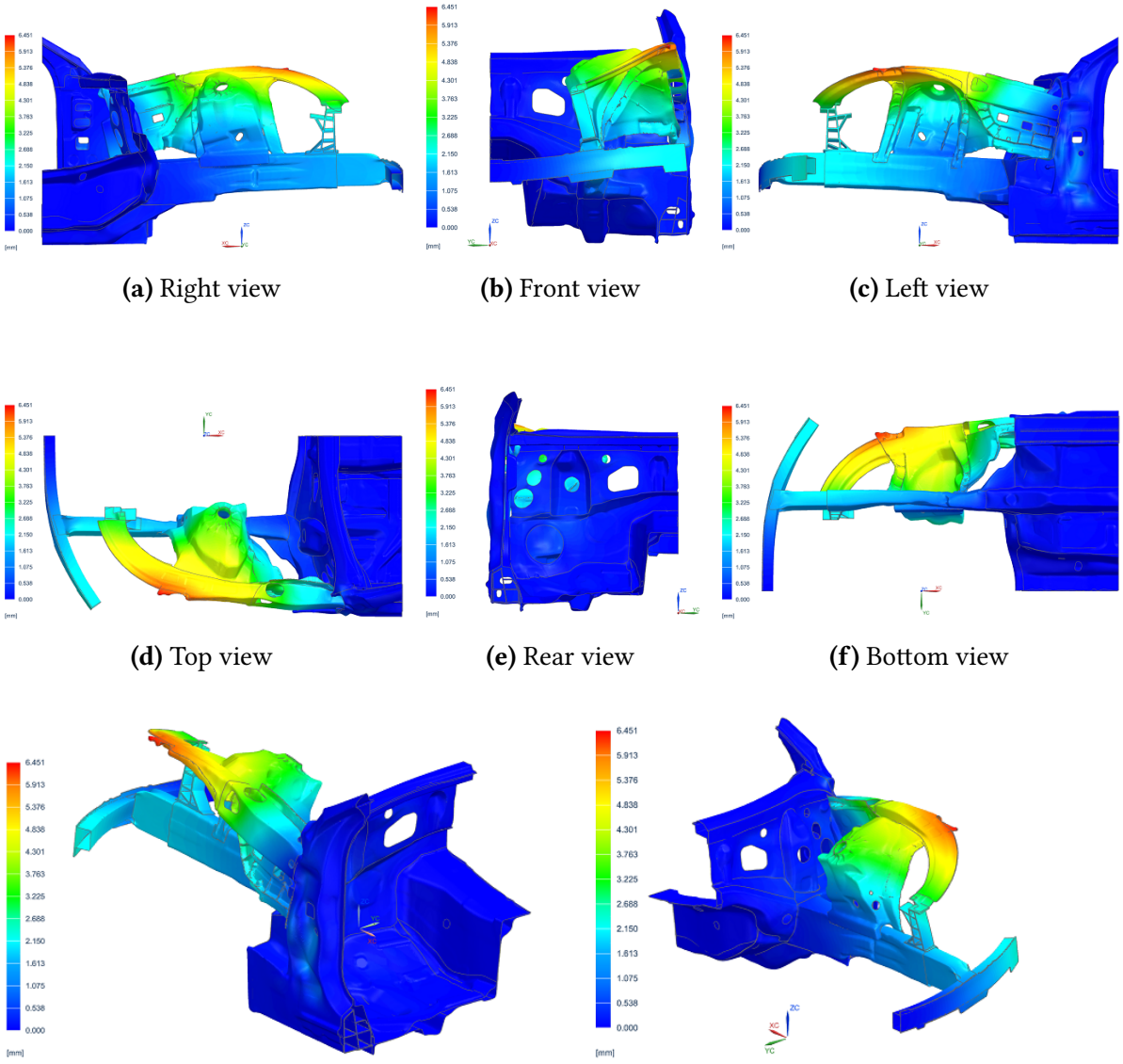

(a) Right view **(b)** Front view **(c)** Left view

(d) Top view **(e)** Rear view **(f)** Bottom view

(g) 3D view 1 **(h)** 3D view 2

Figure C.2: Initial model: Static analysis - composed torsion (additional views)
Classic loading, 10% model deformation

C.2 Model improvement : subframe

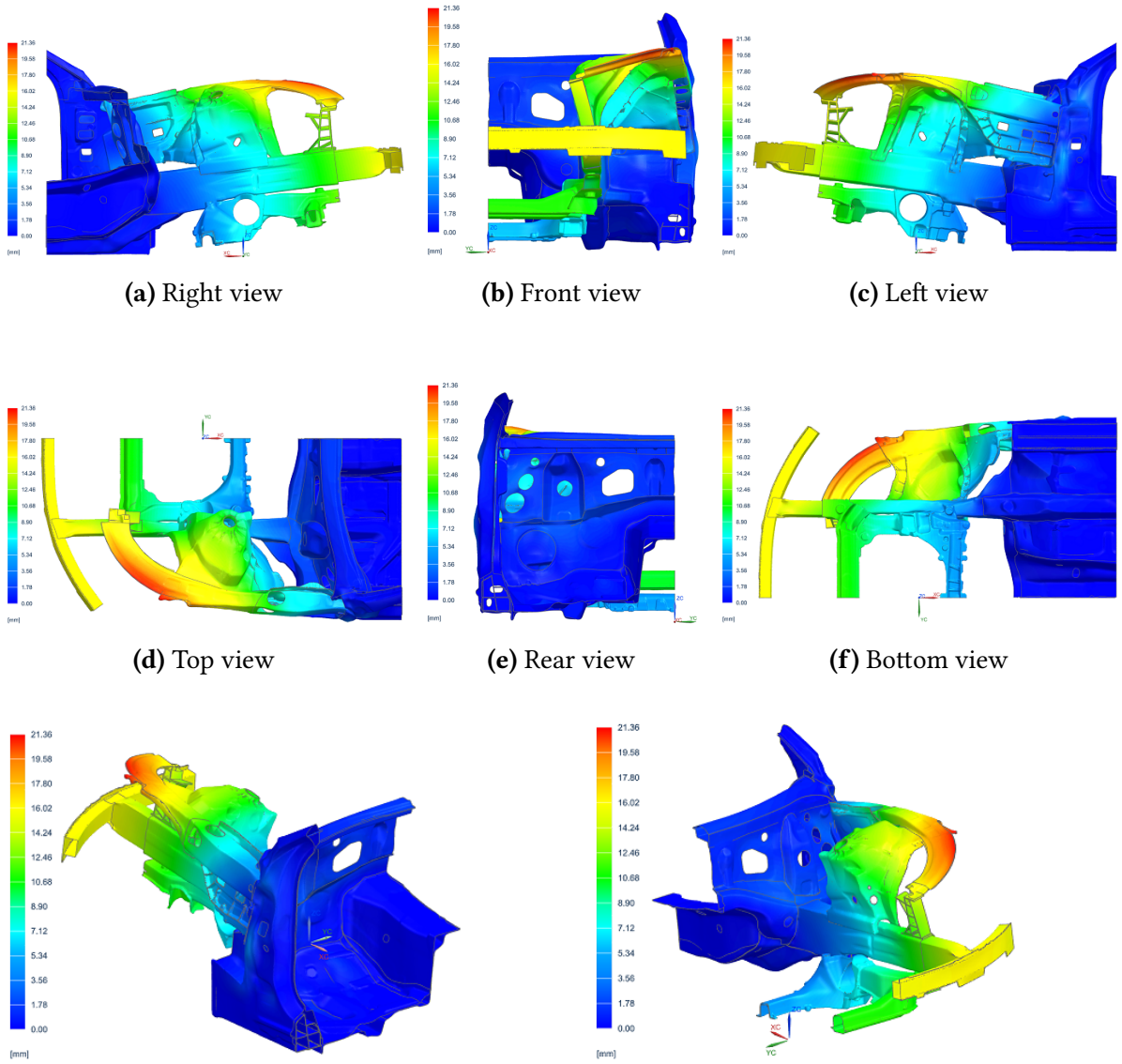

(a) Right view **(b)** Front view **(c)** Left view

(d) Top view **(e)** Rear view **(f)** Bottom view

(g) 3D view 1 **(h)** 3D view 2

Figure C.3: Subframe addition: Static analysis - bending (additional views)
Classic loading, 10% model deformation

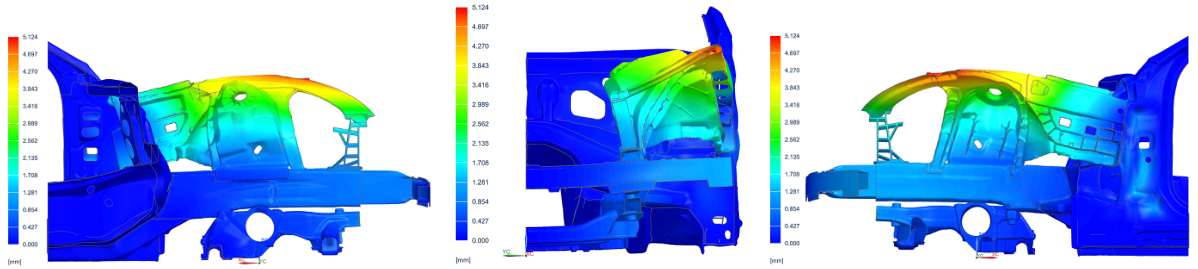

(a) Right view **(b)** Front view **(c)** Left view

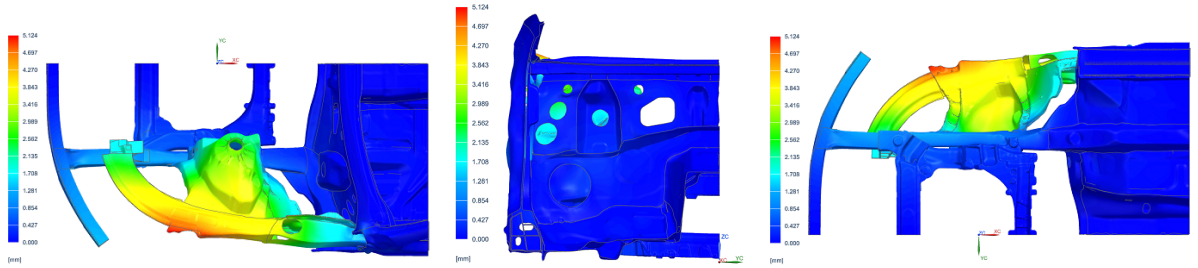

(d) Top view **(e)** Rear view **(f)** Bottom view

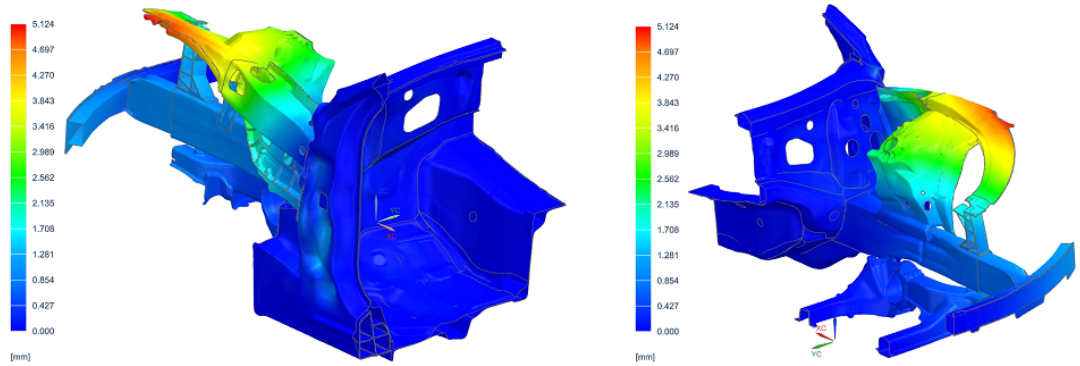

(g) 3D view 1 **(h)** 3D view 2

Figure C.4: Subframe addition: Static analysis - composed torsion (additional views)
Classic loading, 10% model deformation

C.3 Model improvement : suspension load paths

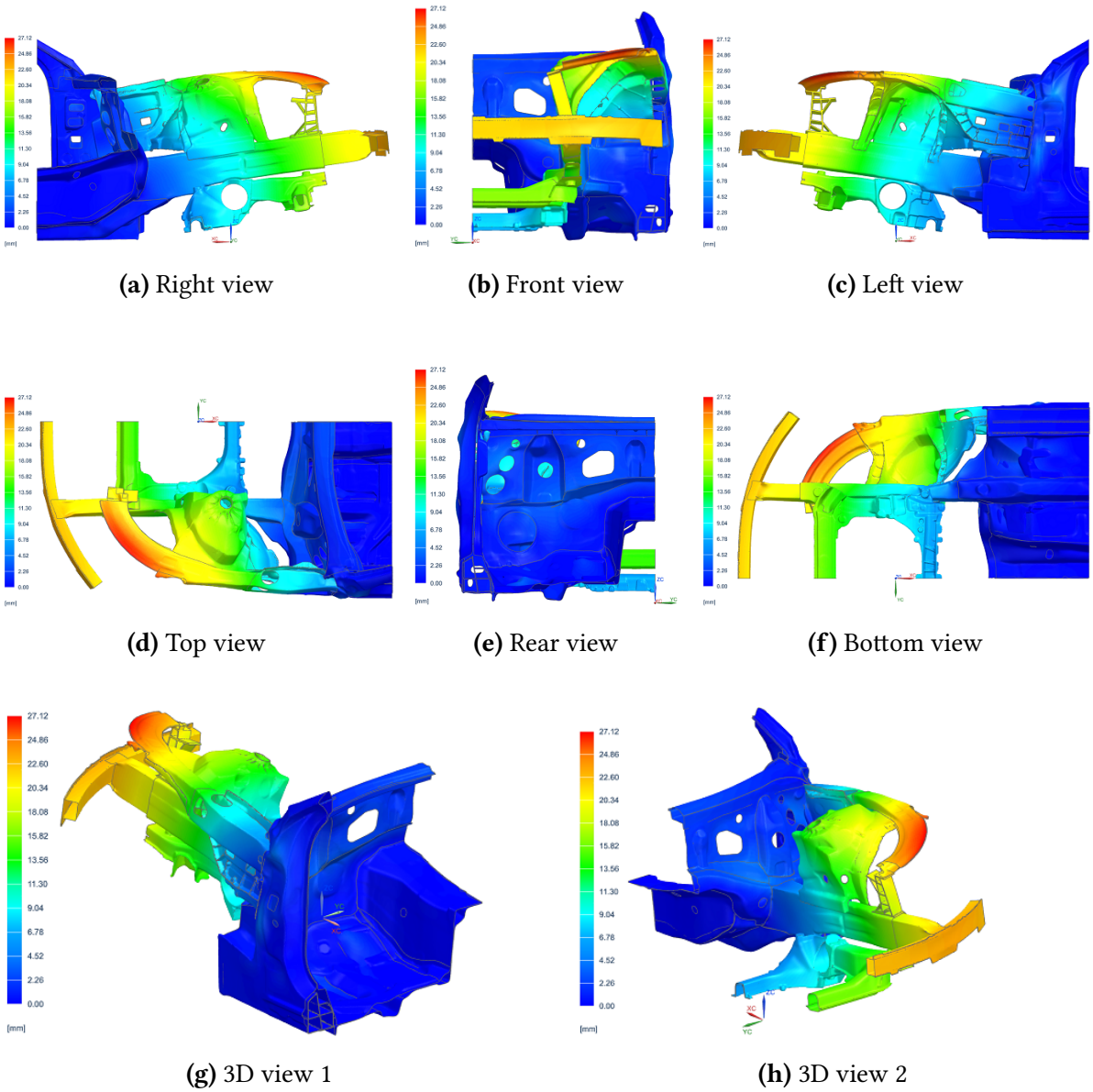

(a) Right view **(b)** Front view **(c)** Left view

(d) Top view **(e)** Rear view **(f)** Bottom view

(g) 3D view 1 **(h)** 3D view 2

Figure C.5: Suspension load paths: Static analysis - bending (additional views)
Classic loading, 10% model deformation

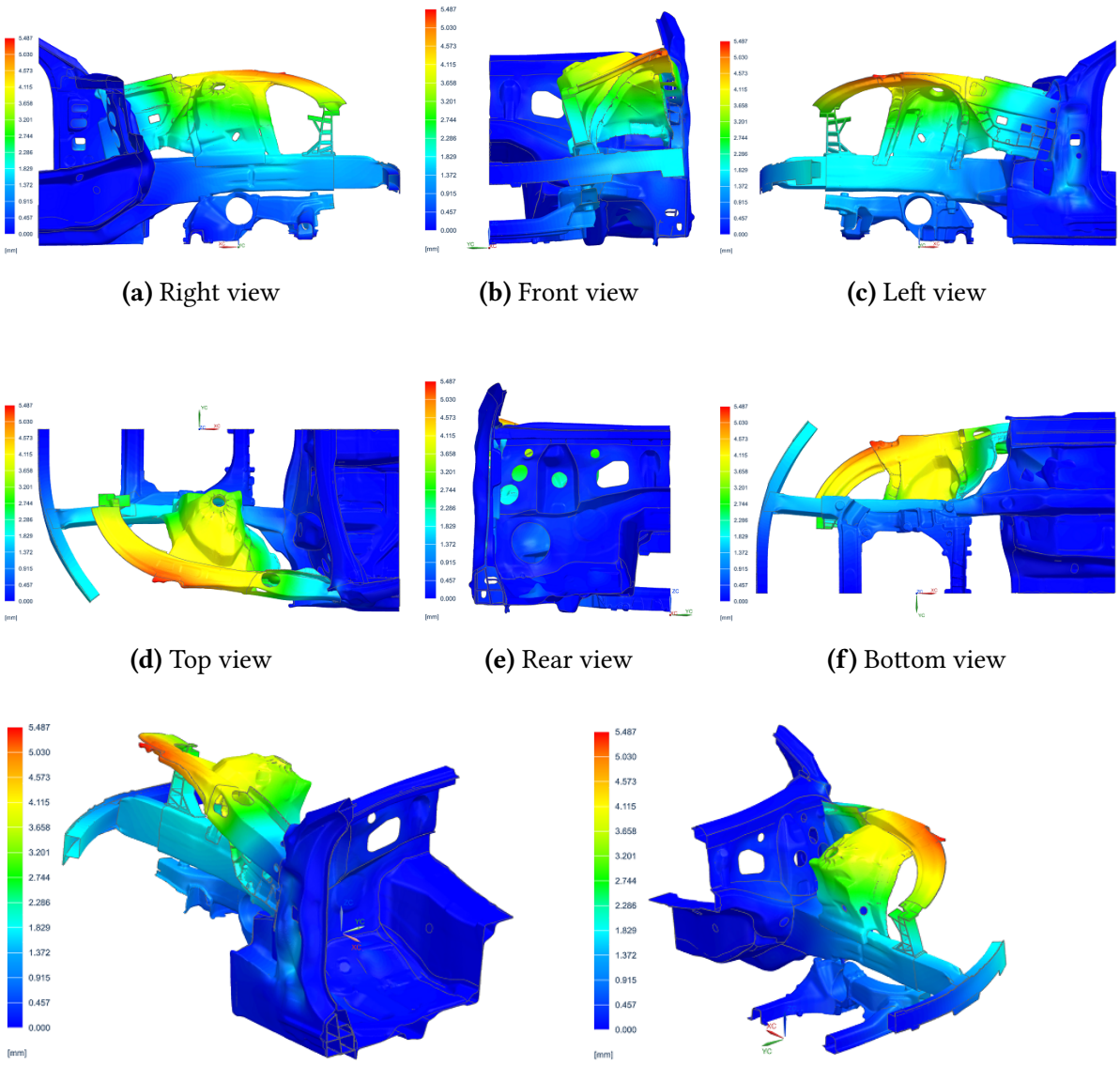

(a) Right view **(b)** Front view **(c)** Left view

(d) Top view **(e)** Rear view **(f)** Bottom view

(g) 3D view 1 **(h)** 3D view 2

Figure C.6: Suspension load paths: Static analysis - composed torsion (additional views)
Classic loading, 10% model deformation

C.4 *Carat-Duchatelet* reinforcement

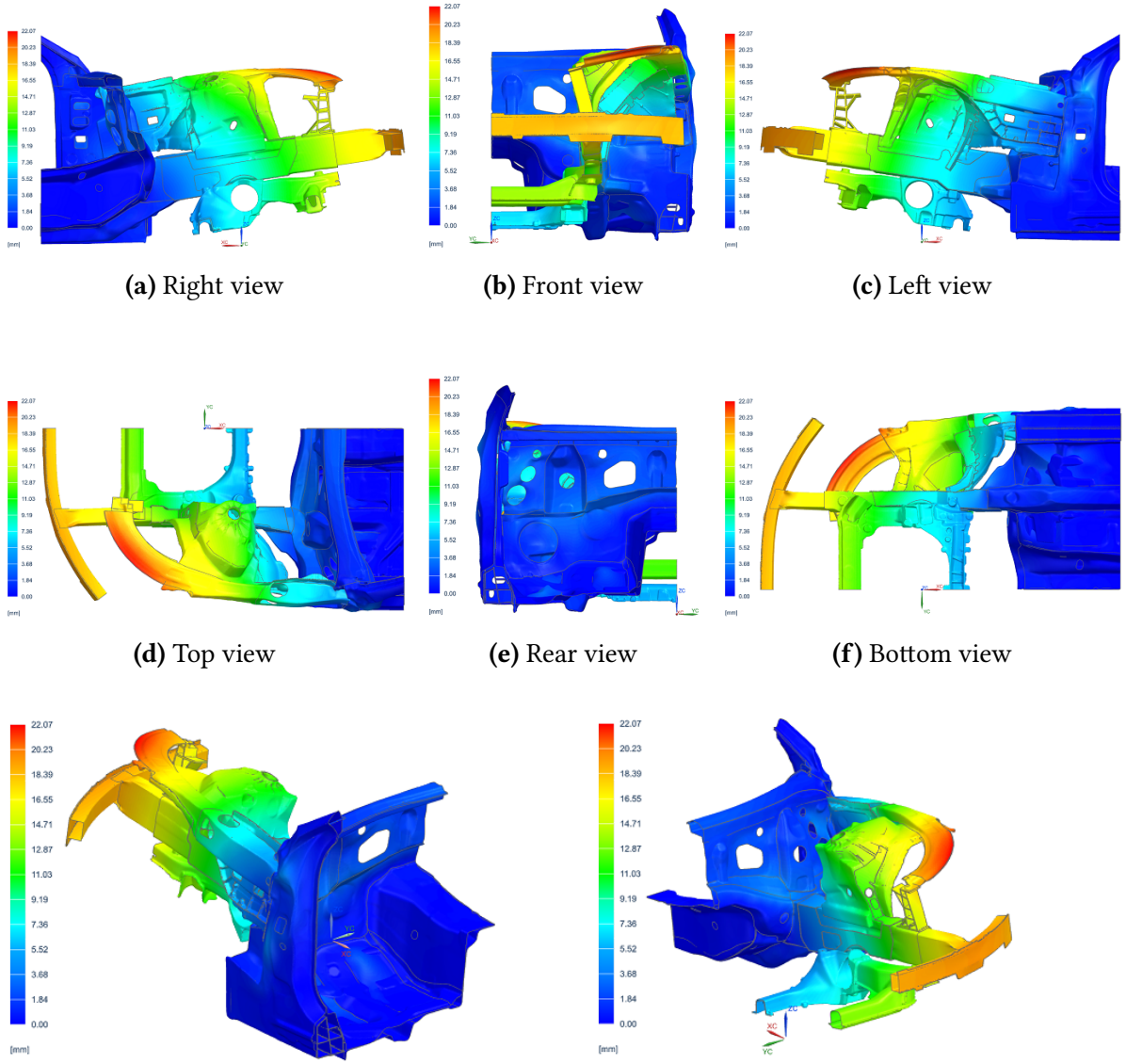

(a) Right view **(b)** Front view **(c)** Left view

(d) Top view **(e)** Rear view **(f)** Bottom view

(g) 3D view 1 **(h)** 3D view 2

Figure C.7: *Carat-Duchatelet* reinforcement: Static analysis - bending (additional views)
Classic loading, 10% model deformation

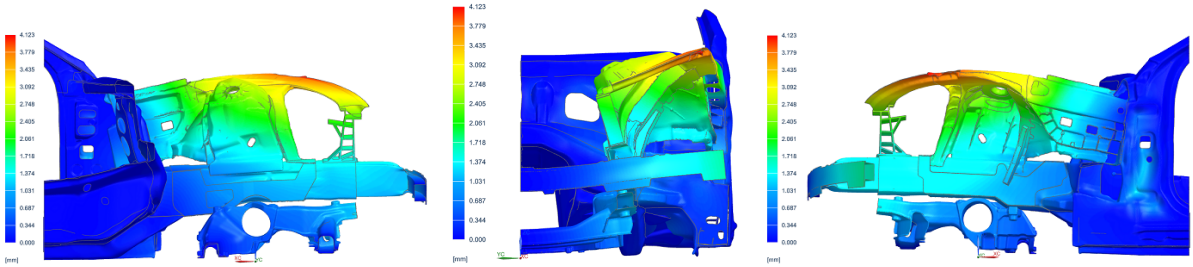

(a) Right view **(b)** Front view **(c)** Left view

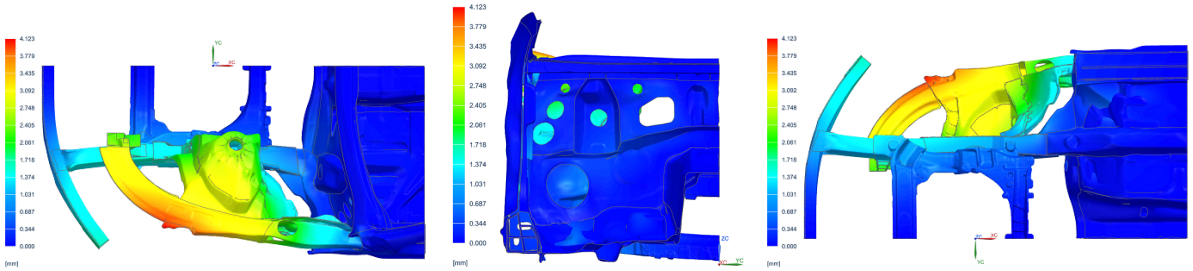

(d) Top view **(e)** Rear view **(f)** Bottom view

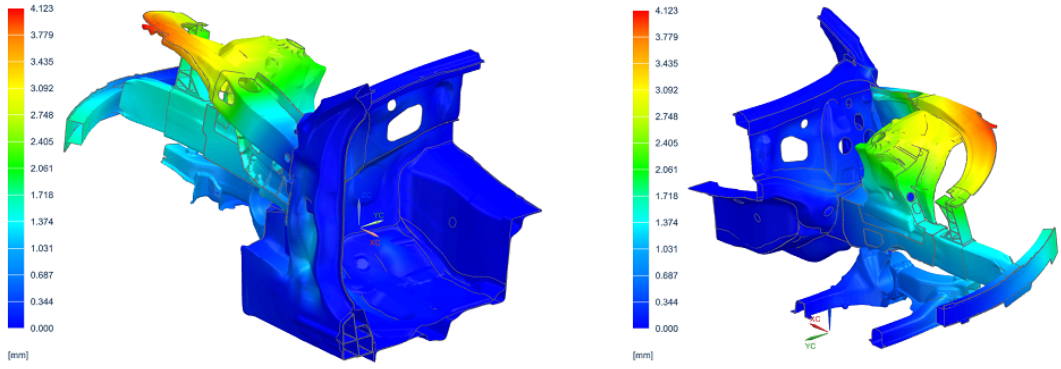

(g) 3D view 1 **(h)** 3D view 2

Figure C.8: *Carat-Duchatelet* reinforcement: Static analysis - composed torsion (additional views)
Classic loading, 10% model deformation

C.5 Flexural reinforcement

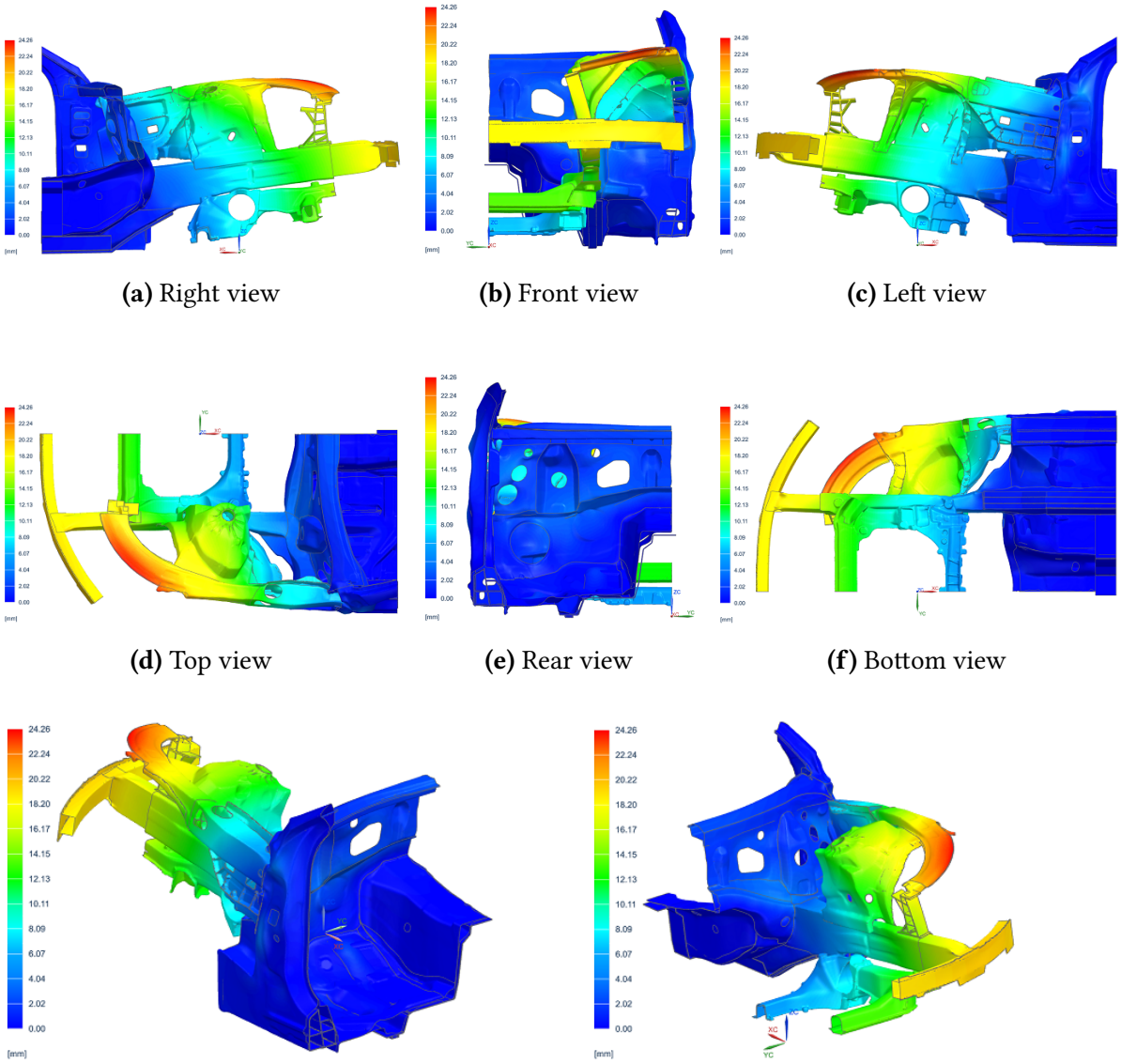

(a) Right view **(b)** Front view **(c)** Left view

(d) Top view **(e)** Rear view **(f)** Bottom view

(g) 3D view 1 **(h)** 3D view 2

Figure C.9: Flexural reinforcement: Static analysis - bending (additional views)
Classic loading, 10% model deformation

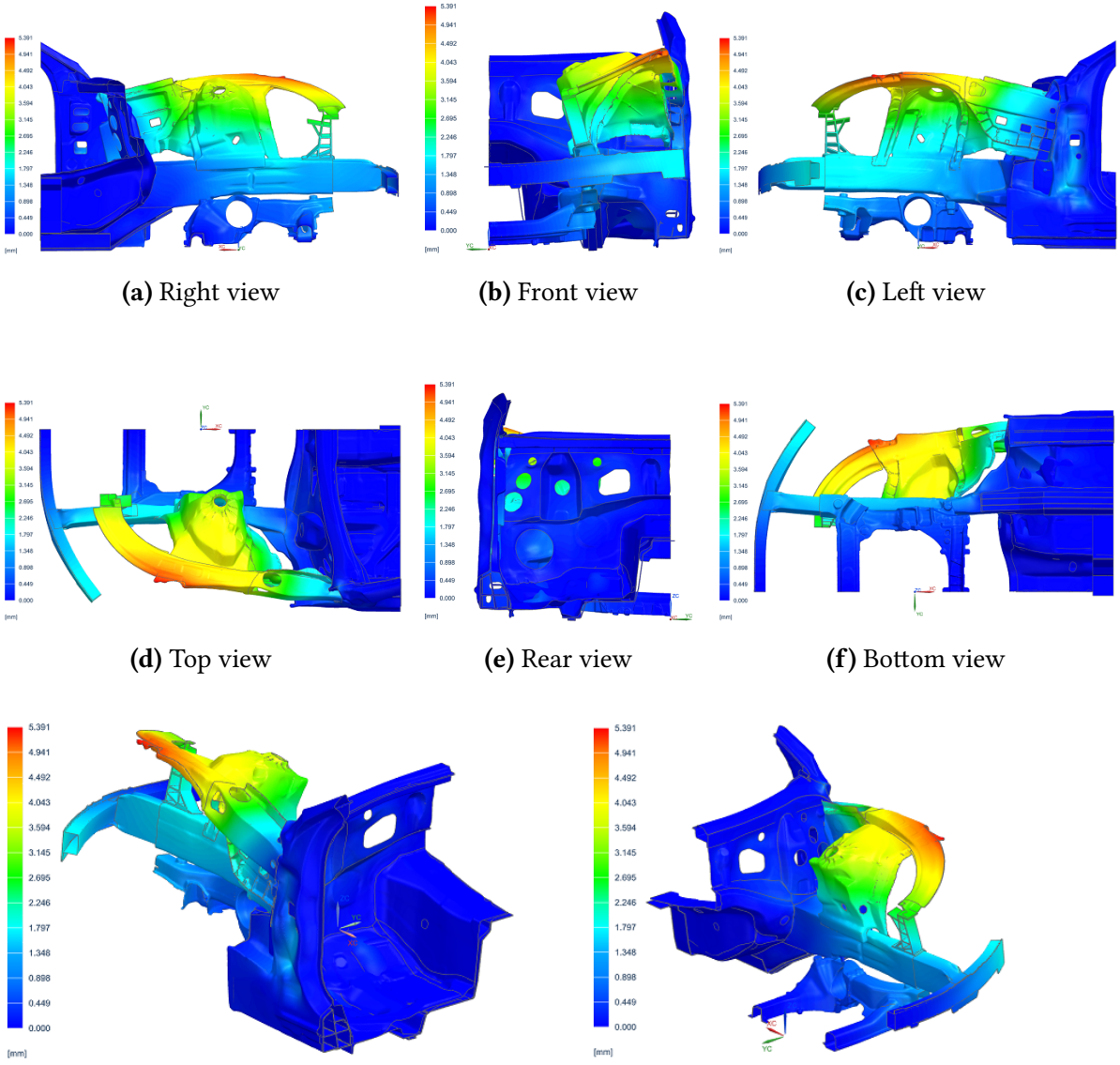

(a) Right view **(b)** Front view **(c)** Left view

(d) Top view **(e)** Rear view **(f)** Bottom view

(g) 3D view 1 **(h)** 3D view 2

Figure C.10: Flexural reinforcement: Static analysis - composed torsion (additional views)
Classic loading, 10% model deformation

C.6 Combination of *Carat-Duchatelet* and flexural reinforcements

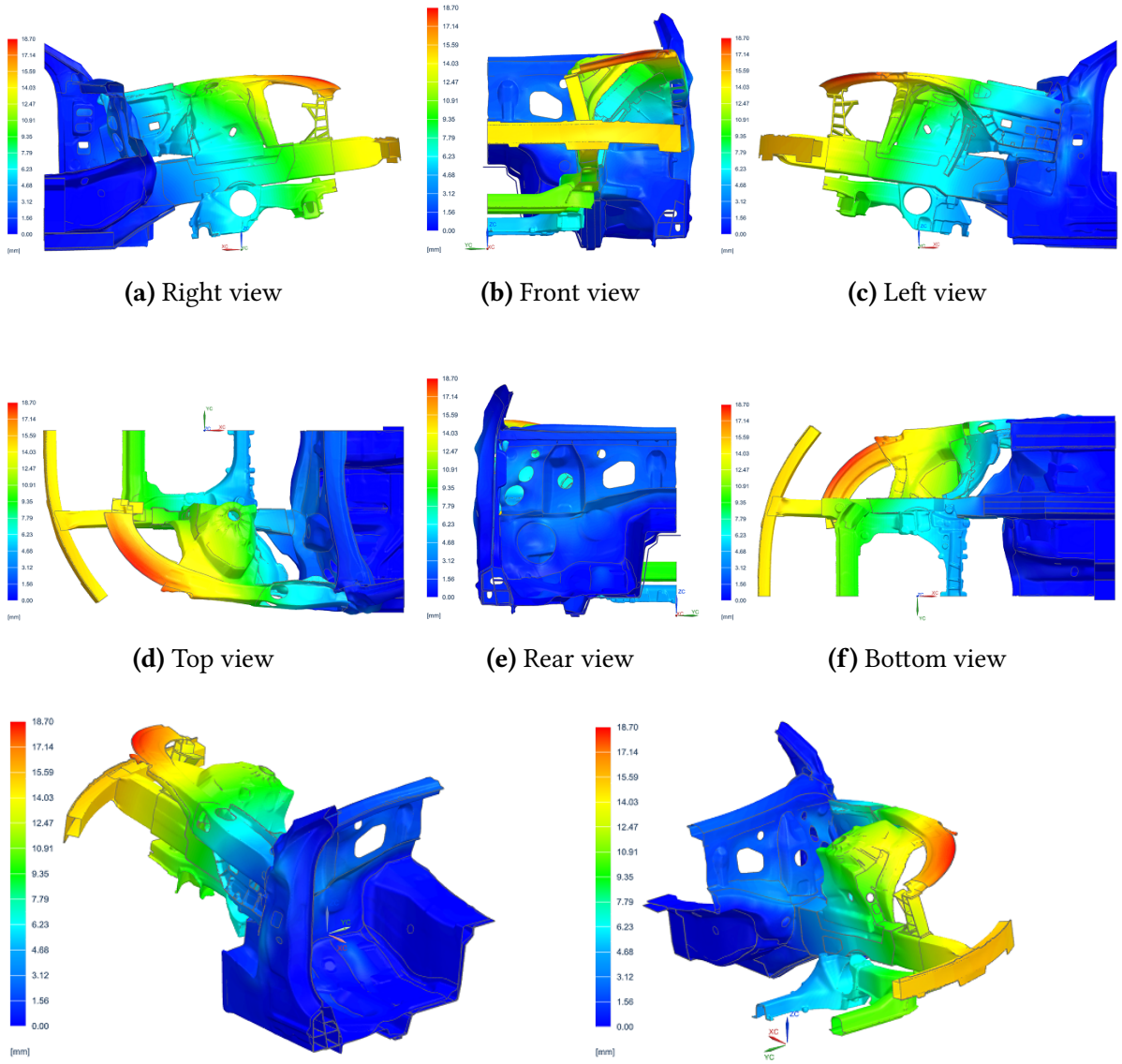

(a) Right view **(b)** Front view **(c)** Left view

(d) Top view **(e)** Rear view **(f)** Bottom view

(g) 3D view 1 **(h)** 3D view 2

Figure C.11: Reinforcements combination: Static analysis - bending (additional views)
Classic loading, 10% model deformation

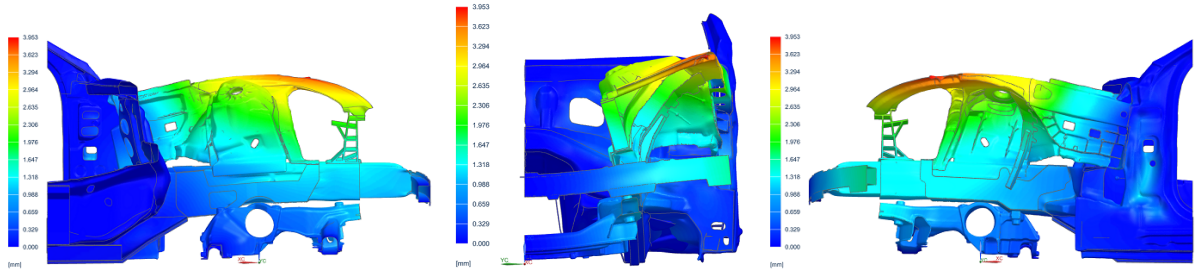

(a) Right view **(b)** Front view **(c)** Left view

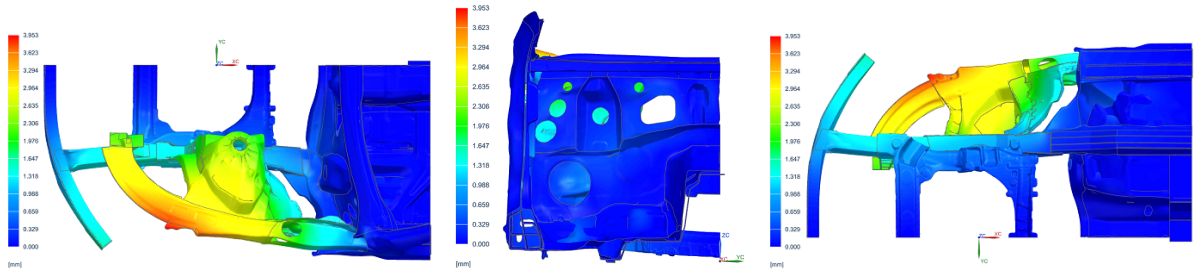

(d) Top view **(e)** Rear view **(f)** Bottom view

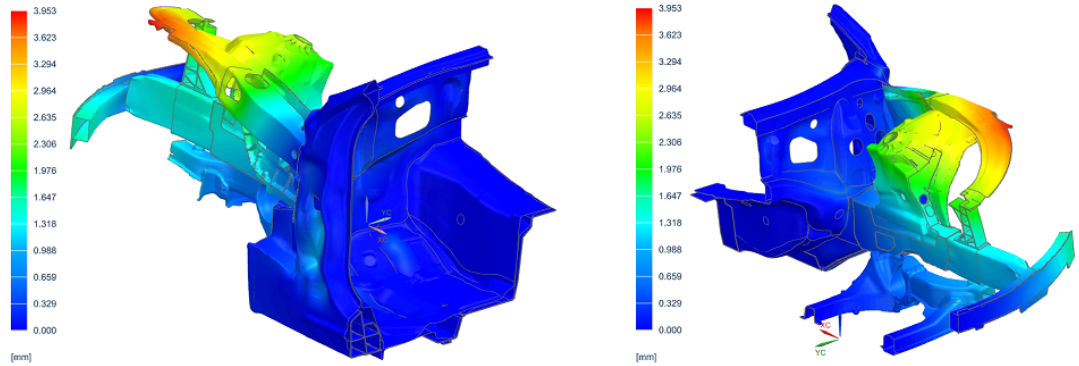

(g) 3D view 1 **(h)** 3D view 2

Figure C.12: Reinforcements combination: Static analysis - composed torsion (additional views)
Classic loading, 10% model deformation

D | Suspension load paths appendix

Support	X [N]	Y [N]	Z [N]
1	31	159	-53
2	0	-1	0
3	0	0	0
4	-209	292	-11
5	108	369	1516

Table D.1: Suspension load paths: 1000 N loading

Support	X [N]	Y [N]	Z [N]
Pure bending			
1	602	3145	-1038
2	9	-17	3
3	0	0	0
4	-4126	5756	-225
5	2121	7279	29890
Composed torsion			
1	261	1363	-450
2	4	-7	1
3	0	0	0
4	-1788	2494	-97
5	919	3154	12950

Table D.2: Suspension load paths: Classic loading

Support	X [N]	Y [N]	Z [N]
Pure bending			
1	1091	5702	-1882
2	17	-31	5
3	0	0	0
4	-7482	10440	-408
5	3846	13200	544210
Composed torsion			
1	473	2471	-815
2	7	-14	2
3	0	0	0
4	-3242	4523	-177
5	1666	5720	23490

Table D.3: Suspension load paths: Armoured loading